

Beneficial Use of Iowa Waste Ashes in Concrete through Carbon Sequestration

**Final Report
January 2025**

IOWA STATE UNIVERSITY
Institute for Transportation

Sponsored by
Iowa Highway Research Board
(IHRB Project TR-807)
Iowa Department of Transportation
(InTrans Project 22-797)

About the Institute for Transportation

The mission of the Institute for Transportation (InTrans) at Iowa State University is to save lives and improve economic vitality through discovery, research innovation, outreach, and the implementation of bold ideas.

Iowa State University Nondiscrimination Statement

Iowa State University does not discriminate on the basis of race, color, age, ethnicity, religion, national origin, pregnancy, sexual orientation, gender identity, genetic information, sex, marital status, disability, or status as a US veteran. Inquiries regarding nondiscrimination policies may be directed to the Office of Equal Opportunity, 3410 Beardshear Hall, 515 Morrill Road, Ames, Iowa 50011, telephone: 515-294-7612, hotline: 515-294-1222, email: eooffice@iastate.edu.

Disclaimer Notice

The contents of this report reflect the views of the authors, who are responsible for the facts and the accuracy of the information presented herein. The opinions, findings and conclusions expressed in this publication are those of the authors and not necessarily those of the sponsors.

The sponsors assume no liability for the contents or use of the information contained in this document. This report does not constitute a standard, specification, or regulation.

The sponsors do not endorse products or manufacturers. Trademarks or manufacturers' names appear in this report only because they are considered essential to the objective of the document.

Iowa DOT Statements

Federal and state laws prohibit employment and/or public accommodation discrimination on the basis of age, color, creed, disability, gender identity, national origin, pregnancy, race, religion, sex, sexual orientation or veteran's status. If you believe you have been discriminated against, please contact the Iowa Civil Rights Commission at 800-457-4416 or the Iowa Department of Transportation affirmative action officer. If you need accommodations because of a disability to access the Iowa Department of Transportation's services, contact the agency's affirmative action officer at 800-262-0003.

The preparation of this report was financed in part through funds provided by the Iowa Department of Transportation through its "Second Revised Agreement for the Management of Research Conducted by Iowa State University for the Iowa Department of Transportation" and its amendments.

The opinions, findings, and conclusions expressed in this publication are those of the authors and not necessarily those of the Iowa Department of Transportation.

Technical Report Documentation Page

1. Report No. IHRB Project TR-807	2. Government Accession No.	3. Recipient's Catalog No.	
4. Title and Subtitle Beneficial Use of Iowa Waste Ashes in Concrete through Carbon Sequestration		5. Report Date January 2025	
		6. Performing Organization Code	
7. Author(s) Kejin Wang (orcid.org/0000-0002-7466-3451) and Yunsu Lee (orcid.org/0000-0002-7360-6439)		8. Performing Organization Report No. InTrans Project 22-797	
9. Performing Organization Name and Address Institute for Transportation Iowa State University 2711 South Loop Drive, Suite 4700 Ames, IA 50010-8664		10. Work Unit No. (TRAIS)	
		11. Contract or Grant No.	
12. Sponsoring Organization Name and Address Iowa Highway Research Board Iowa Department of Transportation 800 Lincoln Way Ames, IA 50010		13. Type of Report and Period Covered Final Report	
		14. Sponsoring Agency Code	
15. Supplementary Notes Visit https://intrans.iastate.edu/ for color pdfs of this and other research reports.			
16. Abstract <p>A significant amount of waste ash in the United States does not meet the necessary specifications for construction and other uses, and power plants are searching for a way to dispose of surplus waste ashes.</p> <p>To address this issue, this research aimed to treat waste ashes using CO₂ injection in order to modify their properties and enable their beneficial use in concrete. The main tasks of the study were to (1) optimize the carbon treatment procedure (pressure, moisture, and time) for the selected waste ashes, (2) determine the effects of the carbon treatment on the properties of the ashes (surface chemistry, morphology, pore structure, etc.), (3) evaluate the effects of carbon-treated ashes on the properties of cement composites such as paste and mortar (set time, flowability, hydration, strength, etc.), and (4) quantify CO₂ sequestration and assess the benefit-to-cost potential of the carbon-curing treatment. Findings indicate that certain types of waste ashes can increase the decarbonation of cement and concrete providing a use for the waste ashes and promoting sustainability.</p>			
17. Key Words carbon sequestration technology—carbon treatment—concrete sustainability—supplementary cementitious materials—waste ashes		18. Distribution Statement No restrictions.	
19. Security Classification (of this report) Unclassified.	20. Security Classification (of this page) Unclassified.	21. No. of Pages 103	22. Price NA

BENEFICIAL USE OF IOWA WASTE ASHES IN CONCRETE THROUGH CARBON SEQUESTRATION

**Final Report
January 2025**

Principal Investigator
Kejin Wang, Professor

Department of Civil, Construction, and Environmental Engineering, Iowa State University

Research Assistant(s)
Yunsu Lee

Authors
Kejin Wang and Yunsu Lee

Sponsored by
Iowa Highway Research Board and
Iowa Department of Transportation
(IHRB Project TR-807)

Preparation of this report was financed in part
through funds provided by the Iowa Department of Transportation
through its Research Management Agreement with the
Institute for Transportation
(InTrans Project 22-797)

A report from
Institute for Transportation
Iowa State University
2711 South Loop Drive, Suite 4700
Ames, IA 50010-8664
Phone: 515-294-8103 / Fax: 515-294-0467
<https://intrans.iastate.edu>

TABLE OF CONTENTS

ACKNOWLEDGMENTS	xi
EXECUTIVE SUMMARY	xiii
1. INTRODUCTION	1
1.1 Research Background	1
1.2 Objectives	2
1.3 Scope and Organization of This Report.....	3
2. SUMMARY OF LITERATURE REVIEW.....	5
2.1 Strategy for Reusing Waste Ashes.....	5
2.2 Concrete Carbon Curing	6
2.3 Importance of Pre-conditioning and Curing Regime.....	6
3. COLLECTION AND CHARACTERIZATION OF WASTE ASHES	8
3.1 Collection of Waste Ashes.....	8
3.2 Characterization of Waste Ashes	10
3.3 Summary of the Physiochemical Properties of RFA, IFA, CFA, and RBA.....	19
4. OPTIMIZATION OF CARBON TREATMENT PROCEDURE	20
4.1 Experimental Setup for the Carbon Treatment	20
4.2 Sample Preparation for Carbon Treatment	22
4.3 Temperature Changes during Carbon Treatment.....	22
4.4 Summary of Exothermic Reactions in the Ashes Studied	27
5. CARBON SEQUESTRATION CAPACITY AND EFFECTS OF CARBON TREATMENT ON PROPERTIES OF WASTE ASHES	29
5.1 Measurement of Carbon Sequestration Capacity.....	29
5.2 Carbon Sequestration Capacity Measured by Thermogravimetry Analysis.....	30
5.3 Surface Morphology of the Carbon-Treated Ashes	33
5.4 Summary of Carbon Sequestration in the Ashes	37
6. EFFECTS OF CARBON-TREATED WASTE ASHES ON FLOWABILITY AND STRENGTH OF MORTAR	39
6.1 Need of Treatment – Expansion of Mortar Containing RFA	39
6.2 Mortar Mixture Proportions and Test Methods	39
6.3 Effect of Carbon-Treated Ashes on Mortar Flowability.....	41
6.4 Effect of Carbon-Treated Ashes on Mortar Strength.....	43
6.5 Summary of Flowability and Strength of Mortar Containing Carbon-Treated Ashes.....	48
7. SYNERGISTIC EFFECTS OF CARBON CURING FOR MORTAR CONTAINING WASTE ASHES	49
7.1 Carbon-Curing Procedure	49
7.2 Results from Carbon-Curing Tests	52
7.3 Summary of the Synergistic Effects of Carbon Curing	58

8. EMBODIED CARBON AND COST SAVINGS ASSESSMENT FOR MORTARS CONTAINING WASTE ASHES	60
8.1 General Considerations	60
8.2 General Assessment	61
8.3 Strength-Normalized Carbon Intensity	64
8.4 Simple Cost Savings Assessment	66
8.5 Summary of Carbon Intensity in the Mortar Containing Waste Ashes	67
9. CONCLUSIONS AND RECOMMENDATIONS	69
9.1 Summary of Observations.....	69
9.2 Conclusions and Recommendations	71
REFERENCES	74
APPENDIX A. ADDITIONAL XRD TEST RESULTS.....	77
APPENDIX B. PHOTOS FROM FLOW TABLE TESTS	78

LIST OF FIGURES

Figure 1.1. Discharge site for Ames Municipal Power Plant ashes.....	2
Figure 3.1. Collection process of (a) RFA and (b) RBA at Ames Municipal Power Plant	8
Figure 3.2. Coarse ash particles in the collected ISU coal ash and the sifted ISU coal ash	9
Figure 3.3. Particle size distribution of RFA, IFA, and CFA	12
Figure 3.4. Gradation curves of RBA and river sand by sieve analysis	12
Figure 3.5. SEM images of (a) RFA, (b) IFA, and (c) CFA.....	13
Figure 3.6. SEM images of (a) RBA and (b) river sand	14
Figure 3.7. X-ray diffraction results of RFA, IFA, CFA, and RBA	17
Figure 3.8. Thermogravimetric test results: (a) weight change and (b) derivative weight loss of RFA, IFA, CFA, and RBA	18
Figure 4.1. Experimental setup for the carbon treatment.....	20
Figure 4.2. Results of the trial tests in the empty pressure pot	21
Figure 4.3. Temperature changes inside the airtight pot during the carbon treatment for RFA	22
Figure 4.4. Temperature changes during the carbon treatment for RFA under different conditions: CO ₂ pressures of (a) 100 kPa and (b) 200 kPa.....	23
Figure 4.5. Trendline of the maximum temperature depending on the moisture content during the carbon treatment for RFA	23
Figure 4.6. Temperature changes during the carbon treatment for IFA under different moisture conditions: CO ₂ pressures of (a) 100 kPa and (b) 200 kPa	24
Figure 4.7. Temperature changes during the carbon treatment for CFA under different moisture conditions: CO ₂ pressures of (a) 100 kPa or (b) 200 kPa	25
Figure 4.8. Setup of the wet carbonation for RBA	26
Figure 4.9. Temperature changes during the carbon treatment for RBA under different moisture conditions: CO ₂ pressures of 100 kPa, 200 kPa, or 500 kPa.....	26
Figure 4.10. Maximum temperature in the carbon treatment under different moisture contents and CO ₂ pressures for the ashes: RFA, IFA, CFA, and RBA	27
Figure 4.11. Hardened samples after carbon treatment and drying at 40°C for 24 hours	28
Figure 5.1. Tangential method to quantify sequestered carbon content in TGA.....	29
Figure 5.2. TGA results of the carbon-treated RFA	30
Figure 5.3. TGA results of the carbon-treated IFA.....	31
Figure 5.4. TGA results of the carbon-treated CFA	32
Figure 5.5. TGA results of the carbon-treated RBA.....	33
Figure 5.6. Surface morphology of (a) RFA, (b) C-RFA-m20-p1, and (c) C-RFA-m20-p2.....	34
Figure 5.7. Surface morphology of (a) IFA, (b) C-IFA-m20-p1, and (c) C-IFA-m20-p2.....	35
Figure 5.8. Surface morphology of (a) CFA, (b) C-CFA-m5-p1, and (c) C-CFA-m5-p2.....	36
Figure 5.9. Surface morphology of (a) RBA, (b) C-RBA-m20-p1, (c) C-RBA-m20-p2, (d) C-RBA-m70-p1, and (e) C-RBA-wet	37
Figure 5.10. Summary of carbon sequestration in RFA, IFA, CFA, and RBA	38
Figure 6.1. Portland cement paste (water-to-cement ratio = 0.45) samples containing RFA (20% replacement) or carbon-treated RFA (20% replacement)	39
Figure 6.2. Flow table test results of mortar containing raw or carbon-treated RFA	41
Figure 6.3. Flow table results of mortar containing raw or carbon-treated IFA.....	42
Figure 6.4. Flow table results of mortar containing raw or carbon-treated CFA.....	42

Figure 6.5. Flow table results of mortar containing raw or carbon-treated RBA	43
Figure 6.6. Compressive strength (a) and strength activity index (b) of mortar specimens containing untreated and carbon-treated RFA ashes.....	44
Figure 6.7. Compressive strength (a) and strength activity index (b) of mortar specimens containing untreated or carbon-treated RFA ashes	45
Figure 6.8. Compressive strength (a) and strength activity index (b) of mortar specimens containing untreated and carbon-treated CFA ashes.....	46
Figure 6.9. (a) Compressive strength and (b) strength activity index of mortar specimens containing raw or carbon-treated RBA ashes.....	47
Figure 7.1. Overall carbon-curing procedure.....	50
Figure 7.2. Surface damage of mortar cubes during early demolding process.....	50
Figure 7.3. Weight change of the cube specimen during the carbon-curing process	51
Figure 7.4. Water released from six mortar cubes during carbonation process.....	52
Figure 7.5. Water evaporation from mortar samples in drying process (pre-conditioning)	53
Figure 7.6. Weight gain of six mortar cubes during carbonation	54
Figure 7.7. Sequestered CO ₂ normalized by the weight of cement content in mortar.....	55
Figure 7.8. Phenolphthalein spray results of the carbon-cured mortar specimens immediately after the carbonation stage: (a) C-RFA-m70-p1, (b) C-IFA20, and (c) C-RBA-m20-p1	55
Figure 7.9. Bulk electrical resistivity of the mortar cubes in the post-curing stage	57
Figure 7.10. Compressive strength of the mortar cubes in the post-curing stage.....	58
Figure 7.11. Phenolphthalein spray results of the carbon-cured mortar specimens at 28 days (the post-curing stage): (a) PLC, (b) C-RFA-m70-p1, (c) C-IFA20, and (d) C-RBA-m20-p1	58
Figure 8.1. Embodied carbon of standard-cured mortar mixtures containing different waste ashes: (a) treated or non-treated RFA, (b) treated or non-treated IFA, (c) treated or non-treated CFA, and (d) treated or non-treated RBA	63
Figure 8.2. Embodied carbon of mixtures treated with carbon curing	64
Figure 8.3. Embodied carbon normalized by compressive strength: (a) 3 days and (b) 28 days	68
Figure A1. XRD patterns of the carbon-treated RFA at a CO ₂ pressure of 100 kPa.....	77

LIST OF TABLES

Table 3.1. Specific gravity, absorption, and moisture content of the collected ashes	10
Table 3.2. Fineness results measured by wet sieve and laser diffraction methods	11
Table 3.3. Oxide compositions of RFA, CFA, IFA, and RBA	15
Table 3.4. Comparison of chemical compositions of RFA, CFA, IFA, and RBA and ASTM C618 requirements	15
Table 4.1. Maximum temperature at the peak during the carbon treatment for RFA.....	23
Table 4.2. Maximum temperature at the peak during the carbon treatment for IFA	24
Table 4.3. Maximum temperature at the peak during the carbon treatment for CFA.....	25
Table 4.4. Maximum temperature at the peak during the carbon treatment for RBA	27
Table 5.1. Sequestered CO ₂ content in the carbon-treated RFA	30
Table 5.2. Sequestered CO ₂ content in the carbon-treated IFA.....	31
Table 5.3. Sequestered CO ₂ content in the carbon-treated CFA	32
Table 5.4. Sequestered CO ₂ content in the carbon-treated RBA	33
Table 6.1. Mixture proportions of mortar containing raw or carbon-treated ashes	40
Table 7.1. Mix proportions of the mortar selected for carbon-curing study	49
Table 7.2. Bulk density of the mortar cubes after post-curing.....	56
Table 8.1. Embodied carbon factors for constituents of mortar	60
Table 8.2. Embodied carbon of the mortar mixes studied	61
Table 8.3. Embodied carbon normalized by compressive strength	65
Table 8.4. Simple calculation of cost savings from use of MSWI fly/bottom ashes in concrete pavement.....	66

ACKNOWLEDGMENTS

The authors would like to thank the Iowa Department of Transportation (DOT) and Iowa Highway Research Board (IHRB) for sponsoring this research.

The technical advisory committee (TAC) for this project included Jeff Devries, Todd Hanson, Chris Brakke, Madeline Schmitt, Jason Omundson, and Brian Moore, Iowa DOT. The authors gratefully acknowledge their valuable suggestions throughout the course of this project. Special help was received from Drs. Yixin Shao and Yogiraj Sargam, whose expert insights, comments, and advice significantly contributed to the success of this research project.

The authors would also like to express their sincere gratitude to the Iowa State University staff and students, including laboratory managers Paul Kremer and Ted Huisman and former graduate student Kwangwoo Wi, at the Department of Civil, Construction and Environmental Engineering, for their daily support of all activities conducted at concrete research labs.

EXECUTIVE SUMMARY

In recent years, many coal-fired power plants in the United States have closed or reduced operations due to the demand for clean energy. This has led to a shortage of coal fly ash that is widely used as a supplementary cementitious material in concrete to improve concrete properties and reduce construction material cost. Currently, many power plants burn natural gas, often together with municipal waste (namely garbage), thus converting waste to energy (called refuse-derived fuel [RDF]) to supplement the coal burned in the power plant. As a result, significant amounts of RDF fly ash (RFA) and RDF bottom ash (RBA) are generated from waste-to-energy power plants and require the use of a landfill. This project aimed to explore the beneficial use of Iowa waste ashes in concrete through carbon sequestration technology. It not only addressed the abovementioned power plant ash problem but also boosted the decarbonation of cement and concrete, thus promoting concrete sustainability.

This project included the following tasks and activities:

Task 1: Collection and characterization of the waste ashes studied. In this task, three fly ashes were collected from the Ames Municipal Power Plant, the Iowa State University (ISU) Power Plant, and the Boral Company, respectively. A bottom ash was collected from the Ames Municipal Power Plant. The physical and chemical properties, including particle size, shape, surface morphology, absorption, oxide composition, crystalline phase composition, and thermal stability and loss on ignition, of these ashes were characterized.

Task 2: Optimization of a carbon treatment procedure for the waste ashes. In this task, waste ash samples with different moisture contents were treated in a tightly sealed carbonation curing chamber, where CO₂ gas was injected under different pressures at a designed rate. Because large fluctuations were observed in the weight changes of the empty carbonation chamber during the carbon injection tests, the team determined that the margin of error was too large to obtain reliable results from the weight change measurements. Therefore, instead of the weight changes, the temperature changes resulting from the exothermic carbonation reaction in the carbonation chamber during the carbon treatment tests were then monitored in real time. The maximum temperature measured in the carbon treatment of a waste ash sample under different treatment conditions was used as a carbonation index for determining the optimal condition in the present study.

Task 3: Evaluation of the effects of the carbon treatment on the properties of the waste ashes. After Task 2, the carbon-treated waste ashes were characterized again, and the modifications to their surface morphology and internal microstructure were realized.

Task 4: Determination of the effects of carbon-treated ashes on mortar properties. In this task, carbon-treated fly ashes (RFA and IFA) were used as a cement replacement in cement pastes, and carbon-treated bottom ash (RBA) was used as a sand replacement in mortar. Samples containing waste ashes with and without carbon treatment were tested for set time, flowability, hydration, and strength. The results were analyzed, and the effects of carbon-treated ashes on paste and mortar properties were recognized.

Task 5: Assessment of the effect of waste ash utilization and carbon curing on the reduction of embodied carbon in mortar. The Inventory of Carbon and Energy (ICE) database and open literature values were used for the assessment of embodied carbon in mortar mixes containing RFA, ISU coal ash (IFA), Class C fly ash (CFA), or RBA. The results were presented as (1) the embodied carbon per unit volume mortar and (2) the embodied carbon normalized by compressive strength of the corresponding mortar mix. These results were compared with the mortar made with 100% portland cement.

The following observations were made in the present study:

1. Physical properties and morphology of raw ashes

- The specific gravity of RFA and IFA was 2.09 and 2.16, respectively, similar to that of CFA (2.13). The moisture content of RFA and IFA satisfied the ASTM C618 requirement (below 3%). RBA had a lower specific gravity of 2.23 and a higher absorption of 8.85%, while the river sand had a specific gravity of 2.67 and an absorption of 1.48%.
- The median particle sizes of RFA (70 μm) and IFA (60 μm) were much larger than that of CFA (16 μm). Their fineness values did not satisfy the ASTM C618 requirement.
- In terms of morphology, RFA and IFA displayed mostly irregularly shaped particles, while CFA displayed mostly spherical particles. The particle shape of RBA was also similar to that of RFA, but there were rod-like crystals on the surface, which were ettringite.

2. Chemical properties and thermal stability of raw ashes

- The CaO content in the waste ashes was 3.14% for RFA and 44.8% for IFA, higher than that of CFA (24.3%), but all met the ASTM C618 requirement of CaO content for Class C fly ash. However, RFA and IFA did not meet the ASTM C618 requirements for $\text{SiO}_2 + \text{Al}_2\text{O}_3 + \text{Fe}_2\text{O}_3$ (>50%) and loss on ignition (LOI) (<6%). In addition, IFA had an SO_3 content of 22.5%, significantly higher than the requirement (<5%), and RFA had an $\text{Na}_2\text{O}_{\text{eq}}$ ($\%\text{Na}_2\text{O} + 0.658 \times \%\text{K}_2\text{O}$) content of 5.7%, significantly higher than the requirement (0.6%). The commercial Class C fly ash, CFA, met all ASTM C618 requirements.
- Based on the X-ray diffraction (XRD) results, relatively higher amounts of calcium carbonate and calcium sulfate in the ashes led to these results. The crystalline phases of RFA were mostly composed of calcite, quartz, and anhydrite. On the other hand, IFA displayed the crystalline phases of anhydrite, quartz, and calcium oxide. The major crystalline phase of CFA was quartz. RBA showed major crystalline phases of ettringite, quartz, gehlenite, and calcite.
- The thermal stability of the ashes was related to the presence of calcite, anhydrite, and ettringite minerals, leading to higher LOI values in RFA, IFA, and RBA.

3. Optimal carbon treatment conditions for waste ashes

- The maximum temperature of an ash sample in the carbon treatment chamber was used as a carbonation index for determining an optimal condition. The maximum temperatures

released from the waste ashes under different carbon treatment conditions were different among the ashes studied. While there was little difference in the maximum temperature resulting from different pressures applied ($p_1 = 100$ kPa and $p_2 = 200$ kPa), the optimal moisture content for carbon treatment was 20% to 40% for RFA, 10% to 20% for IFA, around 10% for CFA, and 20% for RBA.

- At a high moisture content ($>30\%$), some reactive fly ashes, like IFA and CFA, started to harden during carbon treatment due to hydration and carbonation reactions.
- CFA, a conventional Class C fly ash, is highly reactive in water, requiring its carbon treatment under low moisture conditions. RFA is the least reactive of all the fly ashes studied, allowing its carbon treatment under a moisture content of up to 70%. IFA contains an amount of lime, and its reaction was vigorous above a moisture content of 20%, leading to the ash hardening. Therefore, the moisture content should be controlled in a range of 10% to 20% during the carbon treatment of IFA.

4. Carbon sequestration capacity and effect of carbon treatment on properties of waste ashes

- Carbon sequestration was highest in IFA, followed by RFA, RBA, and CFA. At a high CO_2 pressure (200 kPa), the optimal moisture content for carbon sequestration was lower, and the carbon sequestration was improved.
- The optimal moisture content at a CO_2 pressure of 100 kPa was 40% for RFA, 20% for IFA, and 20% for RBA. Under optimal conditions, the amount of CO_2 uptake in IFA, RFA, and RBA was approximately 10, 5, and 2 kg CO_2 /kg anhydrous ash, respectively. However, the carbon treatment was not effective for the conventional fly ash, CFA.
- Morphological changes to the carbon-treated RFA and IFA were observed. On the surfaces of the treated ash samples, calcium carbonate particles between a size of 1 and 5 μm were observed, and the particle surfaces became denser due to the production and aggregation of calcium carbonate. However, for CFA, no significant difference in the morphology before and after carbon treatment was found, although some agglomerations among small particles were noticed.
- The ettringite on the RBA particle surfaces was clearly decomposed after carbon treatment under the treatment condition of 20% moisture content and 100 kPa pressure (sample C-RBA-m20-p1). The decomposition of ettringite due to carbonation was also seen in the TGA results. In addition, some irregularly shaped calcite particles were found on the surfaces of carbon-treated RBA particles.

5. Effects of carbon-treated ashes on properties of cement-based materials

- This research confirms that without any treatment, RFA contained a given amount of metallic aluminum and zinc, which could hydrate and generate air bubbles, causing severe cement expansion. During the carbon treatment, the metallic aluminum was oxidized, and therefore the use of carbon-treated RFA in cement-based materials will cause no damage due to expansion. Carbon treatment can be a promising technology for utilizing waste ashes, including metallic aluminum and zinc.
- The carbon treatment effectively improved RFA and RBA to mitigate the strength reduction of mortar (20% replacement) without significant flowability loss. When carbon treated at the

moisture condition of 70% under 100 kPa and 200 kPa pressure, 20% carbon-treated RFA (C-RFA) replacement for cement led to a reduction in compressive strength of less than 10% and 15% compared with the control mortar mix (100% portland cement) at the age of 28 days. When carbon treated at the moisture conditions of 20% and 70% under 100 kPa pressure, 20% saturated surface-dry (SSD) carbon-treated RBA (C-RBA) replacement for river sand led to a reduction in compressive strength of less than 7% compared with the mix made with 100% dry river sand at the age of 28 days. (Note: The mortar made with 100% dry river sand actually had a lower water/binder (w/b) ratio than the mortar made with 20% SSD C-RBA replacement for river sand.)

- In the test results of samples containing RFA, the strength activity index at 28 days was improved from 57% (RFA20) up to 90% (RFA20-m70-p1). The effect of carbon treatment for RFA was greatly dependent on moisture content. A moisture content of 70% was the best for the treatment, leading to the effective removal of the metallic aluminum and the mitigation of strength reduction.
- In the test results of samples containing RBA, the carbon treatment for RBA improved the compressive strength, increasing the strength activity index at 28 days from 75% (RBA20) up to 93% (RBA20-m70-p1). This may be due to the surface refinement of the ash with calcium carbonate.
- The carbon treatment was not effective for IFA and CFA and had no positive effect on mortar strength. Although the carbon treatment effectively transformed CaO in IFA into calcium carbonate, the excessive sulfate content in the raw or carbon-treated IFA did not change, which hindered the strength development of the mortar.
- The carbon-treated CFA caused particle agglomeration and the prehydration of CFA, leading to negative effects on both flowability and strength development.

6. Strength-normalized carbon intensity of mortar mixes studied

- The strength-normalized embodied carbon values decreased with the age of the mortar due to increased strength with age.
- At the ages of 28 and 56 days, the mortars with a lower value of strength-normalized embodied carbon than the control mortar are those containing RFA20-m70-p1/p2, IFA10, CFA10/CFA20, CFA20-m0-p1, and CFA20-m5-p1/p2, among which only the mortar with RFA20-m70-p1 also had a value of strength-normalized embodied carbon lower than the control mortar at 3 days.
- From the viewpoint of strength-normalized embodied carbon, use of up to 20% CFA with or without carbon treatment or 20% RFA carbon treated under the 70% moisture condition with 100kPa pressure (RFA20-m70-p1) to replace cement in mortar is the most beneficial.

The following are the conclusions and recommendations drawn from the present study:

1. The particle size and chemical composition of as-received RFA and IFA do not meet the requirement of ASTM C618, and therefore they cannot be used as supplementary cementitious materials directly.
2. Test results show that different CO₂ pressures (100 kPa or 200 kPa) have limited effects on the effectiveness of their carbon treatment, but the moisture content of waste ashes has a

significant effect on the effectiveness of their carbon treatment. Different ashes require different carbon treatment conditions to reach optimal carbon sequestration capacity. Generally, reactive fly ash (like IFA and CFA) requires low moisture content to reach optimal carbon treatment, and high moisture content can lead to ash hardening during the treatment. Differently, less reactive ash (like RFA and RBA) allows high moisture content for carbon treatment without hardening. This observation can be used to assist in the selection of carbon treatment conditions of waste ashes.

3. Under their optimal carbon treatment conditions, the CO₂ uptake of IFA, RFA, and RBA is approximately 10, 5, and 2 kg CO₂/kg of anhydrous ash, respectively. Such carbon sequestration capacity will offer additional benefits for embodied carbon reduction when the waste ashes are used in concrete.
4. After being carbon treated at the moisture condition of 70% under 100 kPa pressure, the strength activity index at 28 days of the RFA mortar was improved from 57% (RFA20, with no treatment) up to 90% (RFA20-m70-p1, with carbon treatment). After being carbon treated at the moisture condition of 70% under 100 kPa pressure, the strength activity index at 28 days of the RBA mortar was improved from 75% (RBA20, with no treatment) up to 93% (RBA20-m70-p1, with carbon treatment). These results suggest that from the strength viewpoint, carbon-treated RFA and RBA can be used as cement replacement and sand replacement in concrete, respectively.
5. Carbon treatment is not recommended for reactive ashes like IFA and CFA. Although the carbon treatment effectively transformed the CaO in IFA into calcium carbonate, it did not change the excessive sulfate content in IFA, which critically hindered the strength development of the mortar.
6. The embodied carbon of mortar mixes is primarily controlled by their portland cement content. Therefore, maximizing the replacement of cement with low embodied carbon materials is greatly effective for reducing the embodied carbon of mortars. Although it does not play a significant role in embodied carbon reduction, carbon treatment of waste ashes can effectively help oxidize the metallic aluminum and zinc in waste ashes, such as the RFA studied, thus preventing gas generation, abnormal expansion, and strength reduction of the mortar containing waste ashes.
7. Among all of the waste ashes studied, only the mortar containing 20% RFA carbon treated under the 70% moisture condition with 100 kPa pressure (RFA20-m70-p1) showed a lower value of strength-normalized embodied carbon than the control mortar (made with 100% portland cement) at all ages up to 56 days. From the embodied carbon reduction viewpoint, 20% carbon-treated RFA is encouraged for use as cement replacement in mortar and concrete.
8. In terms of cement and transportation costs, the use of 20% carbon-treated waste fly ashes to replace cement in normal-strength concrete (3000 to 5000 psi) can result in concrete material cost savings of over 20%.
9. The durability of concrete containing carbonation-treated waste ashes, which was not covered in this study, must be investigated before the waste ashes can be practically used in field concrete.
10. Although the City of Ames produces 6 tons of waste ash daily, this amount is insufficient to meet the concrete industry's needs. This may be a concern in terms of industry investment in production lines for waste ash treatment and adoption of these ashes as a viable material in concrete.

1. INTRODUCTION

1.1 Research Background

In the United States, annual cement consumption has increased steadily from approximately 94.4 to 120 million metric tons over the past decade, equivalent to approximately 960 million metric tons of concrete production (Jaganmohan 2024). According to the National Ready Mixed Concrete Association, each pound of concrete releases 0.93 lb of carbon dioxide (CO₂). Therefore, the CO₂ released in the construction of a mile of a single Interstate lane is $0.93 \times 8.7 \text{ million} = 8.1 \text{ million pounds}$ (EcoR1 News 2019).

To reduce the negative environmental impacts, recycled wastes (e.g., slag and fly ash) are widely used as supplementary cementitious materials (SCMs) in concrete. The Iowa Department of Transportation (DOT) has also been using concrete mixes containing 20% or more SCMs (e.g., slag and fly ash) and blended cement, like Types IS, IP, and recently IL. According to the American Coal Ash Association (2020), about 13 million metric tons of coal fly ash is used annually in concrete in the United States. However, a significant amount of the power plant ashes are not currently used beneficially, mainly because these ashes don't meet the national and state material specifications. This generates a great challenge for power plants, concrete producers, and users, as well as our society.

By 2019, Iowa was the 16th in the nation in coal power generation, with 72 operating coal-fired power units at 28 locations totaling 6,492 megawatts. The Iowa State University (ISU) Power Plant on the ISU campus is a coal-fired power station, and it uses 155,000 tons of coal and generates 28,000 tons of coal ash per year. Over the years, 77 tons of coal waste (off spec ashes) have been sent to Waterloo, Iowa, to be dumped into a quarry. The Ames Municipal Power Plant, in Ames, Iowa, opened in 1975 and was the nation's first municipally operated waste-to-energy plant. It converts municipal waste (namely garbage) to energy (called refuse-derived fuel [RDF]), which supplements the coal burned in the power plant. In 2016, the plant converted from burning coal to running on natural gas. It currently produces approximately 6 tons of combustion residuals (RDF ashes) per day. As shown in Figure 1.1, these RDF ashes (bottom ash mixed with fly ash) are remediated at a nearby ash pond, a landfill to prevent the release of ash into the atmosphere, but this poses serious risks for the surrounding environment, such as leaching of chemicals from the ashes into ground and surface waters. The power plants are urgently looking for an effective way to solve this problem.



Figure 1.1. Discharge site for Ames Municipal Power Plant ashes

This proposed study is to address the above-mentioned power plant ash problem and to convert the waste, hazardous ashes, into a sustainable, beneficial, high-value raw material source for extensive use in concrete through an innovative technology.

1.2 Objectives

The goal of the proposed study is to turn both deleterious green gas (specifically CO₂) and power plant ashes into a beneficial product for concrete construction. More specifically, the goal is to utilize captured CO₂ (from power plants, cement manufacturing plants, air, etc.) to treat Iowa power plant waste ashes (coal and RDF ashes, fly ash, and bottom ash) and improve the properties of the ashes for beneficial use in concrete. The approach of this study is to inject CO₂ into these ashes to alter the surface chemistry, morphology, and pore structure of the ash particles and to optimize the engineering performance of the carbon-treated ashes.

The specific objectives of this proposed study include the following:

1. To determine the effects of carbon treatment on properties (surface morphology, particle size, etc.) of the waste ashes in Iowa
2. To determine the effects of carbon-treated ashes on the properties (flowability and strength) of concrete materials (especially paste and mortar)
3. To investigate how much carbon the waste ashes to be studied can sequestrate
4. To assess the embodied carbon reduction potential of the mortar containing carbon-treated waste ashes

The following tasks were accomplished as part of this research:

Task 1: Collection and characterization of the waste ashes collected from the Ames Municipal Power Plant and the ISU Power Plant.

Task 2: Optimization of carbon treatment procedure for the waste ashes: Ames RDF ashes (RDF fly ash [RFA] and RDF bottom ash [RBA]) and ISU coal ash (IFA).

Task 3: Evaluation of the effects of the carbon treatment on the properties of waste ashes.

Task 4: Determination of the effects of carbon-treated ashes on mortar properties.

Task 5: Assessment of the embodied carbon reduction potential of the mortar containing carbon-treated waste ashes.

1.3 Scope and Organization of This Report

This report documents the investigation performed to complete the abovementioned tasks:

Chapter 1 presents the problem statement, goals and objectives, and project tasks.

Chapter 2 summarizes the literature review about waste ashes, carbon treatment, and curing methods for reusing waste ashes in concrete.

Chapter 3 presents the physiochemical properties of Ames RDF ashes (fly ash and bottom ash), ISU coal ash, and general Class C fly ash. The following properties were investigated: specific gravity, particle size distribution, shape/surface morphology, absorption/moisture content, oxide composition, crystalline phase composition, and thermal stability and loss on ignition.

Chapter 4 describes experimental methods for carbon treatment and presents the results of carbon treatment for the waste ashes in terms of initial moisture content and temperature change during the carbon treatment.

Chapter 5 presents the results of carbon treatment in terms of the carbon uptake of the ashes.

Chapter 6 presents the results of the flowability and compressive strength of mortars containing the raw waste ashes or the carbon-treated ashes.

Chapter 7 presents the carbon-curing results for the selected mortar mixtures. The results were compared with the standard curing method in terms of normalized embodied carbon to investigate synergistic effects of the carbon curing.

Chapter 8 describes embodied carbon assessment for a unit volume of the mortar mixtures studied in this project and subsequently presents the normalized embodied carbon by compressive strength of the mortar mixtures.

Chapter 9 summarizes and concludes this research work. Recommendations for effective application of the waste ashes are also presented.

2. SUMMARY OF LITERATURE REVIEW

2.1 Strategy for Reusing Waste Ashes

Reusing solid waste ashes is one way of reducing landfill waste and embodied carbon emissions. Accordingly, replacing cement in concrete, reducing clinkers in cement, and using alternative fuels have already been applied for a long time. Furthermore, the Paris Agreement (Delbeke et al. 2019) accelerated action to limit global warming, resulting in research about carbon capture technology in fresh or hardened concrete. The offset effect on embodied carbon emissions can be expected by reusing industrial gases, including CO₂, in carbon capture technology.

To maximize the reduction of embodied carbon emissions, cement replacement by waste solids and carbon sequestration into concrete are required at the same time. Unfortunately, solid waste ashes produced from a feedstock of municipal solid wastes or a fluidized bed combustion process have very different properties, unlike conventional ashes, limiting their reuse in concrete. For example, RDF ashes mostly contain metallic aluminum, causing hydrogen gas in alkaline solutions through oxidation reactions and a significant decrease in concrete strength (Aubert et al. 2004, Chen and Ye 2024). On the other hand, fly ashes from a fluidized bed combustion process (lower burning temperature ranges of 800°C to 950°C) usually have more crystalline phases, mostly anhydrite, quartz, and lime, and display irregularly shaped particles in contrast to conventional fly ashes (Ohenoja et al. 2020). When these ashes are replaced with cement, strength reduction is typically observed.

Therefore, controlling metallic alumina (Al), soluble sulfate, and free lime is essential to solidify the waste ashes in concrete without strength degradation. To remove metallic Al in RDF ashes, mechanical milling and water treatment have been proposed (Bertolini et al. 2004, Joseph et al. 2020, Chen and Ye 2024). The oxidation reaction can be accelerated in water treatment when water is heated up to 105°C even though it is energy-intensive (Joseph et al. 2020). In water treatment, however, a higher water-to-solid ratio can be an issue in wastewater disposal. That is why Chen and Ye (2024) used a slurry of RDF ashes without disposing of wastewater after the water treatment by making a slurry with a water-to-solid ratio of 0.40.

In the present report, the researchers suggest a slurry carbonation method as distinguished from the water treatment. Because metallic Al can dissolve in a low pH solution and carbon treatment of cement-based materials under moisture and pressure can produce CO₂-saturated pore solutions with a pH of approximately 4 (Li et al. 2012), it is expected that carbon treatment of waste ashes under moisture and pressure can facilitate the dissolution of metallic Al, leading to aluminum-bearing chemicals in the waste ashes studied. In addition, free lime can be restricted by carbon treatment because it is easily converted into calcium hydroxide; thus, the calcium hydroxide can be carbonated in a CO₂-rich environment. Notably, the ashes produced in fluidized bed combustion will have higher carbon sequestration capacity due to higher free lime content.

Before waste ashes are used, the slurry carbon treatment can reduce and stabilize the harmful chemicals in the ashes in addition to the benefit of carbon sequestration. Furthermore, carbon-curing technology can also be applied to cement composites containing the treated ashes for

additional carbon sequestration and property enhancement of the cement composites. Carbon curing has been applied to mainly three different types of concrete: compressed concrete block (Liu et al. 2020), plain or reinforced precast concrete (Zhang and Shao 2016, Zhang et al. 2021), and fresh concrete (Monkman and MacDonald 2017), where the processes of carbon curing for different types of concrete products are different.

2.2 Concrete Carbon Curing

In the carbon curing of compressed cement composites, a water-to-binder ratio of 0.10 to 0.18 is used in the compaction process to simulate the manufacturing of concrete blocks (Lu et al. 2022). A significant advantage of this method is that much of any nonhydraulic or low-hydraulic materials such as γ -dicalcium silicate (γ -2 CaO·SiO₂), rankinite (3CaO·2SiO₂), and wollastonite (CaO·SiO₂) can be used for carbon curing because they are reactive with the carbonate ion (Ashraf and Olek 2016, Smigelskyte et al. 2020). A compressed concrete technique is usually favorable for production of small-sized products (such as concrete blocks). The formwork can be removed soon after compression, and carbon curing can start right after.

On the other hand, the carbon curing of precast concrete requires some time for concrete to be cured in-mold. Carbon curing can be applied after demolding. It takes more time for precast concrete to reach carbon curing after mixing than the compressed concrete. This method, however, allows the use of a variety of formwork to produce concrete beams, walls, slabs, and panels. A primary concern is that a higher water-to-binder ratio is used in precast concrete than compressed concrete, which demands both in-mold curing and a predrying process before carbon curing can be applied. Because CO₂ penetration into concrete is greatly dependent on the water saturation of the concrete's pores (Zhang and Shao 2016), proper drying is needed to make a path for CO₂ in concrete and prevent overdrying of pore water for dissolving calcium ions. (Note: A drying process can be conducted to improve carbon sequestration in the compressed concrete type as well.) The carbon curing in the precast concrete type starts once the in-mold curing and predrying process are finished.

Lastly, carbon sequestration into fresh concrete while mixing can be performed in the ready-mixed concrete industry. Monkman and MacDonald (2017) reported that the estimated direct carbon sequestration into concrete was 2.3 kg CO₂ in an 8 m³ truckload of concrete. It is an insignificant amount compared to the estimated embodied carbon of general concrete with a strength of 28 to 34 MPa (4000 to 5000 lb/in.²), approximately 250 to 400 kg CO₂ in 1 m³ concrete (Anderson and Moncaster 2020). However, the cement reduction in a unit volume of concrete was achieved by compensating strength reduction using CO₂ injection into fresh concrete, leading to a decrease of embodied carbon without strength loss.

2.3 Importance of Pre-conditioning and Curing Regime

Consequently, both compressed concrete and precast concrete types can be widely used for considerable carbon sequestration into concrete. For carbon sequestration, enough time is required to produce reactants reactive with carbonate ions. Prehydration is essential, especially in portland cement-based binders, because Ca(OH)₂ is the main reactant for carbon curing at an

early age (Zhang et al. 2018, Chen et al. 2019, Zajac et al. 2023). Therefore, prehydration, as well as predrying for a CO₂ path, are required for carbon curing. In the predrying stage, an empirical method of evaporating water in concrete using artificially generated wind is suggested to reach the target condition in a few hours. Approximately 30% to 40% water loss of cement paste is recommended for ideal carbon sequestration (Zhang and Shao 2016, Chen and Gao 2019). The limitation of this method is that the moisture content at every depth from the core of a specimen is uneven because of the extent of moisture evaporation near the surface. Nevertheless, it is a simple and reasonable method of improving carbon sequestration within a daily cycle of carbon curing.

Generally, carbon curing significantly improves the strength of nonhydraulic γ -dicalcium silicate, rankinite, and wollastonite binders at both early and later ages because they are less reactive in general water. Contrarily, carbon curing must be used carefully for hydraulic binders, mostly portland cement-based systems. Because excessive carbonation can prevent subsequent hydration of cement by covering the surface of cement grains with stable calcium carbonate after carbon curing, proper prehydration and predrying must be conducted to gain the beneficial effects on carbon sequestration and strength of concrete (Chen and Gao 2019). Accordingly, both carbon-curing time and CO₂ pressure are also important factors in carbon curing of concrete.

3. COLLECTION AND CHARACTERIZATION OF WASTE ASHES

In this study, four different ashes were investigated for use in portland cement paste/mortar as replacements for cement or fine aggregate. Three were fly ashes from different sources (Ames Municipal Power Plant, ISU Power Plant, and Boral Company) and the fourth was bottom ash from the Ames Municipal Power Plant.

3.1 Collection of Waste Ashes

3.1.1 RDF Fly Ash and RDF Bottom Ash Collection

At the Ames Municipal Power Plant, RFA was collected directly from power station cyclones and stored in metal buckets (Figure 3.1(a)). Because of the heat from the ash, it was cooled down for an hour outside. Large ash particles, the floating things in water, were removed using #50 (300 μ m) mesh, as shown in Figure 3.2(a).

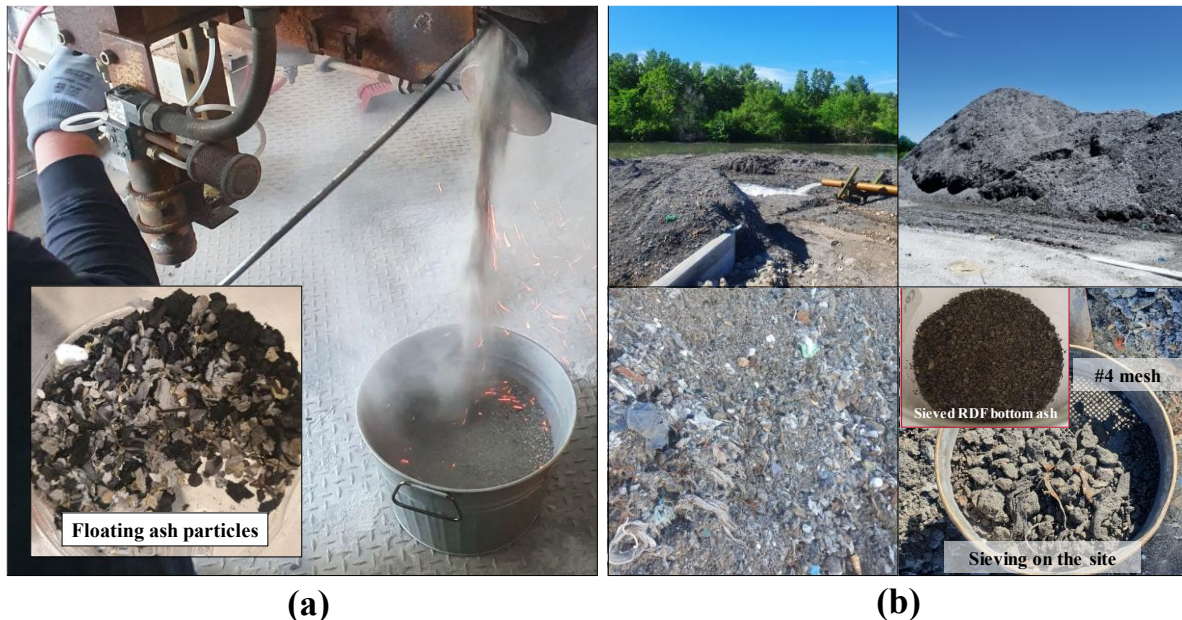


Figure 3.1. Collection process of (a) RFA and (b) RBA at Ames Municipal Power Plant

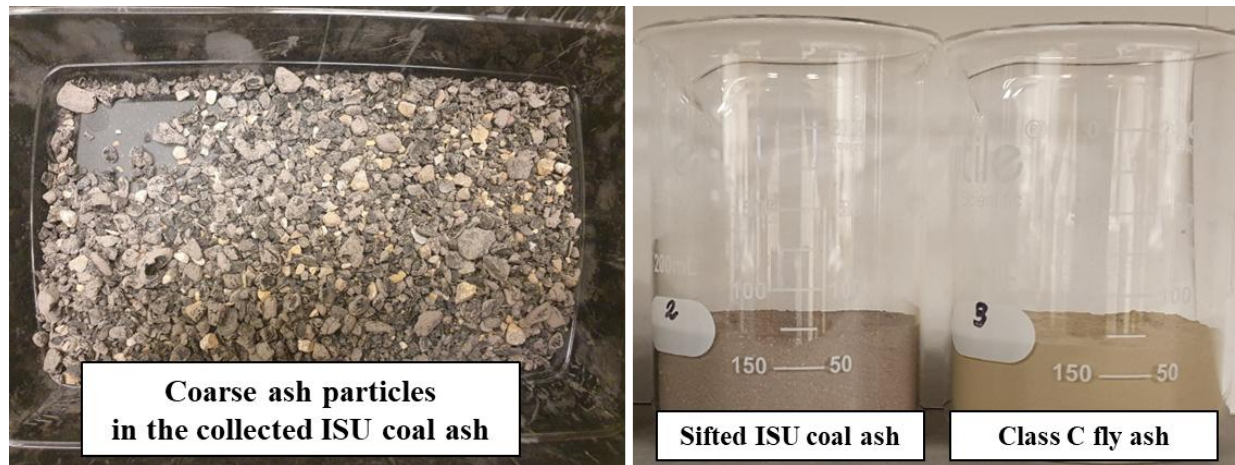


Figure 3.2. Coarse ash particles in the collected ISU coal ash and the sifted ISU coal ash

RBA was collected from an ash pile, near the ash pond. RBA came out of the pond a few days before being collected (Figure 3.2(b)). Thus, it was a water-quenched RBA. During the collection, RBA was sieved using #4 (4.75 mm) mesh to screen out foreign wastes and large particles. The sieved RBA was then placed into buckets.

After being transported to the ISU concrete research laboratory, RFA (or RBA) in different buckets was mixed to homogenize it, and the mixed RFA (or RBA) was then re-stored in different buckets and sealed with lids to prevent weathering and moisture change.

In this project, waste fly ashes, like this RFA, were used for cement replacement, while RBA was used as a fine aggregate for sand replacement, not used as a binder.

3.1.2 ISU Coal Ash Collection

IFA was collected at the ISU Power Plant, where bituminous coal, from southern Illinois, was used in boilers. IFA was collected in several buckets. After being transported to the ISU concrete research lab, all of IFA was mixed together, the coarse ash particles of the ash were removed using #50 mesh, and the sifted IFA was re-stored in different buckets and sealed with lids for later use (Figure 3.2). The sifted IFA was darker and had a similar volume to the Class C fly ash from Boral Company at a given weight of 100 g.

3.1.3 Class C Fly Ash Collection

The commercial Class C fly ash (CFA) was collected from Boral Resources, USA. It complied with the ASTM International (ASTM) specification for fly ash and was used as a reference fly ash in this project. That is, the physical and chemical properties of the abovementioned waste ashes (RFA and IFA) were compared with those of CFA.

3.2 Characterization of Waste Ashes

The collected ashes were characterized by their physical properties (specific gravity, moisture content, particle size, particle shape, and surface morphology) and chemical properties (oxide composition and mineralogical composition). The characterization results are presented below.

3.2.1 Specific Gravity, Absorption, And Moisture Content

Specific gravity was measured by pycnometer for all fly ashes. Kerosene with a specific gravity of 0.798 at room temperature, compliant with ASTM C188, was used to measure the specific gravity of fine ashes below 300 μm (RFA, IFA, and CFA) in a pycnometer. The calculation process of specific gravity for these ashes was in accordance with ASTM D2320. On the other hand, the specific gravity of RBA was measured following ASTM C128 because it was used as a fine aggregate.

The moisture content of the fly ashes was calculated in accordance with ASTM C311. They were first dried to a constant mass in an oven at 110°C for a day. On the other hand, RBA was dried to a constant mass at 40°C for a day because it contained hydroxide compounds and there was unexpected decomposition of hydroxides at 110°C.

Only absorption of RBA was measured because it was important to identify the saturated surface-dry (SSD) condition of the bottom ash when it was used as a fine aggregate. The absorption measurement was in accordance with ASTM C128 and AASHTO T 84, except that RBA was dried to a constant mass at 40°C for a day.

Table 3.1 shows the specific gravity, moisture content, and absorption of the different ashes and river sand used in this study. All of the different fine fly ashes, RFA, IFA, and CFA (reference), showed similar specific gravity, 2.09 to 2.16. However, RBA had a lower specific gravity than the river sand due to some voids in RBA, resulting in higher absorption.

Table 3.1. Specific gravity, absorption, and moisture content of the collected ashes

Sample name	Specific gravity	Absorption (wt%)	Moisture content (wt%)
RFA	2.09	-	0.42
IFA	2.16	-	0.23
CFA	2.13	-	0.09
RBA	2.23 (2.05, dry)	8.85	18.01
River sand*	2.67	1.48	0.44

* The river sand used in this study was also tested as a reference to RBA.

All moisture contents of the as-received fine fly ashes were below 3%, which met ASTM C618 requirement. The as-received RBA had a moisture content of 18.01%, which was greater than absorption. This is because it was collected in a pile not long after it was lifted from the ash pond.

3.2.2 Fineness and Particle Size Distribution

A fineness test for RFA, IFA, and CFA was conducted using #325 (45 μm) mesh and isopropyl alcohol. Fineness was evaluated by the weight measurement of particles retained on the #325 mesh. A sample of approximately 1.2 g was placed on the round #325 mesh with a bottom pan and sieved with the flow of isopropyl alcohol and vibration on a vibrating table. Fineness was verified by laser diffraction method.

The particle size distributions of RFA, IFA, and CFA were determined using laser diffraction (Mastersizer 3000, Malvern Panalytical) in isopropyl alcohol with continuous stirring (wet dispersion).

In the gradation test for RBA, sieve analysis was conducted following ASTM C136. The river sand used in this study was also tested as a reference for RBA. Based on the results of the gradation test, the fineness moduli of RBA and river sand were calculated.

As seen in Table 3.2, the fineness of RFA measured by wet-sieve and laser diffraction was 90.4% and 78.8%, respectively; the fineness of IFA measured by wet-sieve and laser diffraction was 83.1% and 63.2%, respectively; and the fineness of CFA measured by wet-sieve and laser diffraction was 17.2% and 22.9%, respectively. Note that CFA is a commercial fly ash complying with the standard requirement (ASTM C618), and its fineness was below the maximum requirement of 34% as specified by ASTM C618. However, both RFA and IFA greatly exceeded this requirement.

Table 3.2. Fineness results measured by wet sieve and laser diffraction methods

Sample name	Particles above 45 μm (wt%)	
	Wet-sieve method*	Laser diffraction method
RFA	90.4	78.8
IFA	83.1	63.2
CFA	17.2	22.9

*The required maximum percentage of fineness in ASTM C618 is 34%.

From Figure 3.3 it can be observed that the median values (D_{50}) of RFA, IFA, and CFA in particle size distributions were 70, 60, and 16 μm , respectively.

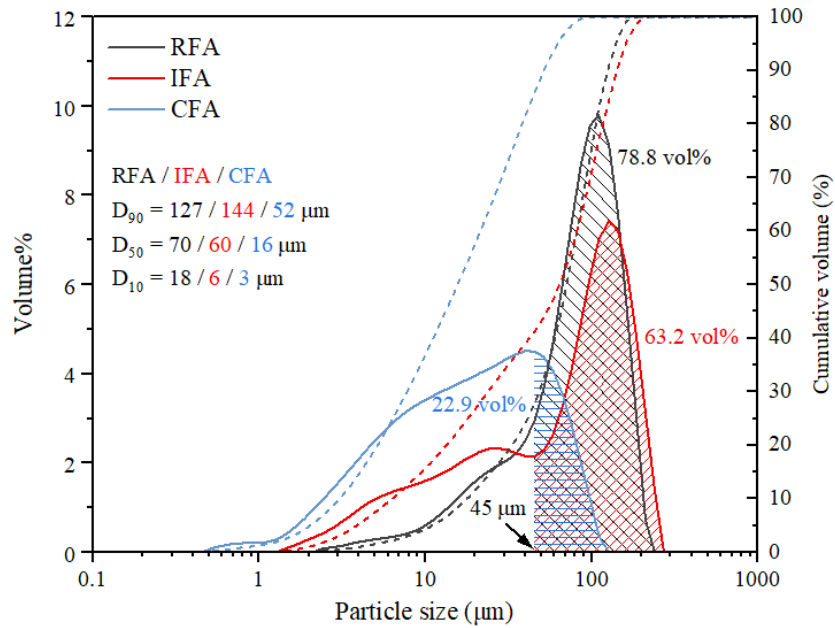


Figure 3.3. Particle size distribution of RFA, IFA, and CFA

Figure 3.4 shows the gradation curves of RBA and river sand resulting from sieve analysis. Both RBA and river sand satisfied the upper and lower limits of ASTM gradation specification. The fineness moduli of RBA and river sand were 3.12 and 2.97, respectively. That is, RBA was slightly coarser than the river sand.

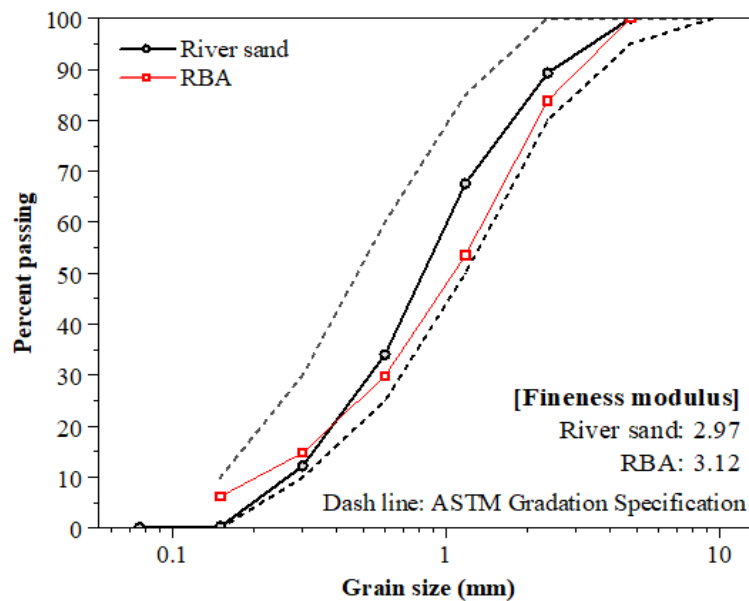


Figure 3.4. Gradation curves of RBA and river sand by sieve analysis

3.2.3 Particle Shape and Surface Morphology

The particle shape and surface morphology of RFA, IFA, and CFA were investigated using a scanning electron microscope (SEM). Inspect F50 was used under 10 kV or 15 kV accelerating voltage and a working distance of approximately 9.5 mm.

Figure 3.5 shows the SEM images of RFA, IFA, and CFA. In RFA, both spherical and irregular particles were seen. In IFA, most particles showed irregular shapes. In CFA, most particles were spherical particles.

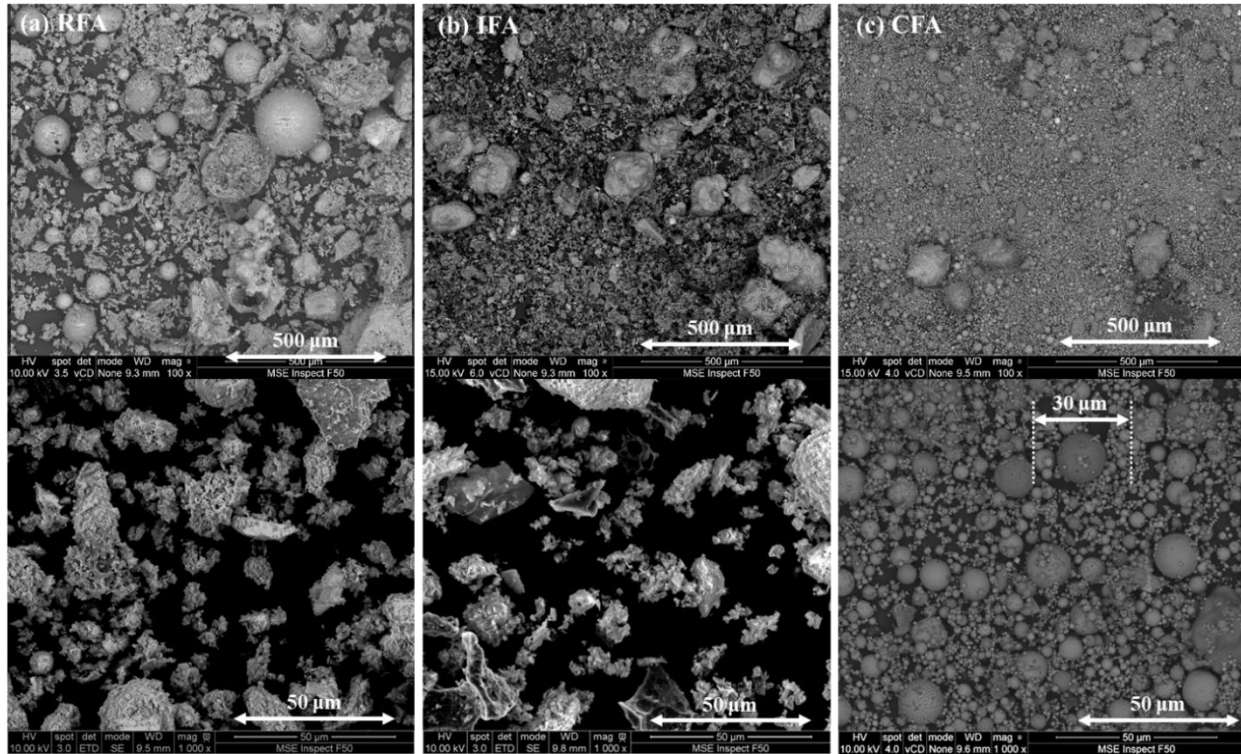


Figure 3.5. SEM images of (a) RFA, (b) IFA, and (c) CFA

The spherical particles in CFA are generally attributed to a high combustion temperature, usually above approximately 1400°C (2550°F), during the coal combustion process. The Ames Municipal Power Plant uses wall-fired or tangential-fired boilers (Stoker grate boiler system) using natural gas, burning up to approximately 1650°C (3000°F). Because of the high temperature combustion, RFA contained some spherical particles. The ISU Power Plant uses circulating fluidized bed boilers that burn coal at low combustion temperature ranges, 800°C to 950°C (1472°F to 1742°F), which significantly affects fusion, sintering, or clinking of ashes, determining particle morphologies. Based on Behr-Andres et al. (1993), spherical particles are rarely formulated in low combustion temperature ranges.

In addition to combustion temperature, the type of feedstock, residence time, and turbulence that influence fused materials and their transformation into fly ash can also influence the fly ash

particle shape formation. Taylor et al. (1982) reported that fly ashes derived from either RDF or RDF/coal mixed feedstock could display four different types of morphologies (shredded sponge, rolled paper, paint chips, and sphere shapes) and most of them were not spherical, even in high combustion temperature ranges.

Figure 3.6 displays the SEM images of (a) RBA and (b) river sand. Unlike in river sand, both spherical and irregularly shaped particles were observed in RBA. The overall shapes of the RBA particles were similar to that of RFA. But, unlike RFA, some rod-like crystals were observed on the surface of the fine RBA particles (100 to 200 μm). The rod-like crystals are supposed to be ettringite ($\text{Ca}_6\text{Al}_2(\text{SO}_4)_3(\text{OH})_{12}\cdot 26\text{H}_2\text{O}$), which can be produced in wet conditions after RBA was lifted from the ash pond (Anthony et al. 2002). The specific mineralogical composition of RBA will be discussed in the mineralogical and oxide compositions section below.

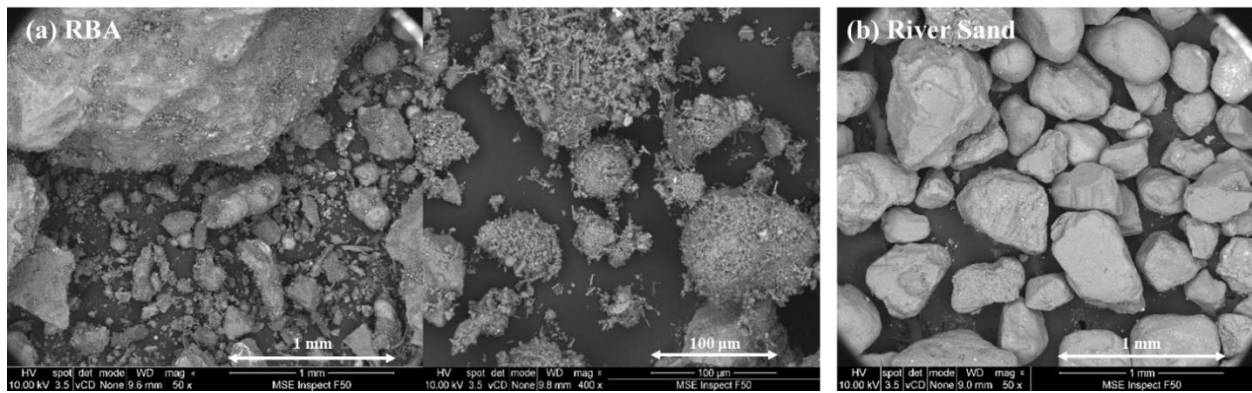


Figure 3.6. SEM images of (a) RBA and (b) river sand

3.2.4 Oxide and Mineralogical Compositions

The oxide compositions of the ashes were detected using X-ray fluorescence (XRF). The XRF results of RFA, CFA, IFA, and RBA are shown in Table 3.3. Additionally, loss on ignition (LOI) from room temperature to 750°C was measured in accordance with ASTM C618. It is noted that the LOI value is intended to be an evaluation of unburnt carbon content in fly ash, but it can be overestimated due to hydrates, carbonates, and organic compounds. Therefore, the LOI indicates various volatile materials with mostly hydrogen oxide and carbon oxide. In this study, RBA was used as a fine aggregate, and its chemical composition was also determined in accordance with ASTM C618 because it can be used as a binder potentially after the grinding process (Chen et al. 2024).

Table 3.3. Oxide compositions of RFA, CFA, IFA, and RBA

Sample name	Oxide compositions (mass%)*												
	SiO ₂	Al ₂ O ₃	Fe ₂ O ₃	CaO	MgO	SO ₃	K ₂ O	Na ₂ O	TiO ₂	ZnO	P ₂ O ₅	BaO	LOI
RFA	29.2	13.1	2.7	31.4	2.7	2.7	1.9	4.4	3.7	0.3	1.8	0.1	6.2
IFA	13.5	5.5	5.0	44.8	0.5	22.5	0.6	0.2	0.3	-	0.1	-	7.2
CFA	36.7	17.8	5.6	24.3	7.6	1.8	0.4	2.0	1.4	-	1.1	0.5	0.8
RBA	35.6	14.0	4.9	21.7	3.1	1.6	1.1	3.2	2.7	0.4	1.7	0.1	9.9

* Sum of Mn₂O₃, SrO, and Cr₂O₃ in all ashes is below 0.3%.

Table 3.4 represents the major chemical requirements in accordance with ASTM C618. The chemical requirements are closely related to the hydration reactivity of ashes in portland cement. As shown in Table 3.4, only CFA meets all of the chemical requirements of Class C fly ash. All three waste ashes collected, RFA, IFA, and RBA, did not satisfy all ASTM C618 requirements.

Table 3.4. Comparison of chemical compositions of RFA, CFA, IFA, and RBA and ASTM C618 requirements

Chemical requirements (ASTM C618)	Sample name			
	RFA	IFA	CFA (ref.)	RBA
CaO, % (Class C: > 18, Class F: ≤ 18)	31.4	44.8	24.3	21.7
SiO ₂ + Al ₂ O ₃ + Fe ₂ O ₃ , % (> 50)	45.0	24.0	60.1	54.5
SO ₃ , % (< 5)	2.7	22.5	1.8	1.6
LOI, % (< 6)	6.2	7.2	0.8	9.9
Na ₂ Oeq (%Na ₂ O + 0.658 × %K ₂ O)	5.7	0.6	2.3	3.9

In terms of chemical composition, all of the waste ashes studied had a CaO content above 18%, meeting the specification requirement for Class C fly ash. As most commercially available fly ashes from North America have CaO content less than 30% (Thomas, 2007), the CaO content of RFA and IFA was higher than that of general fly ashes. The sum of SiO₂, Al₂O₃, and Fe₂O₃ content in RFA, IFA, and RBA was lower than that in CFA, although RBA satisfied the requirement above 50%. The low sum of SiO₂, Al₂O₃, and Fe₂O₃ content may represent the low pozzolanic reactivity of the fly ashes.

The SO₃ content of IFA was much higher than the requirement of below 5%, but on the other hand, the SO₃ content of RFA and RBA satisfied the requirement. The higher sulfate content in IFA was attributed to the use of limestone to reduce the emission of sulfur dioxide in the ISU fluidized bed boilers. In many cases, calcium oxides and anhydrite are usually produced because of the use of limestone in a fluidized bed boiler (Nguyen et al. 2015, Ohenoja et al. 2020).

The LOI of RFA, IFA, and RBA was higher than ASTM C618 requirement below 6%. Although LOI can be an index of how much air entraining agent can be absorbed by ashes (mostly unburnt carbon), it does not necessarily indicate unburnt carbon. The LOI value is often overestimated due to the decomposition of calcium carbonate and other hydrates.

For sodium oxide equivalent (Na_2Oeq), RFA and RBA showed a higher content than CFA, but a negligible content of sodium oxide equivalent was detected in IFA. In the past, Na_2Oeq was usually limited to 0.6% in portland cement due to the possibility of alkali-silica reaction. However, it became obvious that alkali loading is critical to estimate the risk, and therefore only the Na_2Oeq of the cement fraction of the cement composite is included in the calculation of alkali loading in accordance with ASTM C1778. It is expected that the replacement of cement with the ashes could reduce alkali loading.

In addition, ZnO and P_2O_5 were detected in RFA and RBA, which can affect cement hydration as retarders (Tan et al. 2017). Therefore, the refuse-derived fuel ashes RFA and RBA needed to be used carefully because of the higher ZnO and P_2O_5 contents compared to the other ashes.

3.2.5 X-ray Diffraction Test Results

X-ray diffraction (XRD) was conducted on a Rigaku SmartLab using $\text{Cu K}\alpha$ radiation at 40 kV and 44 mA, 2-theta degree of 5° to 65° , and a step width of 0.02° at 0.32 s per step. The diffraction pattern was analyzed using the open-source software Profex to determine crystalline phases in the ashes.

Figure 3.7 shows the XRD patterns of RFA, IFA, CFA, and RBA with highlights of XRD patterns indicating major crystalline phases. Because it is a qualitative analysis, only crystalline phases are discussed in these results, supporting the oxide compositions in Table 3.3. The major crystalline phases of RFA were calcite, quartz, anhydrite, NaCl , metallic Al, CaO , and other different calcium (alumino) silicate minerals. In IFA, anhydrite, quartz, CaO , and hematite were observed. In CFA, quartz, anhydrite, periclase, merwinite, and other different calcium (alumino) silicate minerals were observed. In RBA, calcite, quartz, ettringite, periclase, gehlenite, and other different calcium (alumino) silicate minerals were observed.

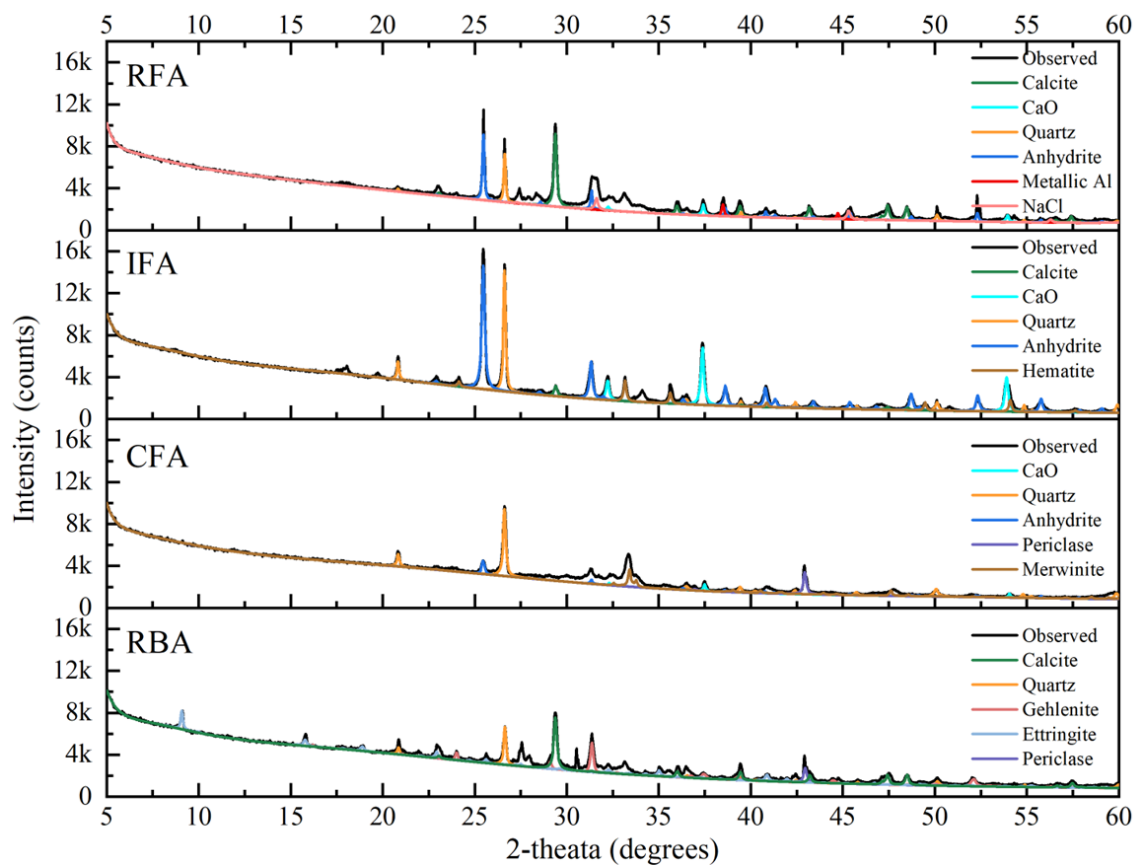


Figure 3.7. X-ray diffraction results of RFA, IFA, CFA, and RBA

Compared to the conventional CFA, RFA and IFA clearly have more anhydrite, displaying higher sulfate content. However, the low sulfate content in the oxide composition of RFA is probably due to a relatively higher amount of amorphous content even though the noticeable anhydrite peak is observed. Notably, a noticeable pattern of CaO was observed in IFA, instead of a calcite pattern, which is clearly observed in RFA. The higher $\text{Na}_2\text{O}_{\text{eq}}$ in RFA is attributed to mostly sodium chloride, of which a pattern is observed in the XRD result. In particular, the metallic Al is observed in the XRD patterns of RFA.

In the XRD patterns of RBA, ettringite is observed instead of anhydrite. This is probably because RBA was stored in the ash pond for a few days, resulting in hydration reactions of anhydrite and other calcium (alumino)silicate minerals.

3.2.6 Thermogravimetric Analysis Results

Thermogravimetric analysis (TGA) was conducted using a TGA 5500 thermal analyzer (TA Instruments). The sample of 10 ± 0.5 mg was heated over the temperature range of 40°C to 990°C at a rate of $20^\circ\text{C}/\text{minute}$ under a nitrogen purge of $20 \text{ mL}/\text{minute}$. Figure 3.8(a) shows the weight change over the temperature range. The derivative weight loss of the raw ashes during heating to 990°C is shown in Figure 3.8(b).

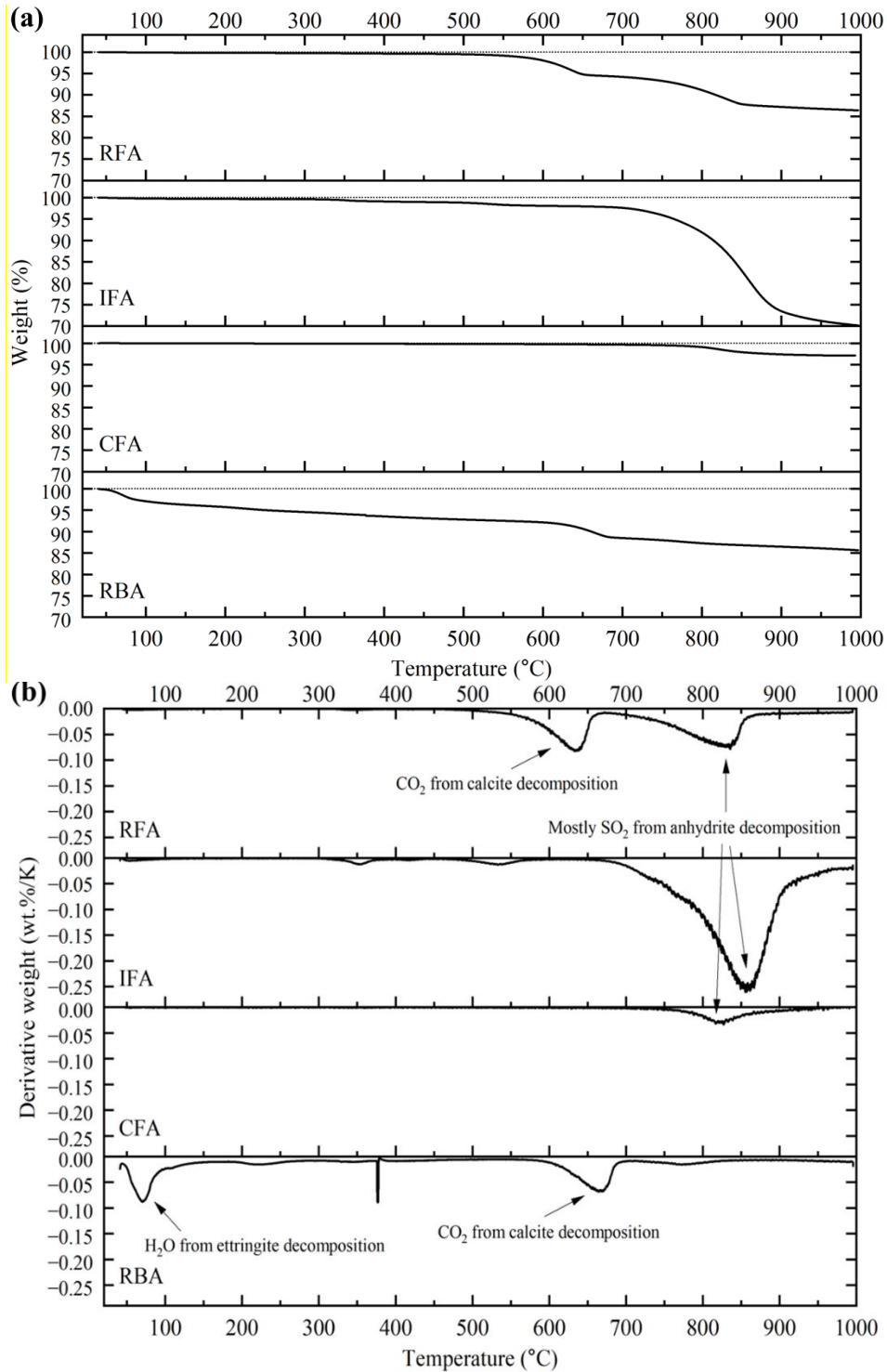


Figure 3.8. Thermogravimetric test results: (a) weight change and (b) derivative weight loss of RFA, IFA, CFA, and RBA

With reference to the above XRD results, the noticeable thermal decomposition in the ashes was mostly from the following minerals: calcite, anhydrite, and ettringite. Calcite in refuse-derived ashes can be decomposed in the slightly lower temperature range of 500°C to 700°C in the

presence of chlorides (Wieczorek-Ciurowa et al. 1980, Ebert et al. 2020). Over 700°C, the mass loss is attributed to the release of SO₂ gas from sulfate compounds such as anhydrite (Zheng et al. 2011, Ebert et al. 2020). The evaporation of water below 100°C in RBA is due to the decomposition of ettringite (Gartner et al. 2011). The size of mass loss corresponding to each mineral correlates with the intensity of each mineral in the XRD results in Figure 3.7.

Therefore, the higher LOI values of RFA, IFA, and RBA in Table 3.4 are attributed to the decomposition of mostly calcite and ettringite in addition to the slight decomposition of sulfate compounds.

3.3 Summary of the Physiochemical Properties of RFA, IFA, CFA, and RBA

The following properties of RFA, IFA, CFA, and RBA were investigated in Chapter 3: specific gravity, absorption/moisture content, particle size distribution, shape/surface morphology, oxide composition, crystalline phase composition, and thermal stability and loss on ignition. The conventional Class C fly ash, CFA, was used as a reference fly ash for comparison with RFA and IFA, which were different from the conventional fly ashes. Through sieving on the ash pond site, the collected bottom ash satisfied the ASTM gradation specification for fine aggregates.

- The specific gravity of RFA (2.09) and IFA (2.16) was similar to that of CFA (2.13), and the moisture content of RFA and IFA satisfied the standard of below 3%. RBA had a lower specific gravity of 2.23 and a higher absorption of 8.85% compared to the general river sand.
- The median particle sizes of RFA (70 µm) and IFA (60 µm) were larger than that of CFA (16 µm). Their fineness values did not satisfy ASTM C618 requirement.
- The morphologies of RFA and IFA displayed mostly irregularly shaped particles compared to CFA. The particle shape of RBA was similar to that of RFA, but there were rod-like crystals on the surface, which were ettringite.
- RFA showed a lower SiO₂ + Al₂O₃ + Fe₂O₃ content of less than 50% and a higher alkali content compared to CFA. IFA displayed a sulfate content of above 20% and a lower SiO₂ + Al₂O₃ + Fe₂O₃ content of less than 25%. Based on the XRD results, relatively higher amounts of calcium carbonate and calcium sulfate in the ashes were responsible for this result. The crystalline phases of RFA were mostly composed of calcite, quartz, and anhydrite. On the other hand, IFA displayed the crystalline phases of anhydrite, quartz, and calcium oxide. The major crystalline phase of CFA was quartz. RBA showed major crystalline phases of ettringite, quartz, gehlenite, and calcite.
- The thermal stability of the ashes was related to the presence of calcite, anhydrite, and ettringite minerals, leading to higher LOI values in RFA, IFA, and RBA.

4. OPTIMIZATION OF CARBON TREATMENT PROCEDURE

In the previous chapter (Chapter 3), the carbon treatment method for the waste ashes and the optimal treatment conditions were presented. Generally, the carbonation reaction of cementitious materials in air depends on the relative humidity and moisture content of the treated ashes because chemical dissolution and precipitation are required for carbonation (Steiner et al. 2020). The precipitation reaction of carbon dioxide during the carbonation process refers to carbon sequestration. Hence, the carbon treatment initiates the carbon sequestration process, and it is expected to reduce the detrimental effects of the waste ashes on portland cement-based composites by stabilizing chemical compounds.

4.1 Experimental Setup for the Carbon Treatment

Figure 4.1 shows the experimental setup for the carbon treatment of the waste ashes. Pure CO₂ is introduced into the airtight pressure pot, and the pressure inside the pot is maintained at a certain pressure. If there is a pressure drop in the pot due to carbon sequestration, CO₂ is introduced automatically according to the set value of the pressure regulator. During the carbon treatment, temperature and relative humidity in the pot were recorded in real time using a portable combined temperature and humidity sensor.

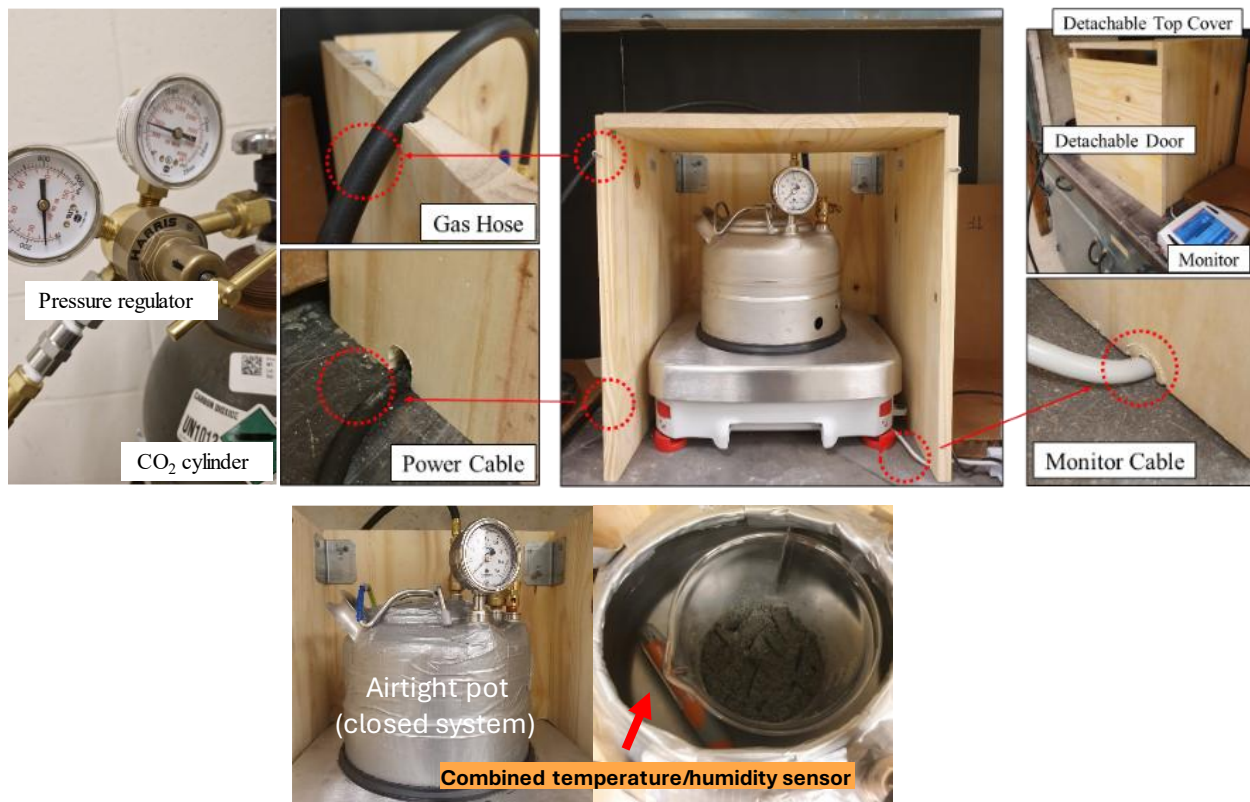


Figure 4.1. Experimental setup for the carbon treatment

At the beginning of the test, a weight change in the pot resulting from carbon sequestration was expected, and therefore the weight change was recorded using a balance, along with serial port data collection (SPDC) software connected to a desktop, as shown in Figure 4.1. However, there was weight change fluctuation in several blank tests, and it was found that the margin of error was critical to measure reliable weight change results in carbon sequestration. For example, if the waste ashes had a CO₂ uptake of less than 3 wt%, the weight gain of the sample was only about 3 g when 100 g of ash was used in the test. The preliminary results showed that the margin of error was approximately ± 2.5 g for the weight change, as shown in Figure 4.2. Therefore, recording weight change was not selected as a carbonation index because only the 200 g ash was used in the glass beaker, resulting in a large deviation in weight change. The sample was limited to 200 g to reduce the thickness of the sample in the beaker and ensure homogeneity in the carbon treatment.

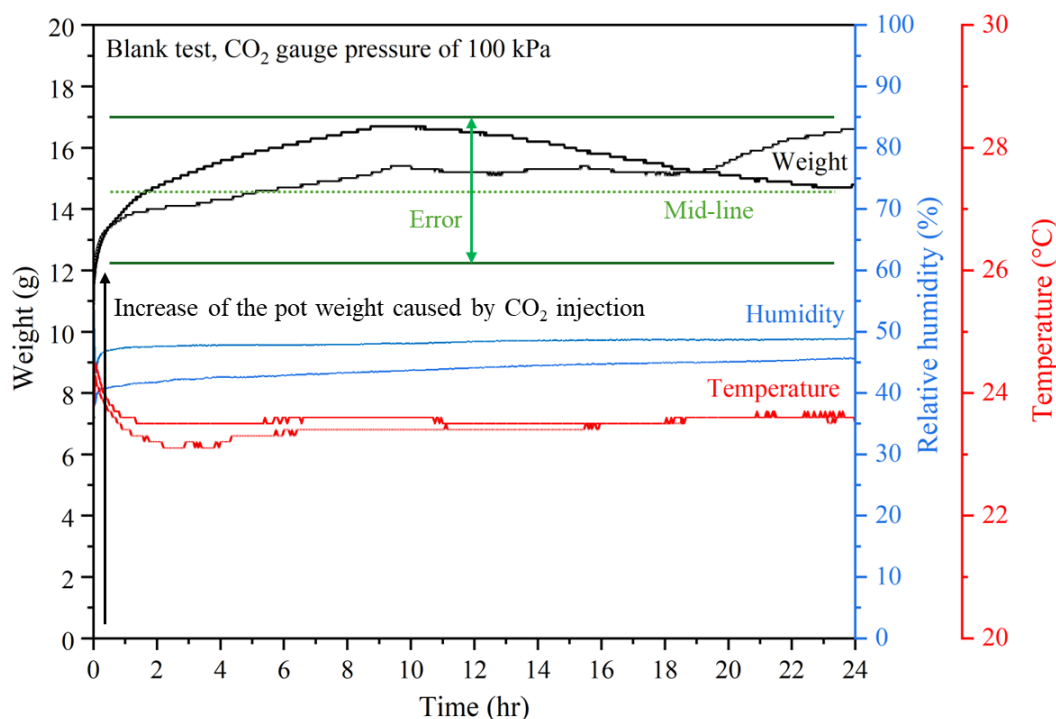


Figure 4.2. Results of the trial tests in the empty pressure pot

Instead of weight change, temperature was measured in real time, as shown in Figure 4.3. An RFA sample with a moisture content of 20% was used to determine the temperature change during the carbon treatment under a CO₂ pressure of 100 kPa. When CO₂ was introduced into the pressure pot, there was a rapid increase in temperature (peaking between 0 and 4 hours) in the pot. This was due to the exothermic carbonation reaction. Therefore, the maximum temperature at the peak in the carbon treatment was proposed as a carbonation index for determining an optimal condition thereafter.

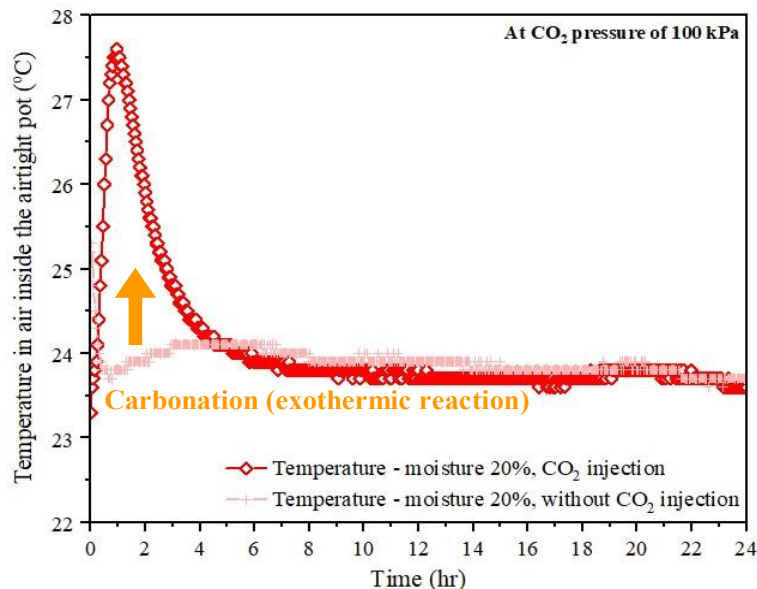


Figure 4.3. Temperature changes inside the airtight pot during the carbon treatment for RFA

4.2 Sample Preparation for Carbon Treatment

RFA, IFA, CFA, and RBA with different moisture contents were carbon treated under different CO_2 pressures to determine the optimal conditions for carbon sequestration.

A sample of 200 g, corresponding to dry weight, was prepared in a beaker. Then, a specific amount of water was added to the sample to achieve a certain moisture content (0% to 70%), and the sample and the water were mixed together for 2 to 3 minutes. After they were homogeneously mixed, the sample in the beaker and the combined temperature and humidity sensor were placed in the airtight pressure pot. Finally, after closing the lid of the pressure pot, pure CO_2 gas was introduced at a rate corresponding to a target pressure (100 and 200 kPa; additionally, 500 kPa was tested only for RBA) for 24 hours. After the carbon treatment, the treated sample was dried at 40°C to reduce unexpected loss and change of carbonates and hydrates. The dry sample was used for TGA to quantify the carbon sequestration.

4.3 Temperature Changes during Carbon Treatment

4.3.1 Treatment of RFA

Figure 4.4 shows the temperature changes during the carbon treatment for RFA under different conditions. When it comes to peak temperature, the carbonation reaction was most intense at a moisture content of 40%, followed by a moisture content of 20%, regardless of the CO_2 pressures in the carbon treatment for RFA. Higher CO_2 pressure was not significant in terms of improving the exothermic reaction related to the carbon sequestration. Table 4.1 shows the maximum temperatures at the peaks, and the trendline of the temperatures depending on the

moisture content is shown in Figure 4.5. The trendline indicates that the carbonation reaction was highest near a moisture content of 30%. In terms of CO₂ pressure, the maximum temperature slightly decreased at the higher pressure.

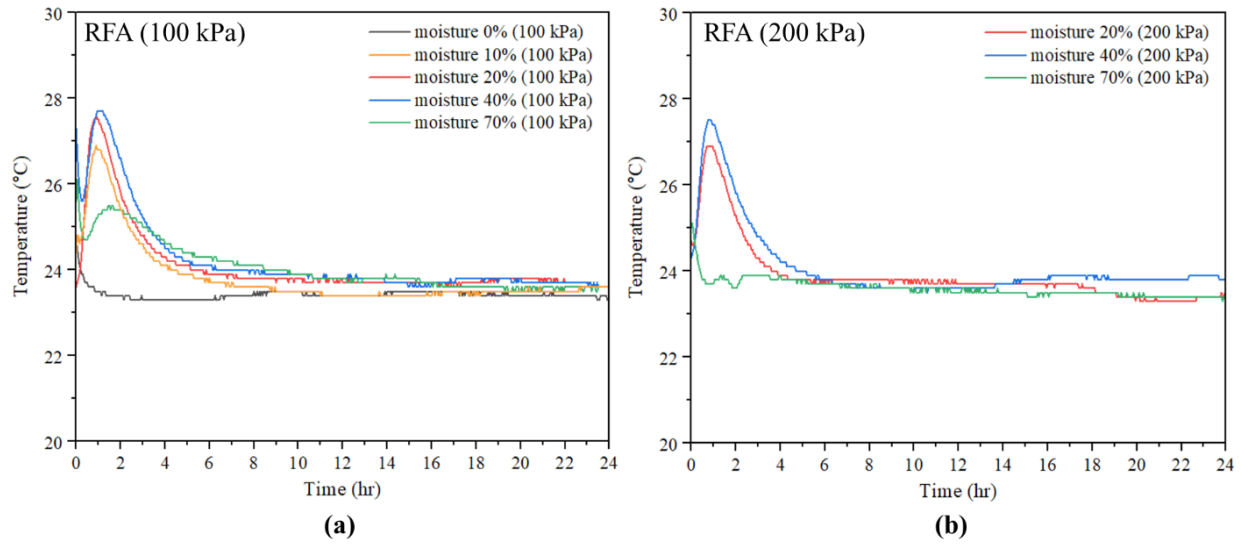


Figure 4.4. Temperature changes during the carbon treatment for RFA under different conditions: CO₂ pressures of (a) 100 kPa and (b) 200 kPa

Table 4.1. Maximum temperature at the peak during the carbon treatment for RFA

CO ₂ pressure	Maximum temperature (°C) in the carbon treatment for RFA				
	Moisture 0%	Moisture 10%	Moisture 20%	Moisture 40%	Moisture 70%
100 kPa	No peak	26.9	27.6	27.8	25.5
200 kPa	No peak	-	26.9	27.6	23.8

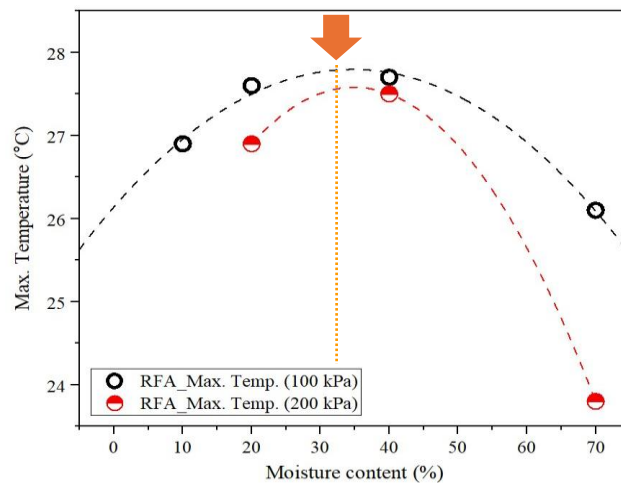


Figure 4.5. Trendline of the maximum temperature depending on the moisture content during the carbon treatment for RFA

4.3.2 Treatment of IFA

Figure 4.6 shows the temperature changes during the carbon treatment of IFA under different conditions. The maximum temperature during the carbon treatment was approximately 40°C. It was much higher than the maximum temperature (26°C to 28°C) during the carbon treatment for RFA. The exothermic reaction was very intense during the carbon treatment for IFA. Higher CO₂ pressure was not significant in terms of improving the carbonation, as in the carbon treatment for RFA.

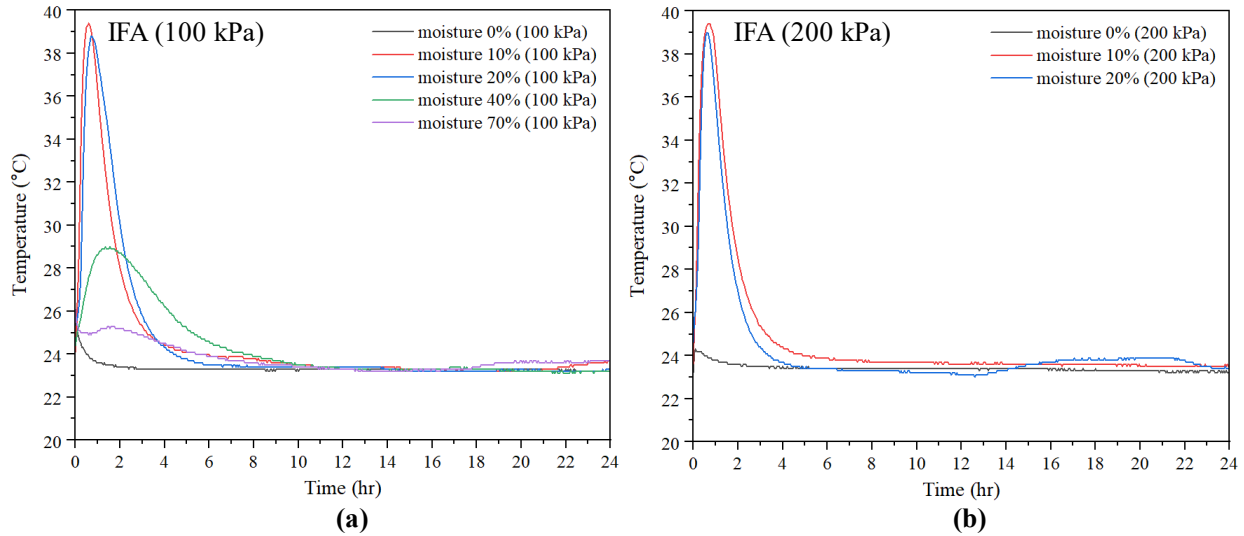


Figure 4.6. Temperature changes during the carbon treatment for IFA under different moisture conditions: CO₂ pressures of (a) 100 kPa and (b) 200 kPa

Table 4.2 shows the maximum temperature during the carbon treatment for IFA with different moisture contents. Unlike the carbon treatment for RFA, the carbon treatment for IFA with a moisture content of 10% to 20% showed considerable exothermic reactions. Thus, significant carbon sequestration is expected in the carbon treatment for IFA.

Table 4.2. Maximum temperature at the peak during the carbon treatment for IFA

CO ₂ pressure	Maximum temperature (°C) in the carbon treatment for IFA				
	Moisture 0%	Moisture 10%	Moisture 20%	Moisture 40%	Moisture 70%
100 kPa	No peak	39.4	38.8	29.0	26.1
200 kPa	No peak	39.4	39.0	-	-

4.3.3 Treatment of CFA

Figure 4.7 shows the temperature changes during the carbon treatment for CFA under different conditions. Table 4.3 shows the maximum temperature during the carbon treatment for CFA with

different moisture contents. During the carbon treatment for CFA, significantly fewer exothermic reactions were observed when compared to the reactions in the carbon treatment for RFA and IFA. Like the carbon treatment for IFA, a moisture content of approximately 10% was favorable for improving carbonation even though the carbonation of CFA with different moisture contents was not as significant as the carbonation of RFA and IFA.

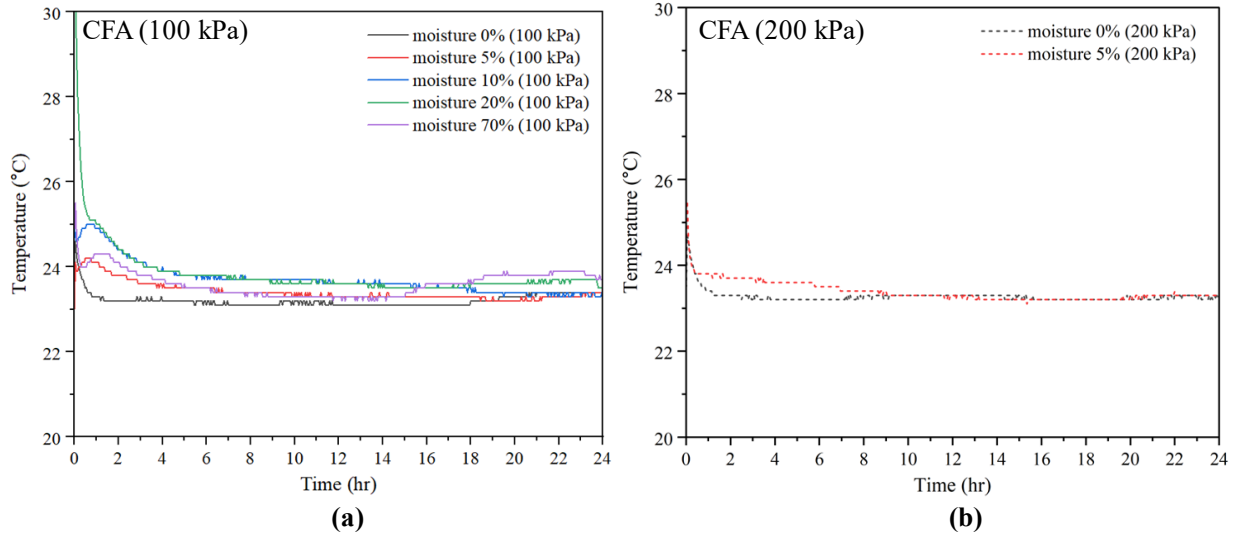


Figure 4.7. Temperature changes during the carbon treatment for CFA under different moisture conditions: CO₂ pressures of (a) 100 kPa or (b) 200 kPa

Table 4.3. Maximum temperature at the peak during the carbon treatment for CFA

CO ₂ pressure	Maximum temperature (°C) in the carbon treatment for CFA				
	Moisture 0%	Moisture 5%	Moisture 10%	Moisture 20%	Moisture 70%
100 kPa	No peak	24.2	25.0	dropping	24.3
200 kPa	No peak	No peak	-	-	-

4.3.4 Treatment of RBA

Unlike the fly ashes (RFA, IFA, and CFA) with an initial moisture content near 0%, the as-received RBA had a moisture content of 18.01% (approximately 20%). Thus, no additional water was added for the carbon treatment of RBA with a moisture content of 20%. However, to have an RBA sample with a moisture content of 70%, additional water was added, and thus a wet sample was obtained. In this project, wet carbonation was conducted for RBA at a CO₂ pressure of 500 kPa only in view of improving the solubility of Ca ions in pore space (Gao et al. 2024). The wet carbonation was conducted at a water-to-solid ratio of 2 (moisture content of 200%) as shown in Figure 4.8.

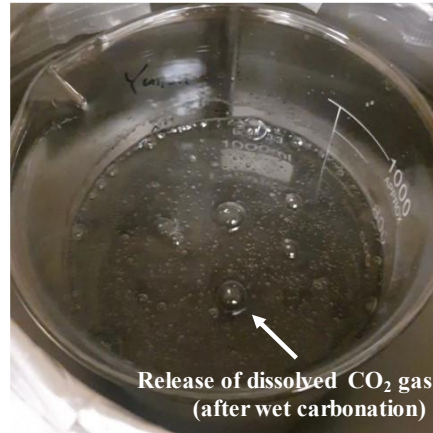


Figure 4.8. Setup of the wet carbonation for RBA

Figure 4.9 shows the temperature changes during the carbon treatment for RBA under different conditions. The maximum temperatures observed in the test are in Table 4.4. No significant peak related to exothermic reaction was observed in the carbon treatment for RBA, regardless of pressure and moisture content. The temperature 5 to 10 minutes after introducing CO_2 showed relatively higher values and dropped over 1 to 3 hours. It seemed that the carbonation of RBA occurred rapidly, briefly, and mostly on the surface. This may result in less of an increase in heat.

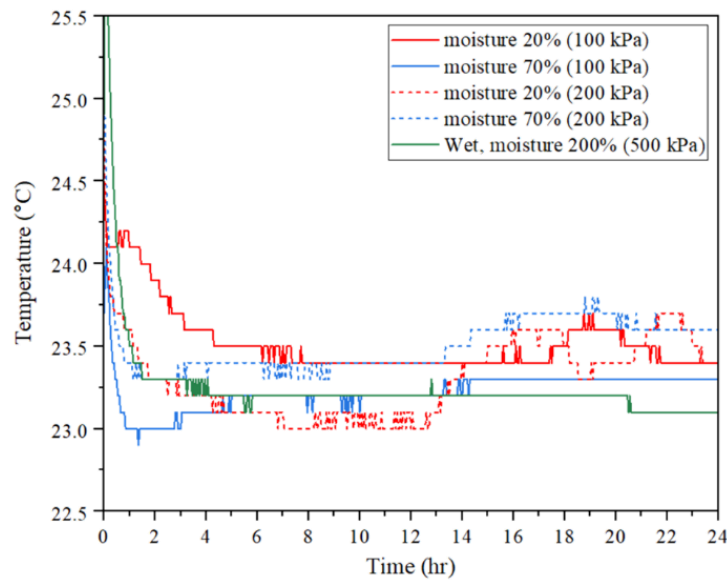


Figure 4.9. Temperature changes during the carbon treatment for RBA under different moisture conditions: CO_2 pressures of 100 kPa, 200 kPa, or 500 kPa

Table 4.4. Maximum temperature at the peak during the carbon treatment for RBA

CO ₂ pressure	Maximum temperature (°C) in the carbon treatment for RBA		
	Moisture 20%	Moisture 70%	Wet carbonation
100 kPa	24.2	Dropping	-
200 kPa	dropping	Dropping	-
500 kPa	-	-	Dropping

4.4 Summary of Exothermic Reactions in the Ashes Studied

Figure 4.10 shows the maximum temperature during the carbon treatment under different moisture contents and CO₂ pressures for all ashes studied. The figure once again reveals that the maximum temperatures released from carbon treatment were different among the ashes studied. While there is little difference in the pressures applied (100 kPa or 200 kPa), the optimal moisture content for carbon treatment is 20% to 40% for RFA, 10% to 20% for IFA, around 10% for CFA, and 20% for RBA.

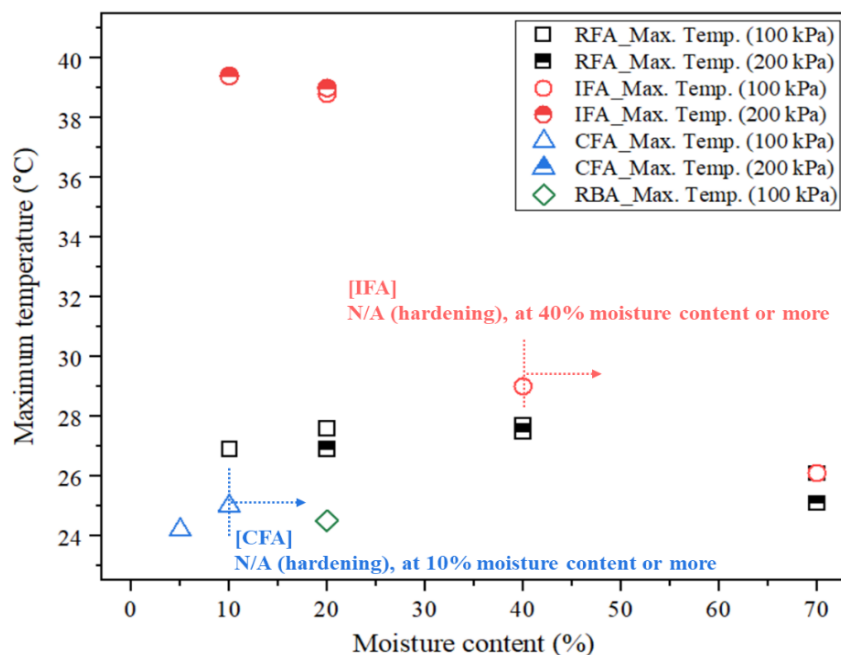


Figure 4.10. Maximum temperature in the carbon treatment under different moisture contents and CO₂ pressures for the ashes: RFA, IFA, CFA, and RBA

It was observed that at a high moisture content (>30%), some reactive fly ashes, like IFA and CFA, may start to harden during carbon treatment due to their hydration and carbonation reactions (Figure 4.11). A limit on the maximum moisture content should be set for each ash to prevent it from hardening during the carbon treatment. CFA, a conventional Class C fly ash, is highly reactive in water, requiring its carbon treatment under low moisture conditions. RFA is the least reactive of all the fly ashes studied, allowing its carbon treatment under a moisture

content of up to 70%. The exothermic reaction was vigorous in IFA with 10% to 20% moisture content because it had a relatively high amount of lime, which is highly reactive with water and subsequently reacts with carbonate easily. However, the moisture content in IFA needs to be controlled carefully because of ash hardening. Therefore, the moisture content should be kept within a range of 10% to 20% during the carbon treatment of IFA.

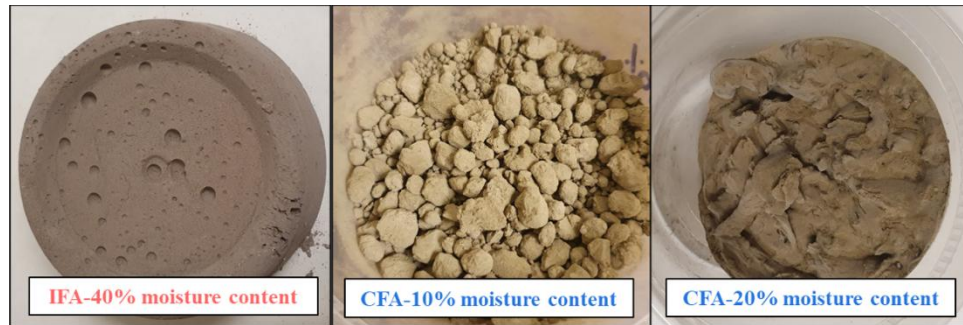


Figure 4.11. Hardened samples after carbon treatment and drying at 40°C for 24 hours

5. CARBON SEQUESTRATION CAPACITY AND EFFECTS OF CARBON TREATMENT ON PROPERTIES OF WASTE ASHES

5.1 Measurement of Carbon Sequestration Capacity

The carbon sequestration capacity of the ashes studied was quantified using TGA. To conduct the quantification, a carbon-treated sample was first dried at 40°C for 24 hours and then gently ground to deagglomerate particles and sieved using #200 (150 μm) mesh. TGA was performed on the sample using a TGA 5500 thermal analyzer (TA Instruments). The sample of 10 ± 0.5 mg was heated over the temperature range of 40°C to 1000°C at a rate of 20°C/minute under a nitrogen purge of 20 mL/minute.

The weight loss of the sample associated with CO_2 release in the obtained TGA curves was quantified using the integration of the peak area (tangential method) of crystalline calcium carbonate in the derivative weight loss (DTG), as shown in Figure 5.1. Here, the CO_2 loss from amorphous CaCO_3 is conservatively ignored because of overlaps between hydrates and carbonates in the lower temperature ranges below 550°C. Usually, CaCO_3 decomposes in the temperature ranges of 600°C to 800°C (Goto et al. 1995). However, the lower temperature ranges (approximately 500°C to 700°C) of the CaCO_3 decomposition in the ashes were observed because of the existence of alkali chlorides (Wieczorek-Ciurowa et al. 1980, Ebert et al. 2019).

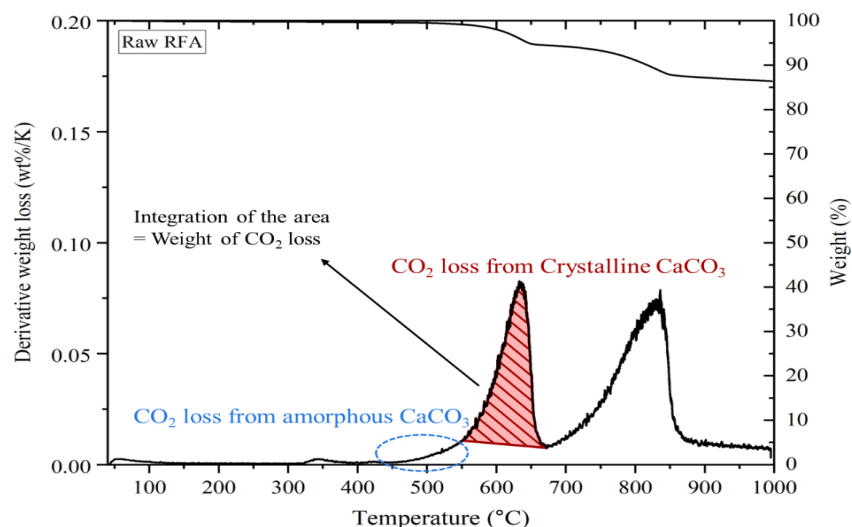


Figure 5.1. Tangential method to quantify sequestered carbon content in TGA

The quantified weight loss due to CO_2 release from the TGA curve was normalized to the anhydrous weight (i.e., final weight loss in TGA). Because there was only water or CO_2 addition during carbon treatment and water evaporation during the drying process, no loss or addition of any other chemicals was expected in the carbon-treated ashes. Therefore, it is assumed that the anhydrous chemical compositions of the carbon-treated ashes are the same as in the anhydrous raw ash. The change in weight of CO_2 in the anhydrous carbon-treated ash was estimated relative to the weight of CO_2 in the anhydrous raw ash.

5.2 Carbon Sequestration Capacity Measured by Thermogravimetry Analysis

5.2.1 Capacity of RFA

Figure 5.2 shows the TGA results of the carbon-treated RFA at different moisture contents under CO₂ pressures of 100 kPa and 200 kPa. Table 5.1 shows the normalized sequestered carbon content in the carbon-treated RFA. The initial CO₂ content in the raw anhydrous RFA (wt%) was 4.12%, and the change in the sequestered CO₂ content of the carbon-treated RFA was determined. The carbon sequestration was highest under 20% moisture content and 200 kPa. The results follow the trend of maximum temperatures in the carbon treatment (Figure 4.10). Especially at the moisture content of 70%, excess water on the particles seems to impede the CO₂ gas diffusion and reduce the carbonation. However, anhydrite was largely consumed and transformed to ettringite at 70% moisture content (Appendix A, Figure A1).

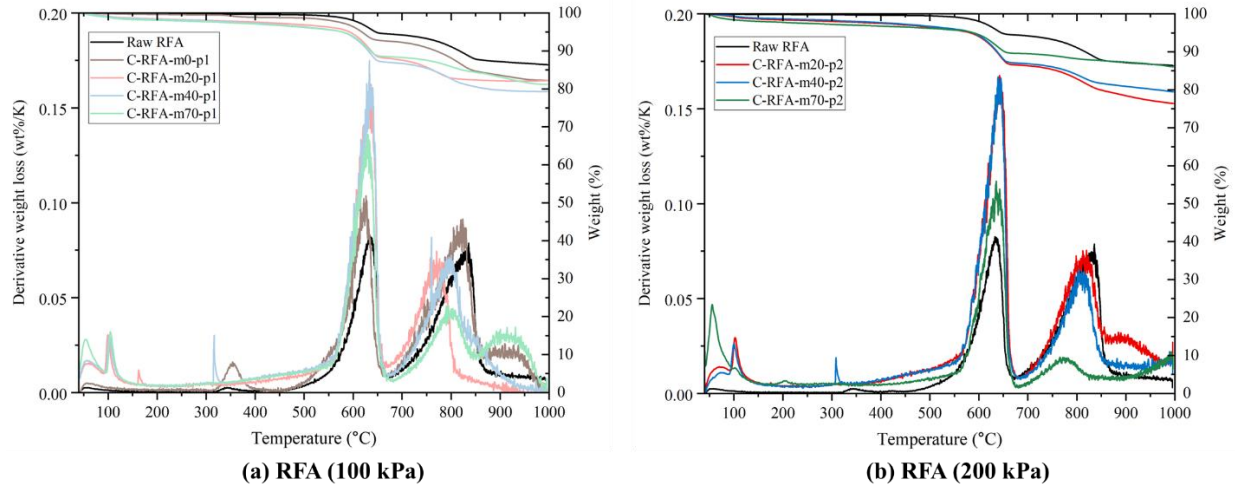


Figure 5.2. TGA results of the carbon-treated RFA

Table 5.1. Sequestered CO₂ content in the carbon-treated RFA

CO ₂ pressure	Sequestered CO ₂ content (and final CO ₂ content) (wt% of the anhydrous RFA*)			
	Moisture 0%	Moisture 20%	Moisture 40%	Moisture 70%
100 kPa	+ 0.18 (4.30)	+ 3.73 (7.85)	+ 4.71 (8.83)	+ 3.12 (7.24)
200 kPa	-	+ 5.70 (9.82)	+ 5.16 (9.28)	+ 2.02 (6.14)

* The initial sequestered carbon content in the raw RFA (wt% of the anhydrous RFA): 4.12%

5.2.2 Capacity of IFA

Figure 5.3 shows the TGA results of the carbon-treated IFA at different moisture contents under CO₂ pressures of 100 kPa and 200 kPa. Table 5.2 shows the normalized sequestered carbon content in the carbon-treated IFA. The initial CO₂ content in the raw anhydrous IFA (wt%) was 0.74%, and the change in the sequestered CO₂ content of the carbon-treated IFA was

determined. The carbon sequestration was highest at 10% moisture content and under 200 kPa. The lower CO₂ pressure of 100 kPa was less effective for the carbon sequestration of IFA. Because of the high quicklime content in IFA, its capacity for carbon sequestration was higher than that of RFA.

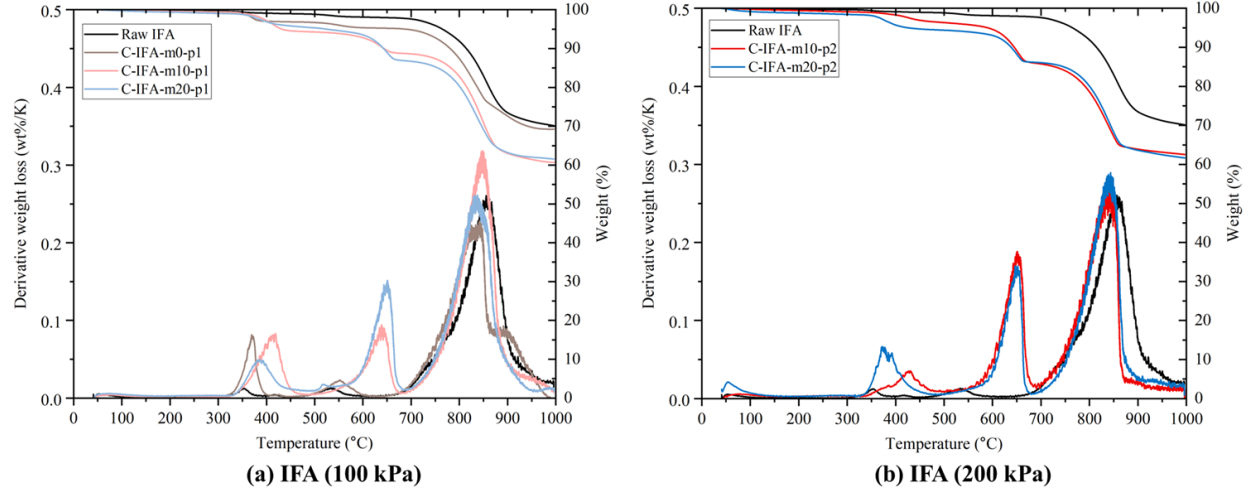


Figure 5.3. TGA results of the carbon-treated IFA

Table 5.2. Sequestered CO₂ content in the carbon-treated IFA

CO ₂ pressure	The sequestered CO ₂ content (and final CO ₂ content) (wt% of the anhydrous IFA*)		
	Moisture 0%	Moisture 10%	Moisture 20%
100 kPa	+ 0.93 (1.68)	+ 6.69 (7.44)	+ 9.97 (10.71)
200 kPa	-	+ 12.47 (13.22)	+ 10.05 (11.40)

* The initial sequestered carbon content in the raw IFA (wt% of the anhydrous IFA): 0.74%

5.2.3 Capacity of CFA

Figure 5.4 shows the TGA results of the carbon-treated CFA at a different moisture content under CO₂ pressures of 100 kPa and 200 kPa. Table 5.3 shows the normalized sequestered carbon content in the carbon-treated CFA. The initial CO₂ content in the raw anhydrous CFA (wt%) was less than 0.08%. Negligible carbon sequestration of less than 0.44% was observed in the carbon-treated CFA. Because of the moisture limitations, owing to the hardening problem, the carbonation reaction was restricted in the carbon treatment for CFA. The loss on ignition of the carbon-treated CFA until the final temperature was almost the same as that of the raw CFA. This indicated that the reactions for hydrates and carbonates were restricted.

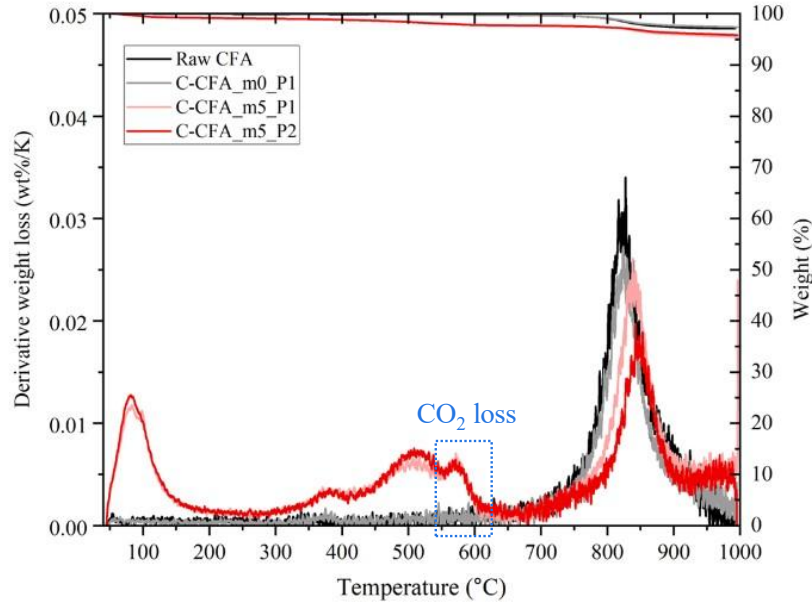


Figure 5.4. TGA results of the carbon-treated CFA

Table 5.3. Sequestered CO₂ content in the carbon-treated CFA

CO ₂ pressure	The sequestered CO ₂ content (and final CO ₂ content) (wt% of the anhydrous CFA*)	
	Moisture 0%	Moisture 5%
100 kPa	+ ~ 0 (< 0.08)	+ < 0.44 (< 0.52)
200 kPa	-	+ < 0.44 (< 0.52)

* The initial sequestered carbon content in the raw CFA (wt% of the anhydrous CFA): < 0.08%

5.2.4 Capacity of RBA

Figure 5.5 shows the TGA results of the carbon-treated RBA at different moisture contents under CO₂ pressures of 100 kPa, 200 kPa, and 500 kPa (wet). Table 5.4 shows the normalized sequestered carbon content in the carbon-treated RBA. The initial CO₂ content in the raw anhydrous RBA (wt%) was 3.43%. The carbon sequestration was effective at 20% moisture content and 100 kPa. The lower moisture content of 20% was generally better than the 70% moisture content for the carbon treatment under a CO₂ pressure of 100 or 200 kPa. A CO₂ pressure of 100 to 200 kPa at the moisture content of 70% was not sufficient for RBA to be carbonated. However, the CO₂ pressure of 500 kPa made for comparable carbonation results in wet conditions. Recently, wet carbonation has been developed to improve the carbonation efficiency of recycled concrete aggregates because it can easily create an undersaturated environment, leading to improvement of the dissolution rate and no limitation on CO₂ diffusion into large solid particles. Therefore, the wet carbonation under the high CO₂ pressure showed a better result, which is comparable to the carbonation under the moisture content of 20% and a CO₂ pressure of 100 or 200 kPa.

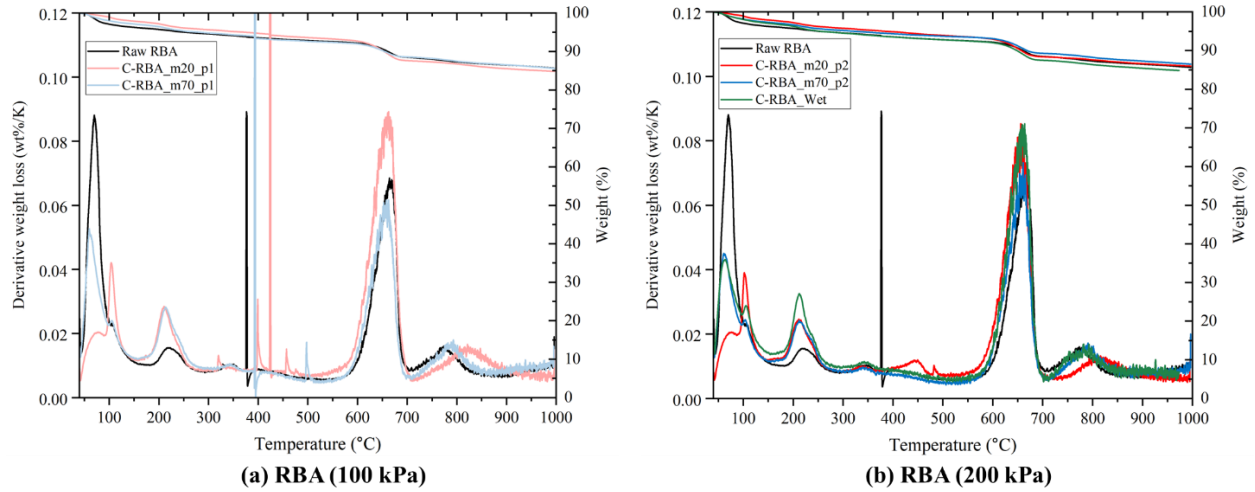


Figure 5.5. TGA results of the carbon-treated RBA

Table 5.4. Sequestered CO₂ content in the carbon-treated RBA

CO ₂ pressure	Sequestered CO ₂ content (and final CO ₂ content) (wt% of the anhydrous RBA*)		
	Moisture 20%	Moisture 70%	Moisture 200% (wet)
100 kPa	+ 2.29 (5.72)	+ ~ 0 (3.35)	-
200 kPa	+ 1.16 (4.59)	+ 0.37 (3.80)	-
500 kPa	-	-	+ 1.21 (4.64)

* The initial sequestered carbon content in the raw RBA (wt% of the anhydrous RBA): 3.43%

5.3 Surface Morphology of the Carbon-Treated Ashes

An SEM analysis was conducted for selected carbon-treated ashes to investigate the change in surface morphology after carbon treatment. The shape and size of calcium carbonate particles after carbonation are dependent on various factors, such as pressure, temperature, humidity, pH, and CO₂ concentration (López-Arce et al. 2011, Oral and Ercan 2018, Lu et al. 2022), leading to various shapes and sizes of calcium carbonate.

Inspect F50 was used under 10 kV accelerating voltage and a working distance of approximately 10 mm.

Figure 5.6 shows the morphology changes of the carbon-treated RFA under a moisture condition of 20% at the different CO₂ pressures of 100 and 200 kPa. Approximately 1 to 5 μm of calcium carbonate particles can be observed on the surface of C-RFA-m20-p1 and C-RFA-m20-p2.

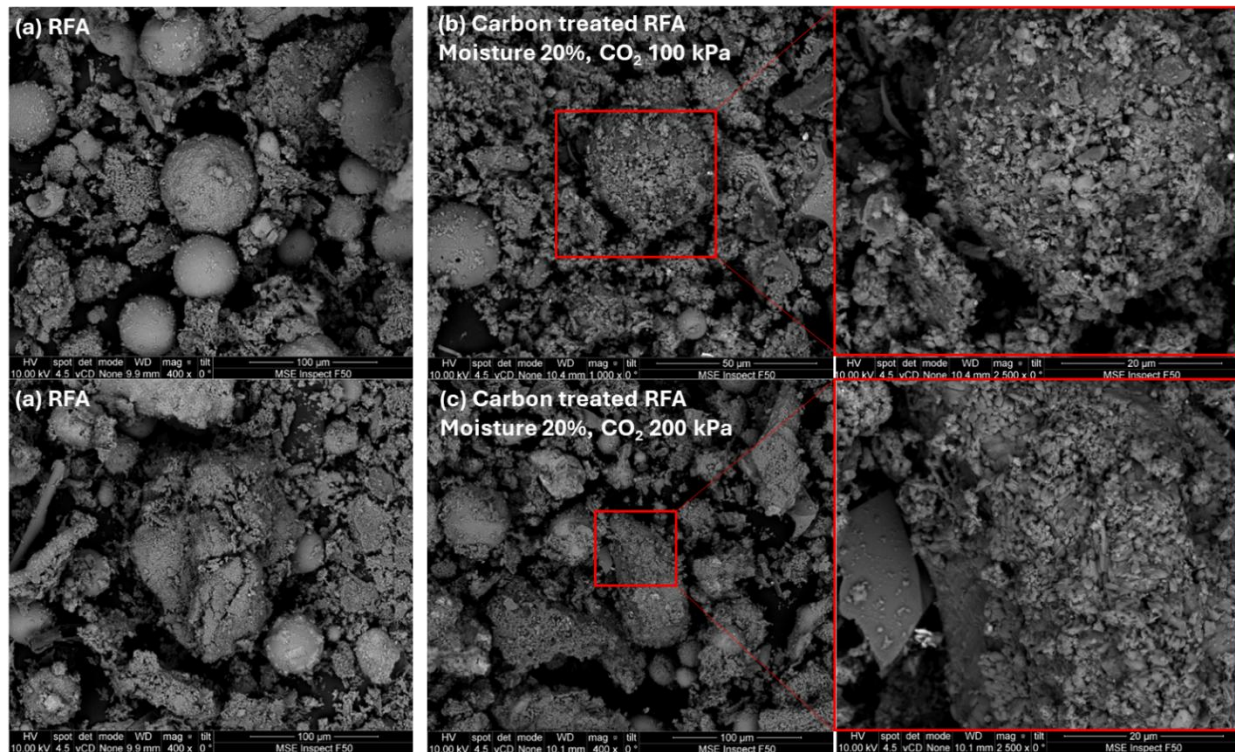


Figure 5.6. Surface morphology of (a) RFA, (b) C-RFA-m20-p1, and (c) C-RFA-m20-p2

Figure 5.7 shows the morphology changes of the carbon-treated IFA under a moisture condition of 20% at the different CO_2 pressures of 100 and 200 kPa. After the carbonation, the surfaces of the C-IFA-m20-p1 and C-IFA-m20-p2 particles became denser due to the production and aggregation of calcium carbonate on the surface.

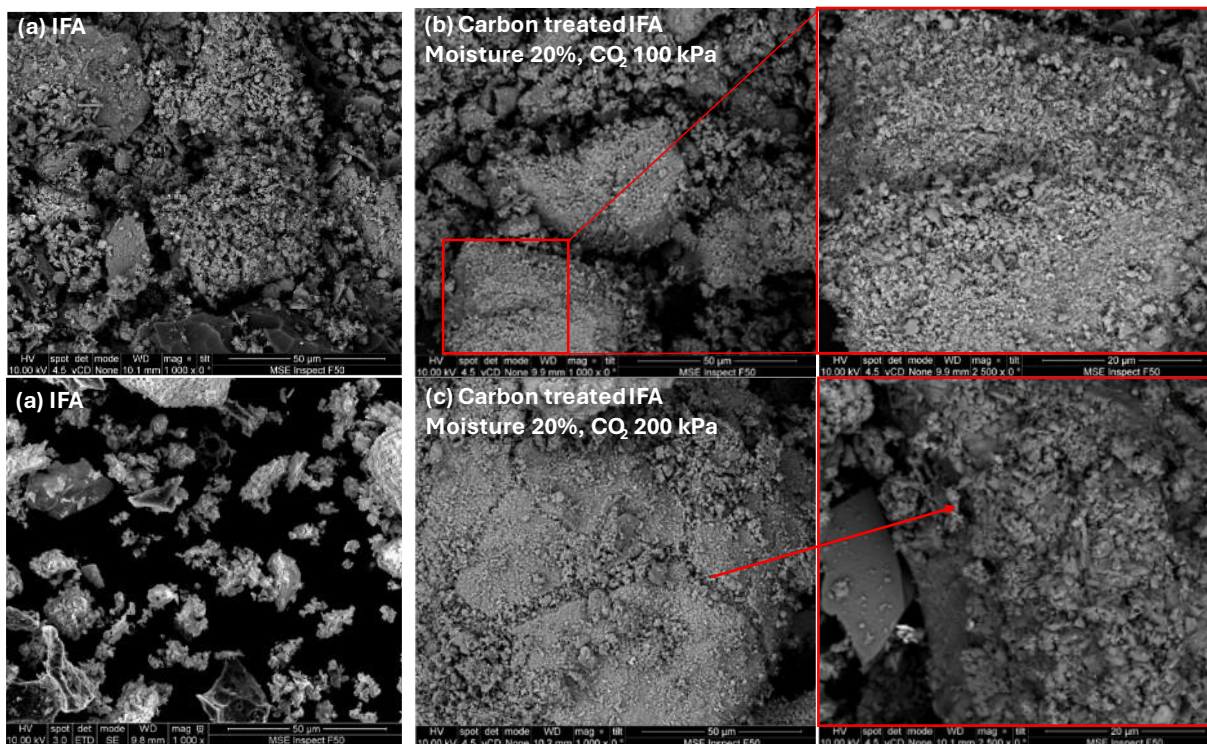


Figure 5.7. Surface morphology of (a) IFA, (b) C-IFA-m20-p1, and (c) C-IFA-m20-p2

Figure 5.8 shows the morphology changes of the carbon-treated CFA under a moisture condition of 5% at the different CO_2 pressures of 100 and 200 kPa. As mentioned in the TGA results, the carbonation reaction was restricted because of the moisture limitation in C-CFA-m5-p1 and C-CFA-m5-p2. Although there was no significant difference in the morphology before and after carbonation, some agglomeration between small particles was observed.

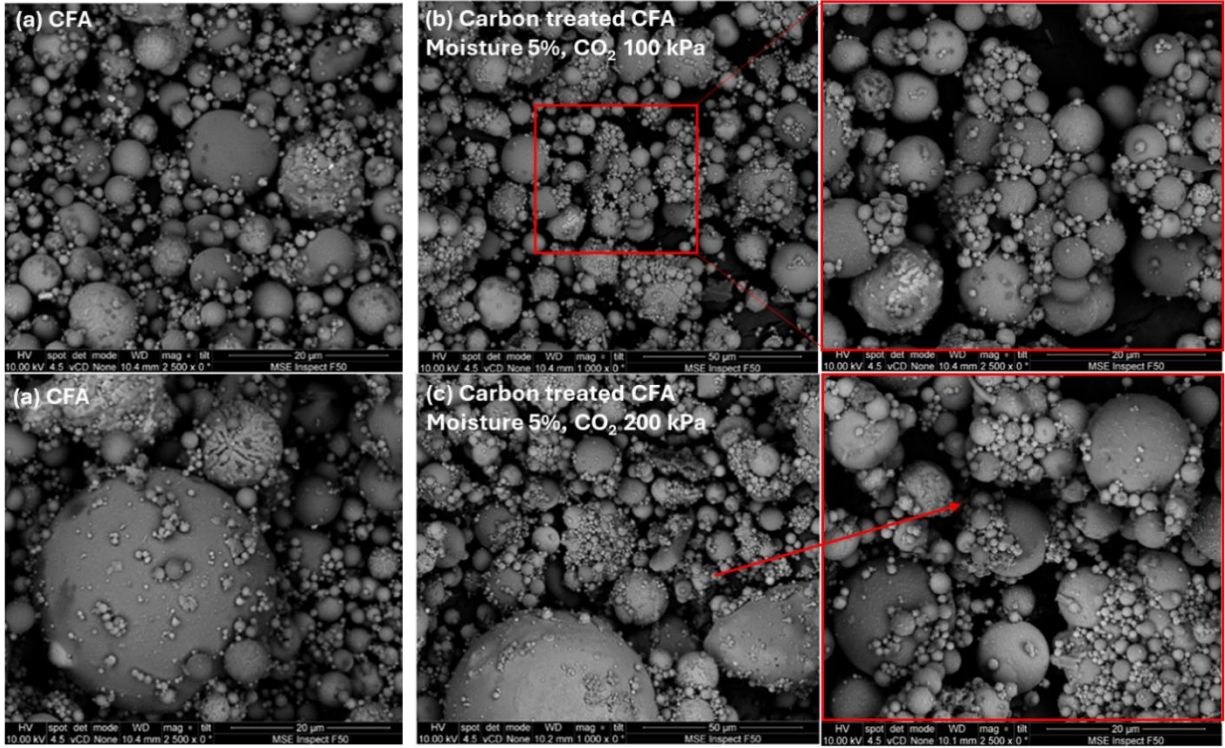


Figure 5.8. Surface morphology of (a) CFA, (b) C-CFA-m5-p1, and (c) C-CFA-m5-p2

Figure 5.9 shows the morphology change of the carbon-treated RBA under different conditions. The ettringite on RBA clearly decomposed on the surface of C-RBA-m20-p1, as also determined in the TGA results, and the irregular type of calcite was produced on the surface. On the other hand, some ettringite rods can still be observed on the surface of C-RBA-m70-p1 and C-RBA-wet. On the surface of C-RBA-m20-p2, the elongated flower-like and smaller calcium carbonate can be observed compared to C-RBA-m20-p1. This is probably due to the pressure effect of excessive carbonate preventing the growth of calcium carbonate crystal (Lu et al. 2022).

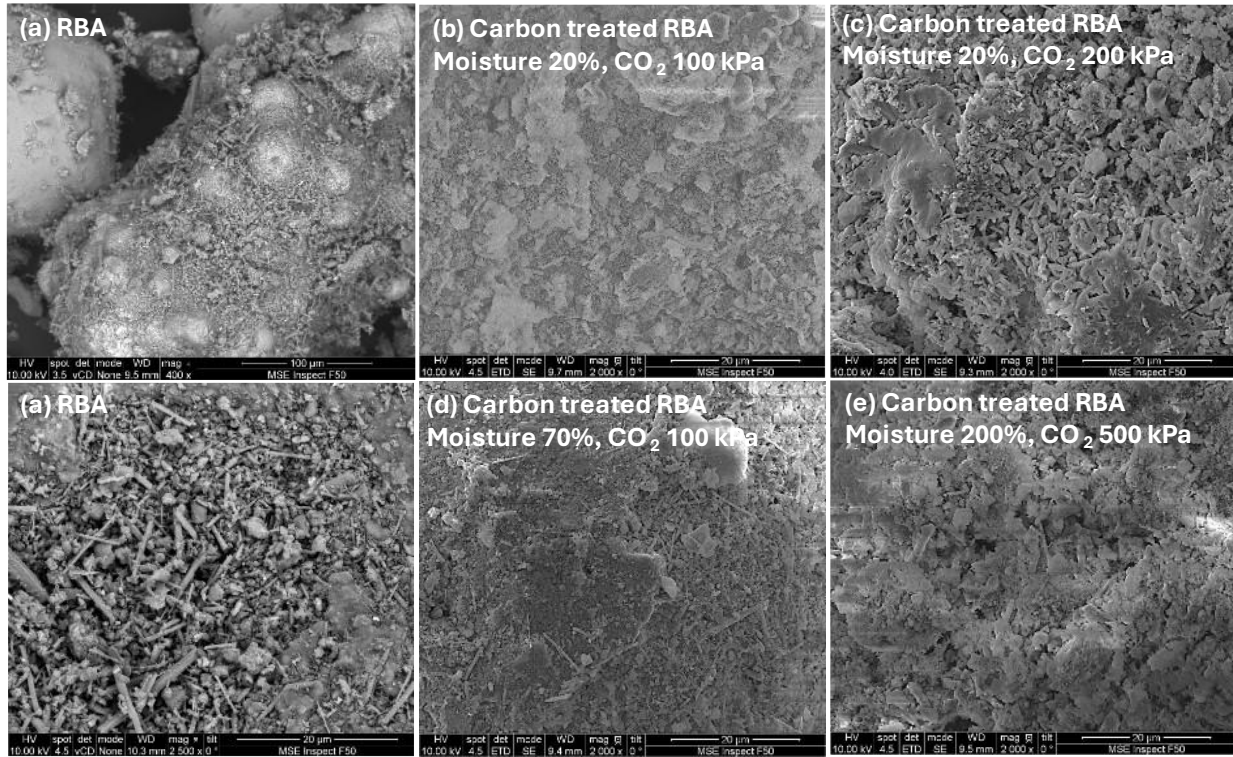


Figure 5.9. Surface morphology of (a) RBA, (b) C-RBA-m20-p1, (c) C-RBA-m20-p2, (d) C-RBA-m70-p1, and (e) C-RBA-wet

5.4 Summary of Carbon Sequestration in the Ashes

Figure 5.10 summarizes the CO₂ uptake in the ashes under different conditions in the carbon treatment. Although the moisture in IFA was limited because of hydration reactions, resulting in hardening, the carbon sequestration was the highest in IFA, followed by RFA, RBA, and CFA. Additionally, the higher CO₂ pressure of 200 kPa lowered the optimal moisture content for carbon sequestration and improved the carbon sequestration. The optimal moisture content for IFA, RFA, and RBA at a CO₂ pressure of 100 kPa was 20%, 40%, and 20%, respectively. In the range of optimal conditions, the amount of CO₂ uptake in IFA, RFA, and RBA was approximately 10, 5, and 2 kg CO₂/kg anhydrous ash, respectively. This carbon treatment for waste ashes will offer additional benefits for reducing embodied carbon when used in concrete. However, the carbon treatment was not effective for the conventional fly ash, CFA.

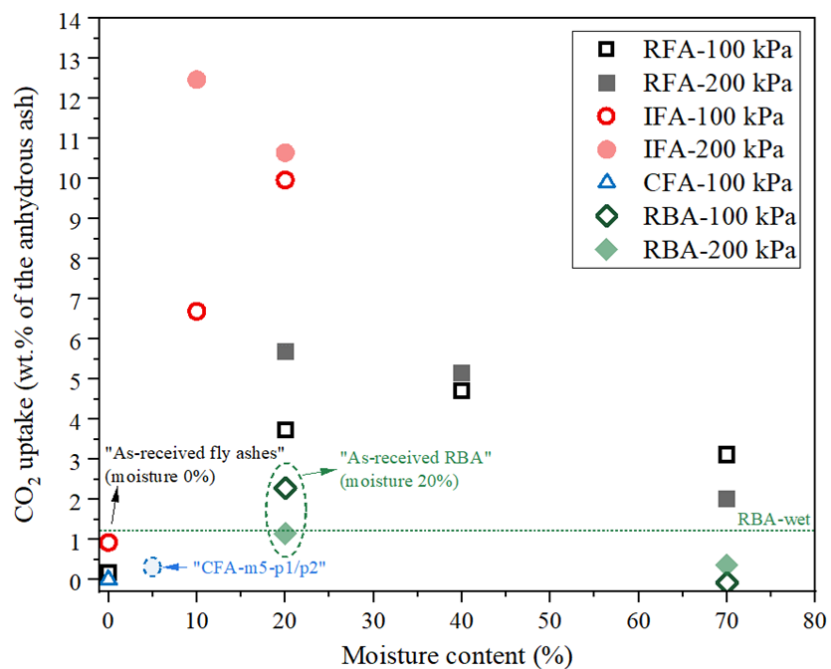


Figure 5.10. Summary of carbon sequestration in RFA, IFA, CFA, and RBA

6. EFFECTS OF CARBON-TREATED WASTE ASHES ON FLOWABILITY AND STRENGTH OF MORTAR

This chapter investigates the flowability and strength properties of mortar containing a raw ash (RFA, IFA, CFA, and RBA) or a carbon-treated ash under different moisture contents and CO₂ pressures. The raw fly ashes (RFA, IFA, and CFA) and their carbon-treated fly ashes (C-RFA, C-IFA, and C-CFA) as introduced in Chapters 4 and 5 were used as a cement replacement, while raw RBA and carbon-treated RBA (C-RBA) were used as a fine aggregate replacement.

6.1 Need of Treatment – Expansion of Mortar Containing RFA

Generally, the expansion of cement paste can be observed in the presence of metallic aluminum, leading to the production of hydrogen gas by its oxidation reaction, thus causing cement paste to expand (Aubert et al. 2004). Because metallic aluminum was observed in RFA (Section 3.2.4, Table 1), visible expansion was observed in the paste with 20% RFA replacement for cement (Figure 6.1). However, no visible expansion was observed in the corresponding paste containing 20% carbon-treated RFA under 70% moisture and a CO₂ pressure of 100 kPa (C-RFA-m70-p1). This was because the metallic aluminum was oxidized during the carbon treatment beforehand (Appendix A, Figure A1), resulting in no influence on the expansion of the paste. This result confirmed that the carbon treatment of RFA can be a promising technology for utilizing waste ashes including metallic aluminum, leading to the use of the treated ashes in concrete as a mineral admixture.

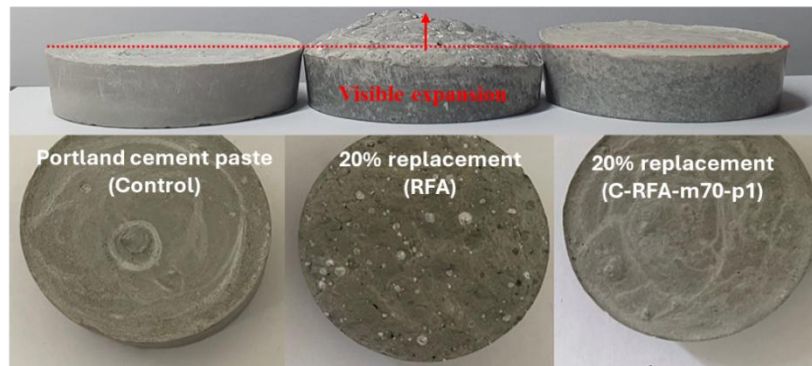


Figure 6.1. Portland cement paste (water-to-cement ratio = 0.45) samples containing RFA (20% replacement) or carbon-treated RFA (20% replacement)

6.2 Mortar Mixture Proportions and Test Methods

The carbon-treated fly ashes were used as cement replacement and the carbon-treated bottom ashes were used as sand replacement in mortar for the quantification. Table 6.1 shows the mixture proportions of mortar containing raw or carbon-treated ashes.

Table 6.1. Mixture proportions of mortar containing raw or carbon-treated ashes

Mixture ID	Mixture proportions (weight ratio)				
	Water	Binder		Fine aggregate	
		Type I/II portland cement	Raw or carbon-treated fly ashes	River sand	Raw or carbon-treated RBA
OPC (reference)	0.45	1.00	-	2.00	-
RFA10		0.90	0.10 (RFA)		
RFA20		0.80	0.20 (RFA)		
RFA20-m0-p1			0.20 (Carbon-treated RFA, under different conditions)		
RFA20-m20-p1					
RFA20-m40-p1					
RFA20-m70-p1					
RFA20-m20-p2					
RFA20-m40-p2					
RFA20-m70-p2					
IFA10		0.90	0.10 (IFA)		
IFA20		0.80	0.20 (IFA)		
IFA20-m0-p1			0.20 (Carbon-treated IFA, under different conditions)		
IFA20-m10-p1					
IFA20-m20-p1					
IFA20-m10-p2					
IFA20-m20-p2					
CFA10		0.90	0.10 (CFA)		
CFA20		0.80	0.20 (CFA)		
CFA20-m0-p1			0.20 (Carbon-treated IFA, under different conditions)		
CFA20-m5-p1					
CFA20-m5-p2					
RBA10		1.00	-	1.80	0.20 (RBA)
RBA20				1.60	0.40 (RBA)
RBA20-m20-p1					0.40 (Carbon-treated RBA, under different conditions)
RBA20-m70-p1					
RBA20-m20-p2					
RBA20-m70-p2					
RBA20-wet					

The mortar had a water-to-binder (w/b) ratio of 0.45 and a sand-to-binder (s/b) ratio of 2. Mortar made with pure Type I/II portland cement (no fly ash replacement) was used as a reference mix. The 20% carbon-treated RFA, IFA, and CFA ashes were used to replace portland cement, and the 20% carbon-treated RBA ash was used to replace river sand in the mortar. The river sand was oven-dried before use. However, all RBA samples were SSD to prevent excessive absorption of mixing water because RBA has a high absorption of 8.85%. Because the absorption of oven-dried river sand is nearly 2.0%, the effective water-to-binder ratio for the mortar with 0%, 10%, and 20% replacement by SSD bottom ash was 0.410, 0.414, and 0.418, respectively. Therefore, the difference in the effective water-to-binder ratio between the 0% replacement and 20% replacement was approximately 0.008. The difference did not seriously affect the strength and flowability of the mortar.

Each mortar mixture was mixed following ASTM C305. Immediately after mixing, the flow table test was conducted according to ASTM C1437. The photos of the flow table test results are in Appendix B.

The mixtures were cast in 2 in. cube molds, and the demolding process was conducted in a day, then the cube specimens were cured in a fog room. The compressive strength of the specimens was tested at the ages of 3, 28, and 56 days according to ASTM C109. Based on the strength results, the strength activity index of mortar containing the treated ashes was evaluated.

6.3 Effect of Carbon-Treated Ashes on Mortar Flowability

The flow table results of mortar containing the raw or carbon-treated RFA are shown in Figure 6.2. The raw RFA did not significantly affect flowability. However, the carbon-treated RFA ashes under a CO₂ pressure of 100 kPa slightly reduced the spread flow diameter (flowability). Interestingly, the carbon-treated RFA ashes under a CO₂ pressure of 200 kPa did not negatively affect flowability.

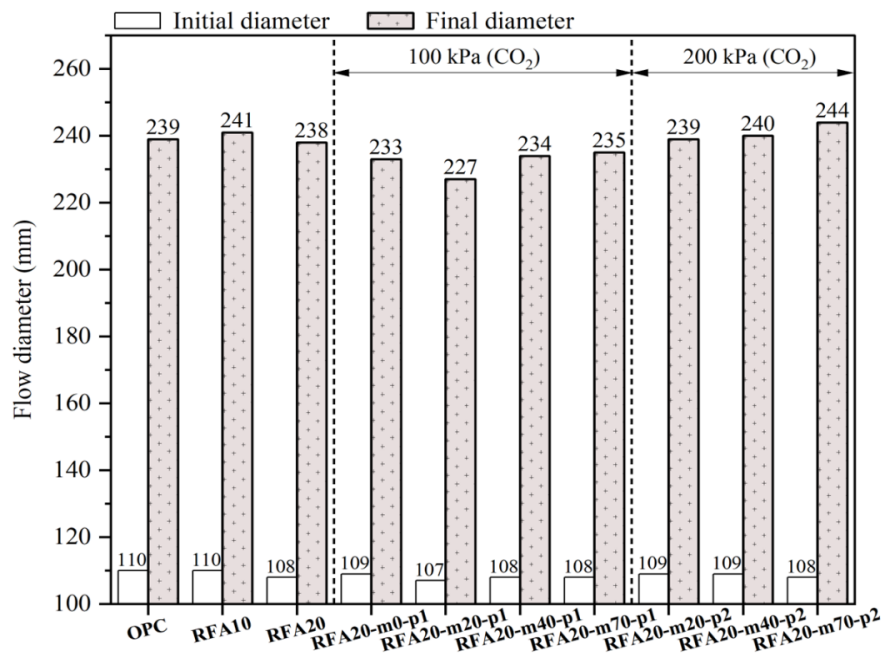


Figure 6.2. Flow table test results of mortar containing raw or carbon-treated RFA

Figure 6.3 shows the flow table results of mortar containing the raw or carbon-treated IFA. As the replacement amount of raw IFA increased, the flowability significantly decreased. The quicklime in IFA can influence the decrease of spread flow diameter (Qadir et al. 2019). Also, high amounts of sulfate can cause rapid set and decrease flowability. However, the carbon-treated IFA ashes under moisture conditions improved flowability. This is due to the consumption of quicklime during carbonation.

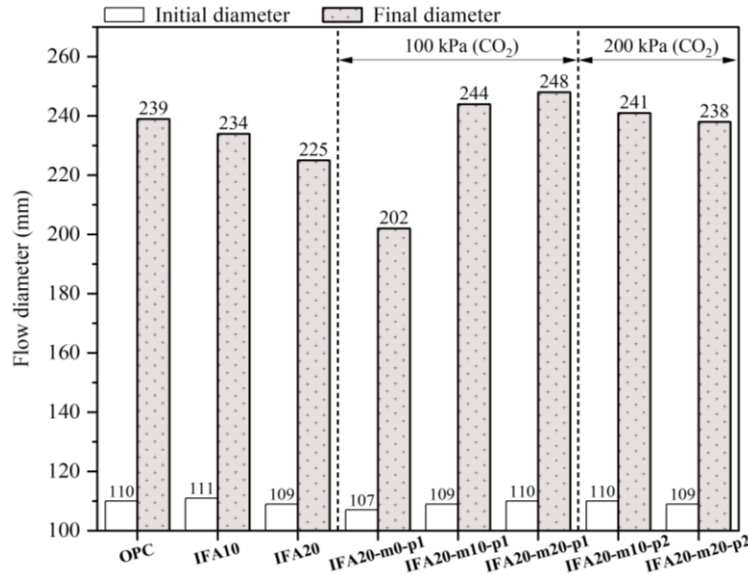


Figure 6.3. Flow table results of mortar containing raw or carbon-treated IFA

Figure 6.4 shows the flow table results of mortar containing the raw or carbon-treated CFA. Generally, spherical particles in fly ash result in ball bearing effects in paste, increasing flowability (Manz 1999). Therefore, the partial replacement of 10% to 20% with CFA increased flowability. However, the carbon-treated CFA under moisture conditions reduced flowability. This is attributed to the influence of the particle agglomeration (Figure 5.8) and the hydrates in CFA, as shown in the TGA results (Figure 5.4), decreasing the ball bearing effects of the fly ash and the flowability of its mortar.

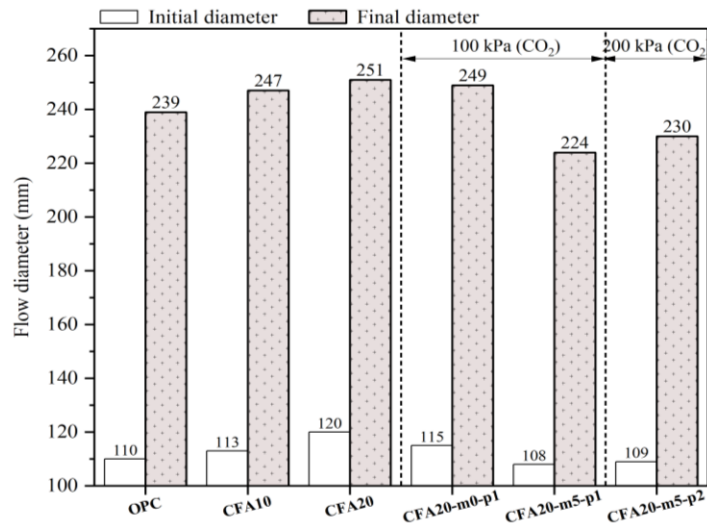


Figure 6.4. Flow table results of mortar containing raw or carbon-treated CFA

Figure 6.5 shows the flow table results of mortar containing the raw or carbon-treated RBA. There was no change in flowability in RBA10. In RBA10, the SSD RBA did not influence the decrease of flowability. However, the addition of more RBA (RBA20) reduced the flowability.

This can be attributed to the increase of RBA volume per unit volume of mortar because of its low specific gravity. When the carbon-treated RBA ashes were used, the flowability was not significantly reduced. The decrease of surface roughness (Figure 5.9) can be the reason for the flowability improvement.

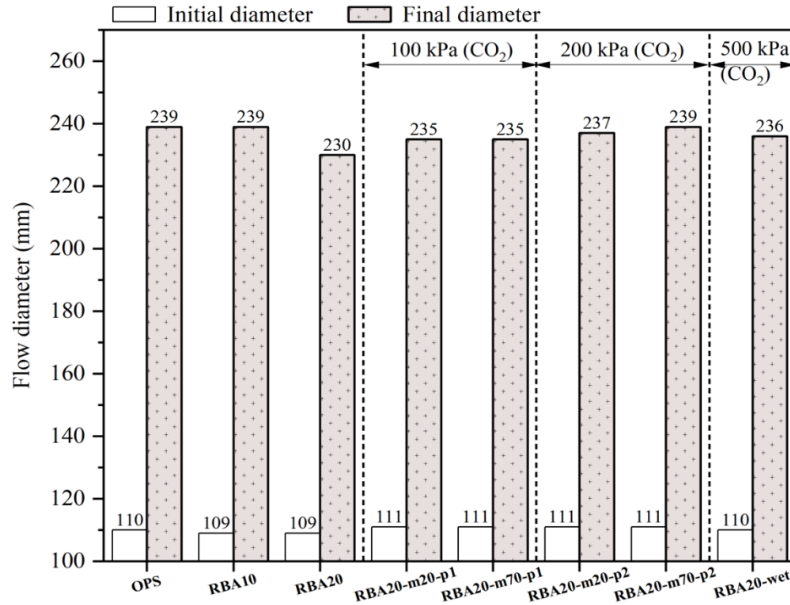


Figure 6.5. Flow table results of mortar containing raw or carbon-treated RBA

6.4 Effect of Carbon-Treated Ashes on Mortar Strength

Figure 6.6 shows the compressive strength and strength activity index of the mortar specimens containing the raw or the carbon-treated RFA ashes. The raw RFA affected the strength reduction greatly, leading to a strength activity index of less than 60% at 28 days for RFA20 (20% raw RFA replacement). This is mostly due to the expansion caused by hydrogen gas generation, increasing porosity in the cubes, as described in the problem statement. However, all carbon-treated RFA ashes mitigated the strength reduction. The mitigation effect was dependent on the moisture content in the carbon treatment. The carbon-treated RFA ashes with a moisture content of 70% greatly impacted the mitigation of strength reduction, leading to a strength activity index of 85% to 90% at 28 days. Only RFA20-m70-p1 and RFA20-m70-p2 met the requirement of a strength activity index of 75%, as shown in Figure 6.6b. The oxidation reaction of metallic Al in the carbon treatment before use is likely the main reason for the strength improvement. The effect of a higher CO₂ pressure during the carbon treatment was slightly less effective or comparable for the strength improvement.

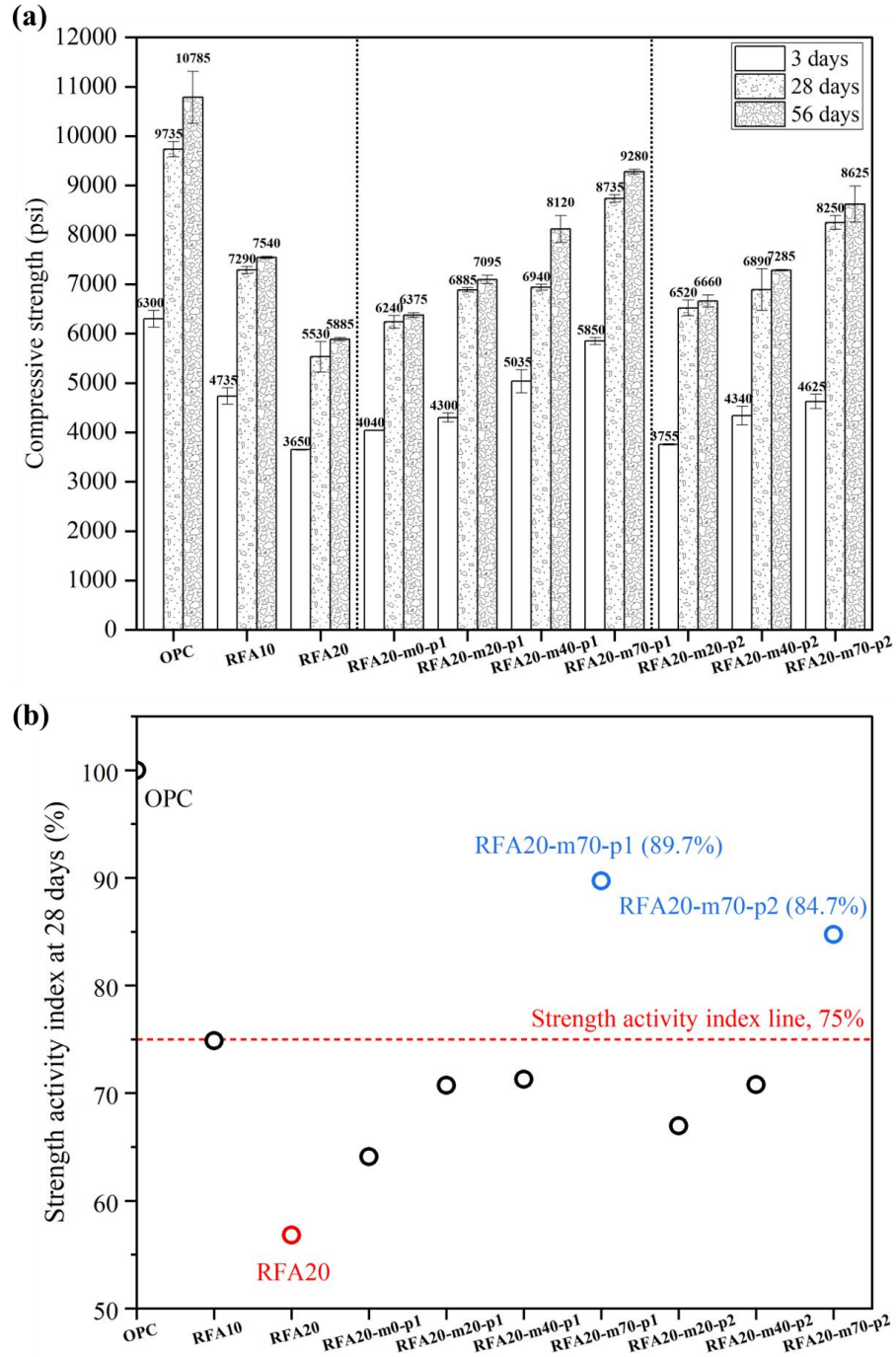


Figure 6.6. Compressive strength (a) and strength activity index (b) of mortar specimens containing untreated and carbon-treated RFA ashes

Figure 6.7 shows the compressive strength and strength activity index of the mortar specimens containing the raw or the carbon-treated IFA ashes. There was a strength reduction of less than 10% in IFA10 at 28 days, but IFA20 had a much lower strength, resulting in a strength activity index of approximately 65% at 28 days. All of the carbon-treated IFA ashes also did not mitigate the strength reduction significantly and did not meet the strength activity index requirement of

$\geq 75\%$. These results are probably related to these ashes' high sulfate content, leading to the strength reduction at later ages (Tsamatsoulis and Nikolakakos 2013, Neto et al. 2021). Above the optimal sulfate content, an increase in ettringite volume and a decrease in calcium silicate hydrate (C-S-H) density can be observed in the cement pastes (Adu-Amankwah et al. 2018).

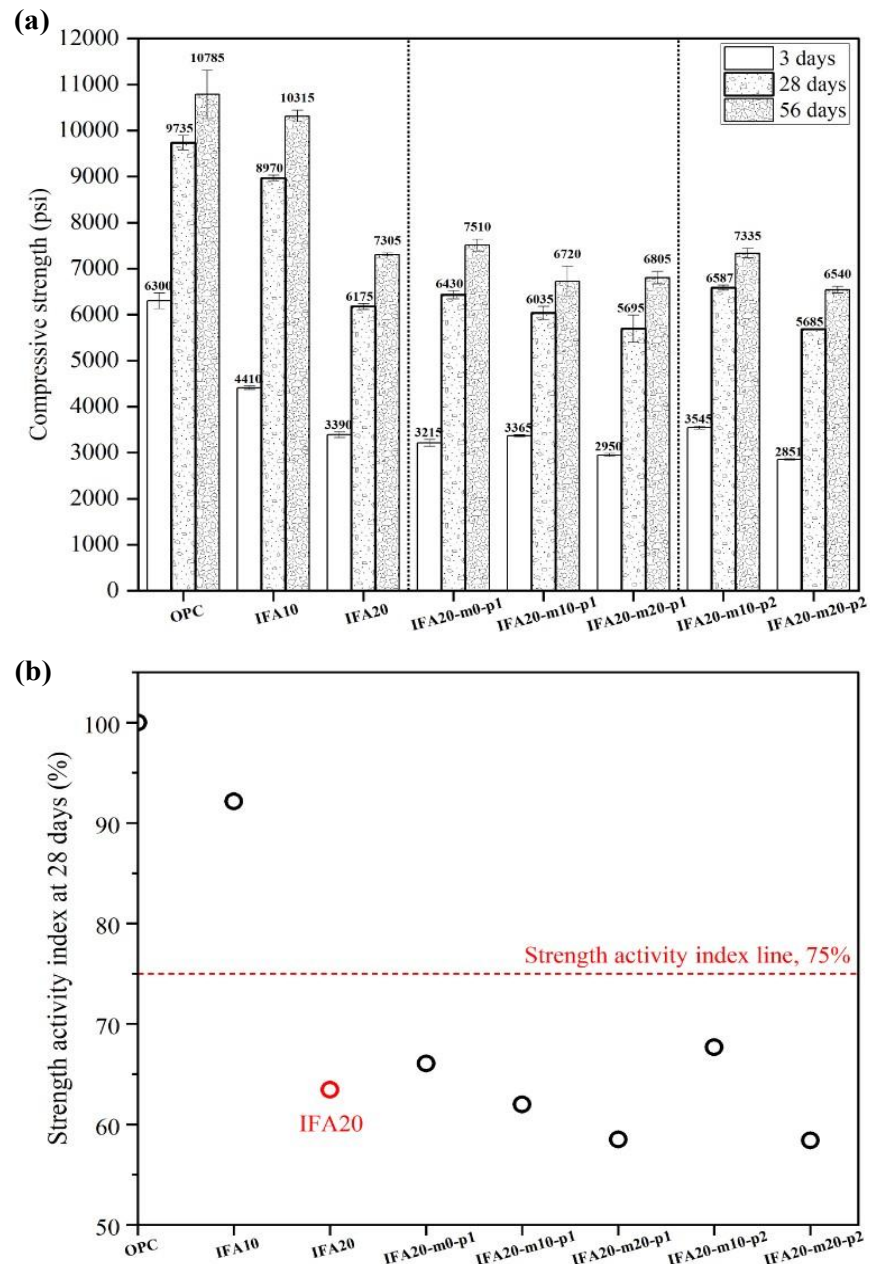


Figure 6.7. Compressive strength (a) and strength activity index (b) of mortar specimens containing untreated or carbon-treated RFA ashes

Figure 6.8 shows the compressive strength and strength activity index of the mortar specimens containing the raw or the carbon-treated CFA ashes. As specified in the technical data sheet,

CFA10 and CFA20 showed a strength activity index of 104% and 93%, respectively, which satisfied the requirement and were comparable to the ordinary portland cement (OPC). However, the carbon treatment had a negative effect on CFA, leading to a decrease in the strength activity index (80% to 90%) even though it met the requirement. The particle agglomeration and the prehydration of CFA during the carbon treatment had a detrimental effect on the strength development.

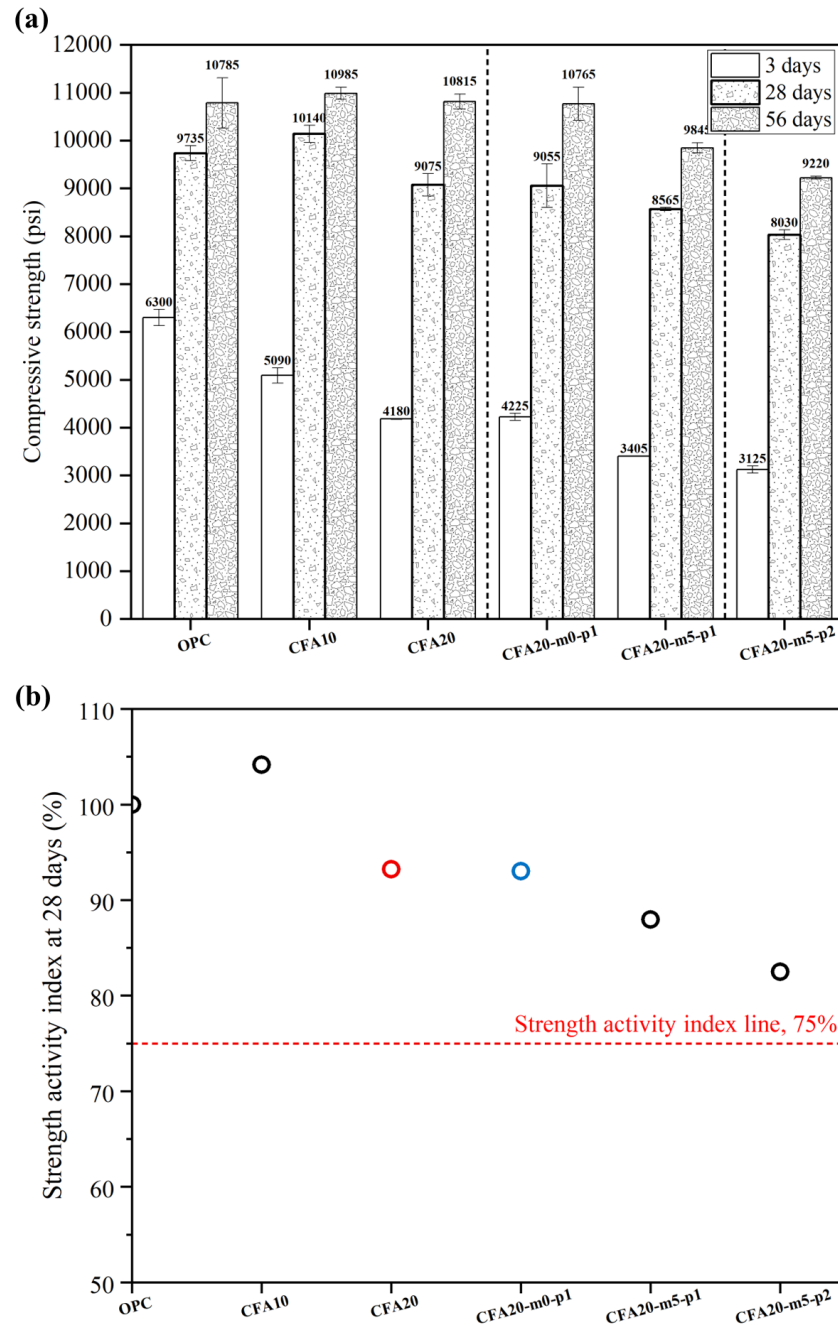


Figure 6.8. Compressive strength (a) and strength activity index (b) of mortar specimens containing untreated and carbon-treated CFA ashes

Figure 6.9 shows the compressive strength and strength activity index of the mortar specimens containing the raw or the carbon-treated RBA ashes.

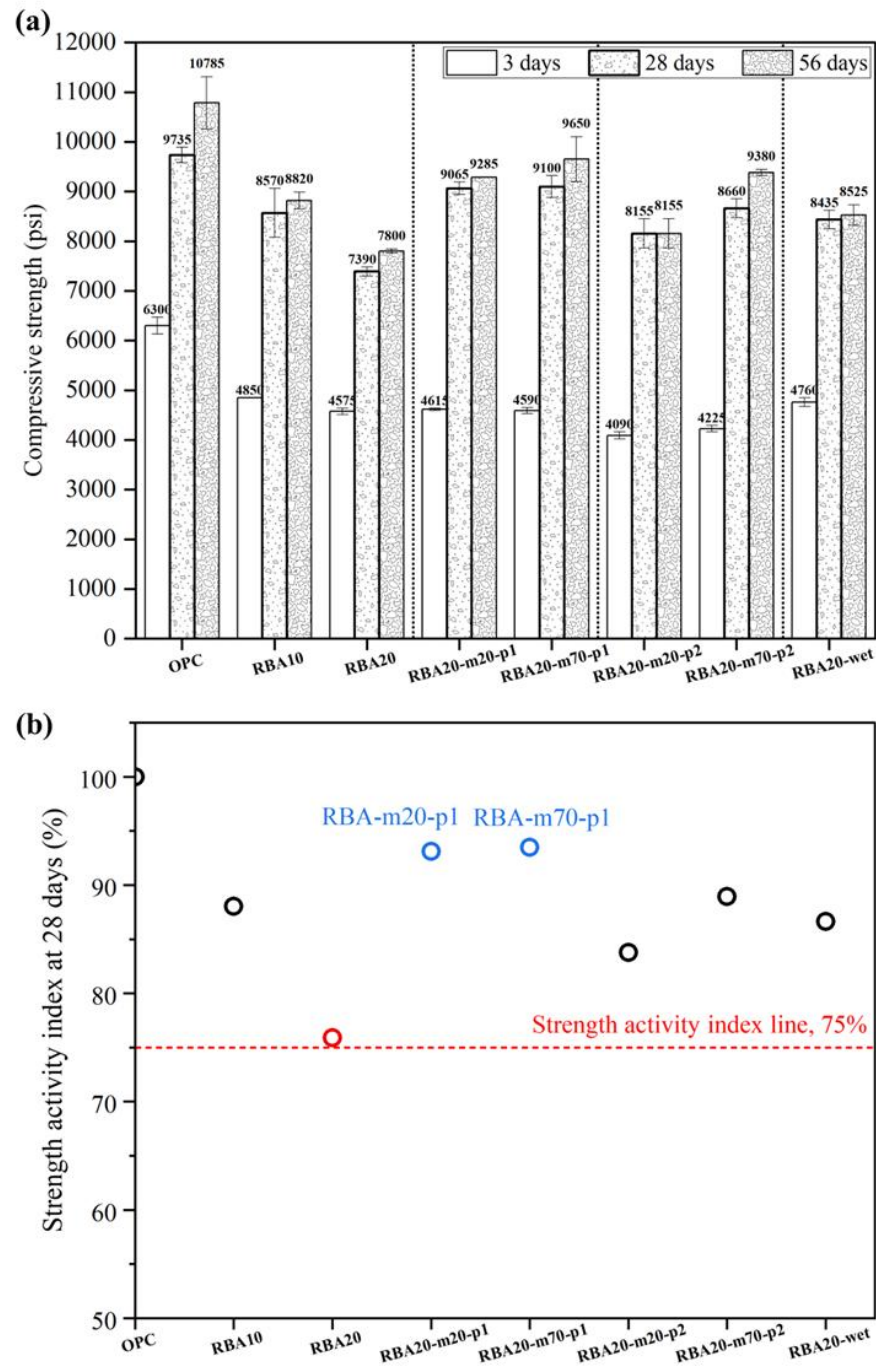


Figure 6.9. (a) Compressive strength and (b) strength activity index of mortar specimens containing raw or carbon-treated RBA ashes

When the raw RBA replaced the river sand, the compressive strength proportionally decreased with every 10% replacement, leading to a strength activity index of approximately 75% at 28

days for RBA20. The relatively porous RBA increased the porosity in mortar, decreasing the strength. However, all carbon-treated RBA ashes impacted the mitigation of strength reduction, resulting in a strength activity index of 84% to 93%. A CO₂ pressure of 100 kPa used in the carbon treatment was the best for strength improvement. A lower CO₂ concentration can allow for controlled carbonation, promoting calcium carbonate growth without causing excessive carbonation (Lu et al. 2022), which thus limits undesirable effects, such as surface cracks or excessive porosity, but densifies the surface of the RBA, as shown in Figure 5.9. This might be one of the reasons that RBA-m20-p1 and RBA-m70-p1 had better results than the other treated RBA ashes.

6.5 Summary of Flowability and Strength of Mortar Containing Carbon-Treated Ashes

This chapter evaluated the flowability and compressive strength of the mortar mixtures containing the carbon-treated ashes. The major findings are as follows:

- The carbon treatment effectively improved RFA and RBA to mitigate the strength reduction of mortar (20% replacement) without significant flowability loss.
- In the RFA results, the strength activity index at 28 days was improved from 57% (RFA20) to 90% (RFA20-m70-p1). The effect of carbon treatment on RFA was greatly dependent on moisture content. A moisture content of 70% was best for the treatment, leading to the effective removal of metallic aluminum and the mitigation of strength reduction.
- In the RBA results, the carbon treatment of RBA improved the compressive strength, increasing the strength activity index at 28 days from 75% (RBA20) to 93% (RBA20-m70-p1). This can be attributed to the surface refinement with calcium carbonate.
- The carbon treatment was not effective for IFA and CFA in terms of improving the compressive strength of mortar.
- The carbon-treated CFA caused particle agglomeration and the prehydration of CFA, leading to negative effects on both flowability and strength development.

7. SYNERGISTIC EFFECTS OF CARBON CURING FOR MORTAR CONTAINING WASTE ASHES

To reduce embedded carbon in concrete, the cement industry is transitioning to ramp up production of portland limestone cement (Type IL). At the same time, carbon-curing technology has been increasingly used to sequester more carbon into concrete while improving the early-age strength of the concrete (Chen and Gao 2019). In this project, the synergistic effects of utilizing Type IL cement and waste ashes in concrete, which is further cured with carbon, are investigated so as to maximize carbon footprint mitigation.

In the previous chapter (Chapter 6), the compressive strength of the mortar containing raw or carbon-treated IFA did not meet the ASTM strength activity index limit of 75%. The carbon-curing method was expected to improve the strength of mortars made with IFA. The carbon-curing method was also applied to the mortar mixes containing the carbon-treated RFA or RBA so as to increase their carbon sequestration capacities.

7.1 Carbon-Curing Procedure

For the investigation of the mortar compressive strength before and after carbon curing and for the estimation of carbon sequestration capacity, 2 in. cube mortar samples were used. Table 7.1 shows the mixture proportions of the selected mortar mixes studied. The mix made with 100% Type IL cement was used as a reference cement. Other mixes contain either 20% carbon-treated waste fly ash replacement for Type IL cement or 20% carbon-treated waste bottom ash for sand replacement. All mixture proportions are expressed by a weight ratio, and the mixing processes were the same as those performed in Chapter 6.

Table 7.1. Mix proportions of the mortar selected for carbon-curing study

Mixture ID	Mixture proportions (by weight ratio)				
	Water	Binder		Fine aggregate	
		Type IL portland cement	Raw or carbon-treated fly ashes	River sand	Raw or carbon-treated RBA
PLC (reference) ¹	0.45	1.00	-	2.00	-
C-RFA20-m70-p1 ²		0.80	0.20 (RFA-m70-p1)	2.00	-
C-IFA20 ³		0.80	0.20 (raw IFA)	2.00	-
C-RBA20-m20-p1 ⁴		1.00	-	1.60	0.40 (RBA-m20-p1)

¹Mortar containing 100% IL cement, and it was not carbon cured; ²Mortar containing 20% carbon-treated RFA under the treatment condition of 70% moisture and 100 kPa carbon pressure, and the mortar was carbon cured;

³Mortar containing 20% IFA (untreated), and the mortar was carbon cured; ⁴Mortar containing 20% carbon-treated RBA under the treatment condition of 20% moisture and 100 kPa carbon pressure, and the mortar was carbon cured.

The carbon-curing process consists of mainly three stages: pre-conditioning, carbon curing, and post-curing (Liu and Meng 2021). Figure 7.1 shows the three-stage process of carbon curing:

pre-conditioning, carbonation, and post-curing. The pre-conditioning process includes in-mold curing and drying after the demolding process. The time for in-mold curing is dependent on the final set time of the mixture to prevent unexpected damage in the demolding process. The demolding time for the mixtures in Table 7.1 was set to approximately 7 hours after starting the mixing of mortar through preliminary tests. Figure 7.2 shows that even with extra care, such as the application of a lubricant to the surface of the mold, the risk of sample surface damage in the demolding process was still high, as some mortar samples might have not reached their final set.

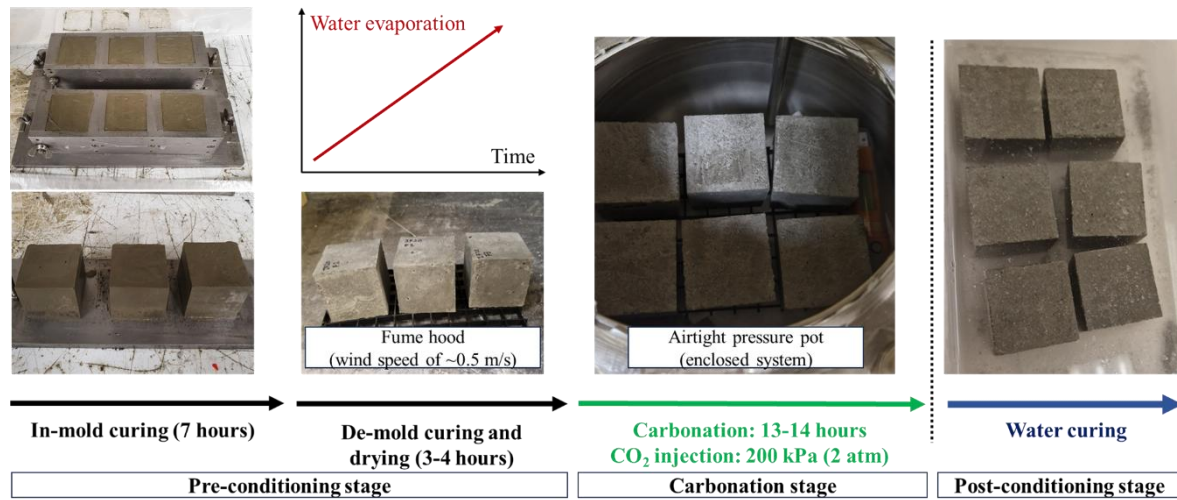


Figure 7.1. Overall carbon-curing procedure

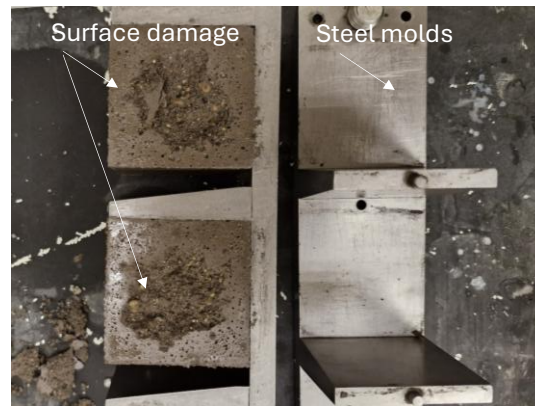


Figure 7.2. Surface damage of mortar cubes during early demolding process

Immediately after the demolding process, the mortar specimens were dried in a fume hood with a wind speed of approximately 100 feet per minute (FPM) (approximately 0.5 m/s). As described in the brief literature review (Chapter 2), the water evaporation in the mortar mixtures was set to approximately 30% to 35% of the initial mixing water immediately before the carbon curing. The weight of the initial mixing water in a cube was estimated based on the mortar mixture proportions (Table 7.1), and it was 45 g water per 345 g mortar, as shown in Figure 7.3.

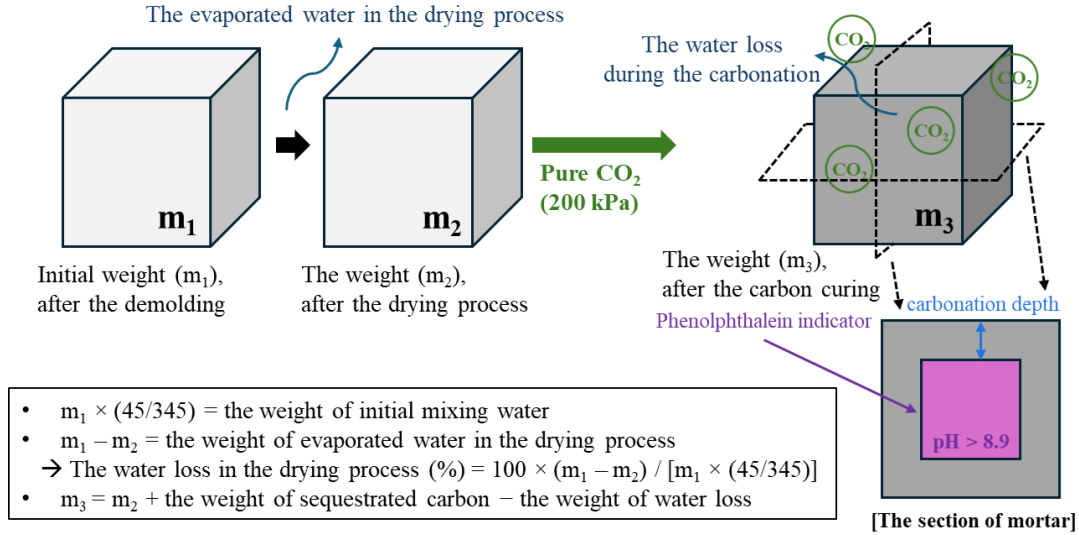


Figure 7.3. Weight change of the cube specimen during the carbon-curing process

In this study, a cycle of 24 hours was considered for the carbon curing, which may be applicable for the precast concrete. During the carbon-curing test, the CO_2 uptake by the unit volume of mortar during curing was investigated. Following the carbon curing, for 24 hours, the carbon-cured cubic samples were cured under water until their testing time. The compressive strength, SSD density, and electrical surface resistivity of the mortars was tested at the mortar ages of 3, 10, and 28 days.

Once approximately 30% to 35% of the mixing water was evaporated in the drying process, the carbonation process was conducted in the airtight pressure pot (Figure 4.1) supplied with pure CO_2 gas at a gauge pressure of 200 kPa. The higher CO_2 pressure is generally advantageous to increase the diffusion of CO_2 into concrete, subsequently improving carbonation efficiency, and increasing the sequestered carbon. It has been reported that the carbonation efficiency increases steeply and reaches almost its highest degree when the carbon-curing pressure is increased to 100 kPa, but after the pressure reaches 400 kPa, the carbonation efficiency goes down (Liu and Meng 2021). Therefore, a CO_2 gauge pressure of 200 kPa was adopted in this study.

During the carbon curing, the weight change of the airtight pressure pot including the six mortar specimens was measured every 15 seconds, using a weight balance with the SPDC software. In a preliminary test, a noticeable weight change by carbonation during the carbon curing was observed. Unlike the carbon treatment for raw ashes, it was not significantly affected, with a margin of error of less than approximately 5% of the weight change. The final weight in the recording was compared to the weight change of the mortar specimens before and after the carbon curing, as shown in Figure 7.2.

In considering the water release during the carbon curing, mainly produced from cement hydrates reacting with CO_2 (Figure 7.4), the weight of sequestered carbon in the carbon-cured samples can be calculated as $m_3 - m_2$ + the weight of water loss during the carbon curing. This estimated amount of sequestered carbon was compared to the weight changes measured in the

corresponding carbon-cured samples. In addition, the carbonation depth of each carbon-cured sample was measured immediately at the end of the carbon-curing process, where a phenolphthalein solution of 0.1% w/v in ethanol was used as a carbonation indicator (Yu et al. 2010).



Figure 7.4. Water released from six mortar cubes during carbonation process

After carbon curing, all specimens were cured in a water bath for post-curing, allowing for subsequent cement hydration by supplying water. Then, the following tests were performed on the 2 in. cube samples at the mortar ages of 3, 10, and 28 days:

1. The SSD density of mortar samples was measured following the same procedure used for bulk density of aggregates (ASTM C29).
2. The compressive strength of the mortar samples was tested in accordance with ASTM C109.
3. The bulk electrical resistivity of the SSD cube samples was measured using a Proceq resistivity meter with an accuracy of ± 0.2 to ± 2 $k\Omega \cdot cm$ (depending on resistivity range). The bulk electrical resistivity of concrete correlates to the durability of concrete regarding strength, porosity, and permeability (Cosoli et al. 2020).

7.2 Results from Carbon-Curing Tests

7.2.1 During the Pre-conditioning Stage

Prior to the pre-conditioning stage, the demolding of all mortar mixtures was conducted 7 hours after casting the mortar mixtures into cube molds. Then, the initial weight of each cube in a set of six samples for each mix was measured to estimate water evaporation during the drying process in the fume hood with a wind speed of approximately 0.5 m/s. The weight change during the drying process was measured every 60 minutes. As shown in Figure 7.5, Mixes C-RFA20-m70-p1 and C-IFA20 showed a similar water evaporation rate, reaching the goal of 30% to 35% water evaporation in 4 hours of drying, while Mix C-RBA20-m20-p1 reached this goal in 3 hours of drying. The difference is probably due to the SSD condition of RBA, and sufficient water retained in carbon-treated RBA particles can be easily dried.

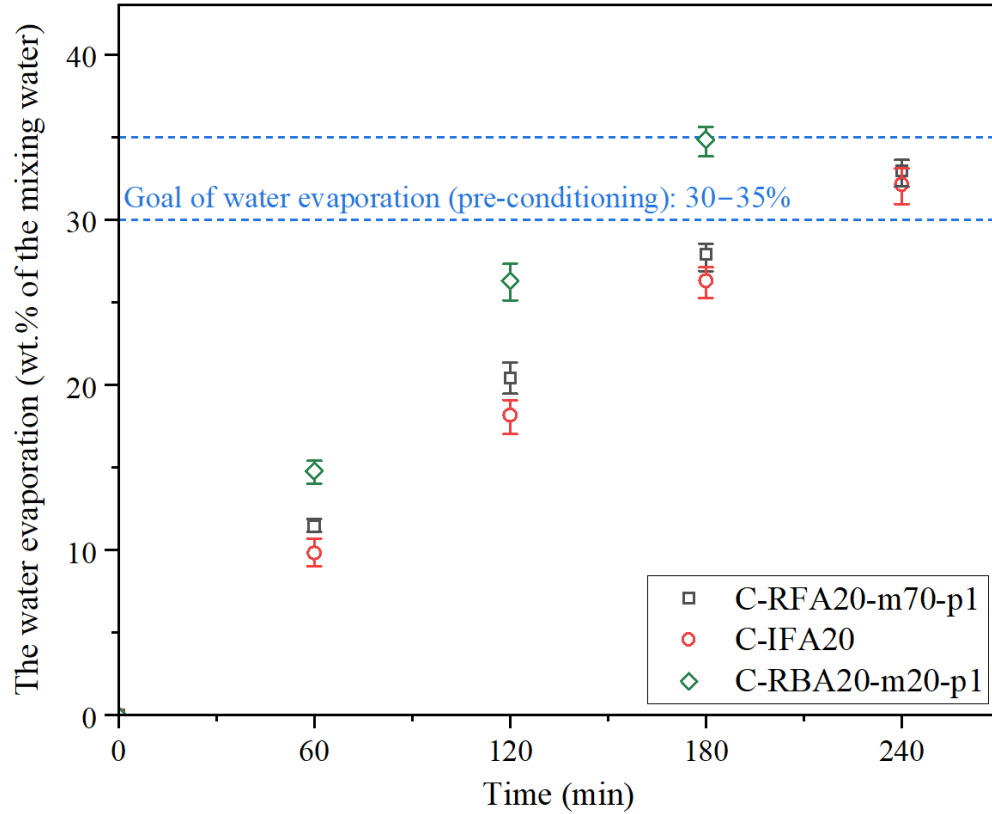


Figure 7.5. Water evaporation from mortar samples in drying process (pre-conditioning)

7.2.2 During the Carbonation Stage

The weight change during the carbonation stage was recorded every 15 seconds using a weight balance with the SPDC software. As mentioned in Section 7.1, the sequestered CO_2 content in the mortar samples was determined using two methods: (1) the weight recorded in real time (the results are shown as the smooth curves in Figure 7.6) and (2) the weight calculated from the process as illustrated in Figure 7.3 (the results are shown by the symbols in Figure 7.6). Figure 7.6 demonstrates that the sequestered CO_2 content obtained from both methods was consistent. The highest weight gain, or the highest sequestered CO_2 content, was found in Mix C-RBA-m20-p1 (122.3 g, from six cubes tested), followed by Mix C-IFA20 (98.6 g), and then Mix C-RFA-m70-p1 (94.9 g). The time for Mixes C-RFA-m70-p1, C-IFA20, and C-RBA-m20-p1 to reach 50% of the highest CO_2 sequestration values were at 1.5, 1.9, and 1.3 hours after the start of the CO_2 curing process, respectively, and the times for these mixes to reach 90% of the highest CO_2 sequestration values were at 8.4, 8.8, and 7.7 hours after the start of the CO_2 curing process, respectively. Most CO_2 sequestration occurred within 9 hours during the carbonation stage.

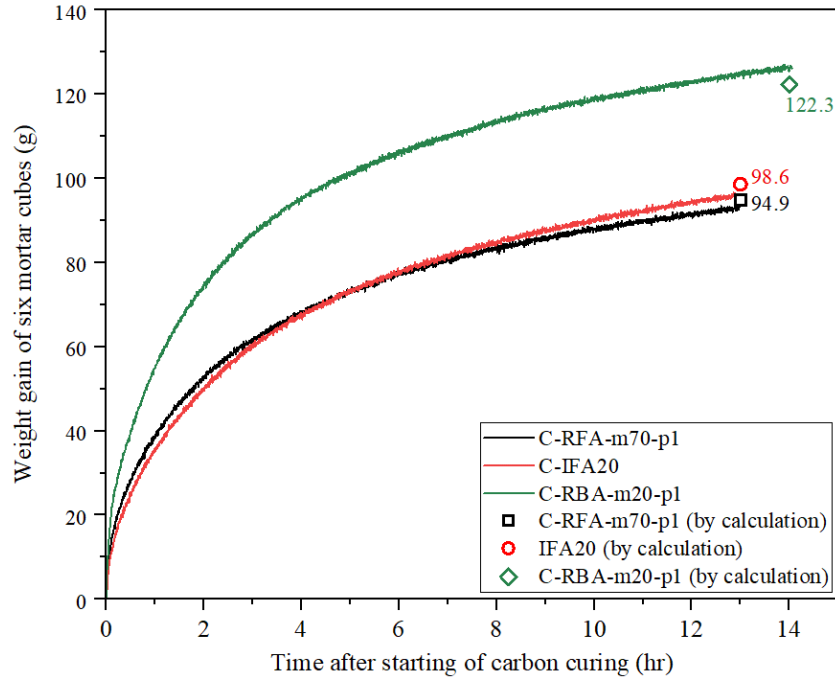


Figure 7.6. Weight gain of six mortar cubes during carbonation

Carbonation in concrete is dependent on the pH of the concrete pore solution as well as gas diffusivity and reactants. The content of calcium hydroxide, a major hydrate in portland cement-based systems, plays an important role in carbonation because it provides a high pH pore solution for CO_3^{2-} dominance (Visser 2014). That is why calcium hydroxide content, which is closely related to cement content and degree of cement hydration, is important in mineral carbonation. Figure 7.7 proves that CO_2 sequestration is closely related to the cement content in mortar. All mixes displayed similar curves of sequestered CO_2 content when the results of Figure 7.6 were normalized by the weight of cement content in the six mortar cubes tested. The 20% waste ashes replacement for cement in Mixes C-IFA20 and C-RFA-m70-p1 reduced the calcium hydroxide content in the six cubic mortar samples, thus resulting in less weight gain from CO_2 sequestration than Mix C-RBA-m20-p1, where the cement content was as high as that of the control mix.

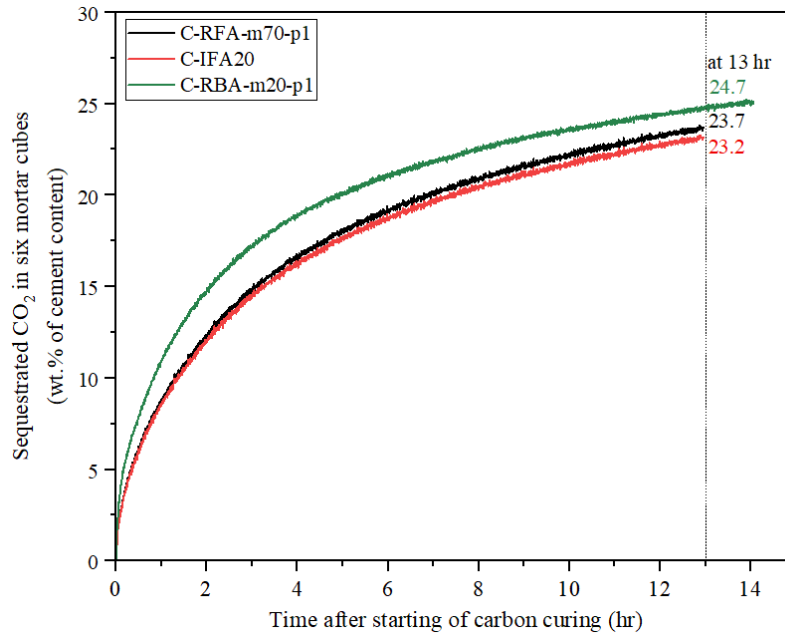


Figure 7.7. Sequestered CO₂ normalized by the weight of cement content in mortar

Figure 7.8 shows the cross sections of mortar samples sprayed with the phenolphthalein solution (Figure 7.3). All samples displayed a carbonation depth of approximately 0.35 to 0.42 in., indicating that the carbonated volume of samples in each mix is similar.

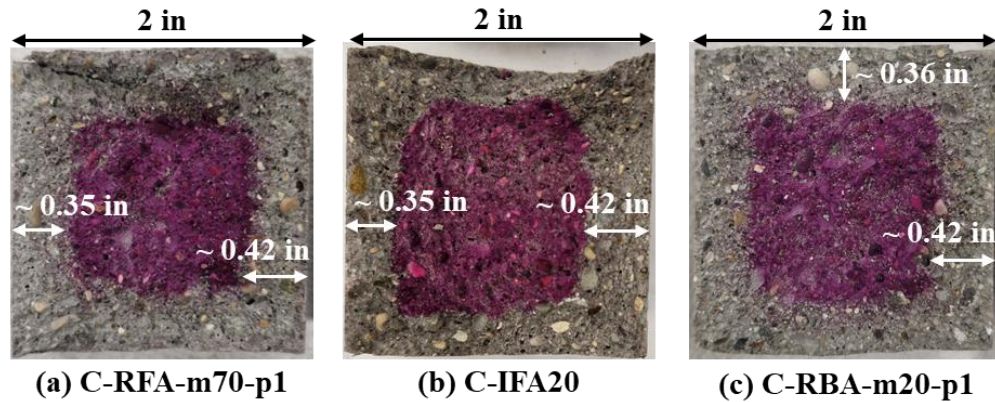


Figure 7.8. Phenolphthalein spray results of the carbon-cured mortar specimens immediately after the carbonation stage: (a) C-RFA-m70-p1, (b) C-IFA20, and (c) C-RBA-m20-p1

Based on the measured and calculated sequestered CO₂ content per unit volume of mortar (Figure 7.7), and the results of carbonation depth (Figure 7.8), it can be inferred that CO₂ sequestration is mostly dependent on cement content. Therefore, Mix C-RBA-m20-p1 experiences more benefits from carbon curing in terms of embodied carbon, compensating for embodied carbon from the higher cement content. Even though the amount of CO₂ sequestration in Mixes C-RFA-m70-p1 and C-IFA20 was lower than that in Mix C-RBA-m20-p1, their

embodied carbon could also be lower because 20% waste ash replacement for cement could cut back on the embodied carbon from reduced cement content.

Figure 7.8 also shows that full carbonation of the cubic samples was not achieved in the present study. Partial carbonation is often observed because carbonation starts from the surface layer of carbon-cured samples and forms a dense layer that prevents further CO₂ penetration. Research has found that similar to the concept of carbon capture coating (Peng et al. 2023), a dense surface layer on carbon-cured concrete could improve the deterioration resistance of the concrete and potentially extend the concrete service life.

7.2.3 During the Post-curing Stage

Immediately after the carbonation stage, all samples were cured in a water bath to compensate for water loss in both the pre-conditioning and carbonation stages. At the ages of 3, 10, and 28 days, the bulk density, bulk electrical resistivity, and compressive strength of the samples were measured. All sample surfaces were dried with a towel before testing, and it was assumed that all samples were at an SSD condition as they were cured in water at least 2 days. Therefore, all test results were not influenced by the degree of water-saturation of the mortar.

Table 7.2 shows the bulk density of the mortar samples at the ages of 3, 10, and 28 days. Except for Mix C-IFA20, whose density was slightly higher, the density values of all other mortar samples were similar.

Table 7.2. Bulk density of the mortar cubes after post-curing

Mixture ID	Bulk density (g/cm ³)		
	3 days	10 days	28 days
PLC (reference)	2.26	2.27	2.27
C-RFA20-m70-p1	2.26	2.27	2.27
C-IFA20	2.31	2.31	2.31
C-RBA20-m20-p1	2.26	2.27	2.27

Figure 7.9 shows the bulk electrical resistivity of the mortar samples at the ages of 3, 10, and 28 days. Mix PLC, portland limestone cement mortar, displayed a much lower bulk electrical resistivity value (only 10 to 20 kΩ·cm) at all ages compared to other mortars subjected to carbon curing. This is attributed to the dense surface layer of the samples, resulting from carbonation. At 3 days, the C-RBA20-m20-p1 displayed the highest resistivity, followed by the C-IFA20 and C-RFA20-m20-p1. Partial cement replacement with the ashes was ineffective for electrical resistivity improvement. This seems to be related to the quantity of carbonate compounds in the outer part of the mortar cube. In Figure 7.6, the sequestered CO₂ in the C-IFA20 was slightly higher than that in the C-RFA20-m70-p1. This can be attributed to the free lime in IFA reacting with carbonate, although most carbonation is greatly dependent on the cement content in mortar, as shown in Figure 7.6 and Figure 7.7. Notably, the electrical resistivity of C-IFA20 has steeply increased compared to that of the other mixtures at later ages. The reason for this still has not

been discovered, but it may be related to the high calcium sulfate content in IFA, which can stabilize calcium carbonate by preventing its transformation to the other polymorphs, and volumetric change (Li et al. 2015). This needs to be investigated further.

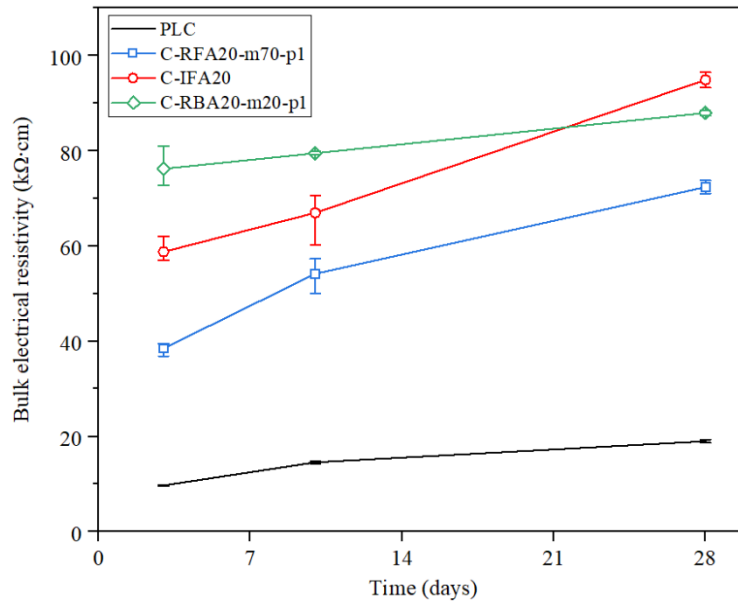


Figure 7.9. Bulk electrical resistivity of the mortar cubes in the post-curing stage

Figure 7.10 shows the compressive strength of the mortar specimens in the post-curing stage at 3, 10, and 28 days. It can be seen in the figure that at 3 days, all carbon-cured samples containing 20% waste ashes had a comparable strength to the control mortar (PLC). But at 28 days, all carbon-cured samples containing 20% waste ashes had a lower strength than the control mortar (PLC). At 3 days, the strength of specimens treated with carbon curing was comparable to or higher than that of PLC. In the previous chapter, the strength activity indexes of RFA-m70-p1, IFA20, and RBA20-m20-p1 at 3 days were 92.9%, 53.8%, and 73.3%, respectively. The carbon curing enhanced the strength activity indexes from 92.9%, 53.8%, and 73.3% to 100.3%, 92.3%, and 105.1%, respectively, compared to the previous standard curing results. The carbon treatment was effective on IFA20 and RBA20-m20-p1, particularly at early ages. However, the strength at 28 days was not significantly improved, except for C-IFA20. RFA-m70-p1 and RBA20-m20-p1 showed a strength activity index of approximately 90% at 28 days. However, the carbon-curing process was ineffective, resulting in a strength activity index of around 80% at 28 days. Unlike them, the strength activity index of C-IFA at 28 days met the minimum requirement of 75%. Research has indicated that carbon-cured concrete may have lower strength at later ages. During carbon curing, CO_2 reacts with not only calcium hydroxide (CH) but also unhydrated cement minerals in the cement paste, thus interfering with further cement hydration and C-S-H formation, reducing long-term concrete strength (Chen and Gao 2019). In addition, the carbonation reactions that form calcium carbonate and water are generally volume reduction reactions. Initially, the rapid calcium carbonate formation might reduce porosity and increase the density of the cement paste. However, fewer pozzolanic reactions along with $\text{Ca}(\text{OH})_2$ reduction by carbonation at early ages (Figure 7.8) could potentially result in the reduction of long-term strength (Bui et al. 2018) although there was pH recovery over time, as shown in Figure 7.11.

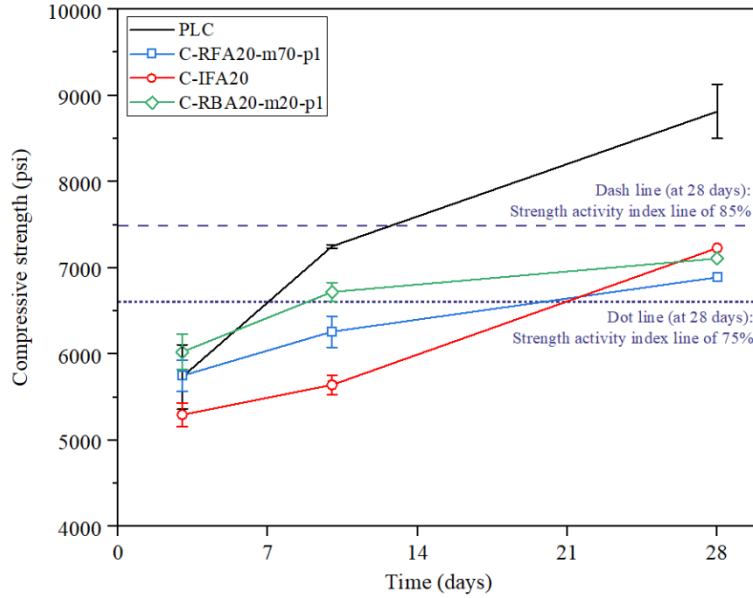


Figure 7.10. Compressive strength of the mortar cubes in the post-curing stage

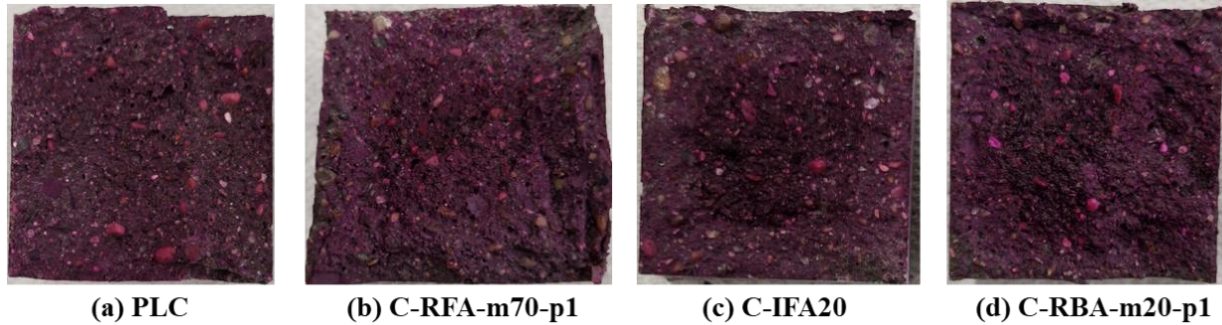


Figure 7.11. Phenolphthalein spray results of the carbon-cured mortar specimens at 28 days (the post-curing stage): (a) PLC, (b) C-RFA-m70-p1, (c) C-IFA20, and (d) C-RBA-m20-p1

7.3 Summary of the Synergistic Effects of Carbon Curing

This chapter investigated the effects of carbon curing on Type IL portland cement containing RFA-m70-p1, IFA, or RBA-m20-p1. The major findings are as follows:

- In the pre-conditioning stage, the water evaporation rate of C-RBA20-m20-p1 was higher than that of C-RFA20-m70-p1 and C-IFA20, which displayed a similar water evaporation rate. This is because of the SSD condition of RBA, which retained water and dried easily in a mortar cube.
- During the carbonation stage, the weight gain from carbonation (CO_2 sequestration) of C-RBA20-m20-p1 was higher than that of C-RFA20-m70-p1 and C-IFA20. This was mostly attributed to the cement content in mortar due to its relationship to calcium hydroxide

content, which is mostly a precursor of calcium carbonate. IFA20 was slightly higher than C-RFA-m70-p1 at the same cement replacement of 20%.

- The carbon-curing process reduced the embodied carbon in cement by 20% to 25%, leading to a synergistic effect when cement was further substituted with supplementary cementitious materials.
- During the post-curing stage, the bulk electrical resistivity of mortars subjected to the carbon-curing process was three times higher than that of the PLC with standard curing at all ages. This is mainly attributed to the dense surface caused by carbonation.
- The compressive strength of mortars subjected to the carbon-curing process at 3 days was comparable to that of PLC, primarily because of the dense surface resulting from the carbonation process. However, the strength development of C-RFA-m70-p1 and C-RBA-m20-p1 at 28 days was ineffective compared to the standard curing results in Chapter 6, even though the strength activity index met the minimum requirement of 75%. This was probably due to the consumption of calcium hydroxide during the carbonation stage, which reduced the pozzolanic reactivity of the ashes in the post-curing stage.
- Carbon curing was essential for IFA with high sulfate and free lime content to be used as a cement substitute. Replacing 20% of the cement with raw or carbon-treated ashes did not meet the minimum strength activity index of 75%, resulting in strength activity indexes of 55% to 70% in all standard curing results. After carbon curing, however, the strength of C-IFA20, with a strength activity index of 82%, met the minimum requirement.

8. EMBODIED CARBON AND COST SAVINGS ASSESSMENT FOR MORTARS CONTAINING WASTE ASHES

Concentrated effort to reach net-zero embodied carbon is being exerted worldwide after the Paris Agreement in 2015 (Delbeke et al. 2019). Embodied carbon in construction materials is generally defined as the total carbon released from direct and indirect processes associated with materials or products production. This includes all activities from material extraction (e.g. quarrying and mining), manufacturing, transportation, and fabrication processes until the product is ready to be used.

8.1 General Considerations

In this project, the Inventory of Carbon and Energy (ICE) database (Hammond et al. 2011) was used to conduct a benefit assessment of the mortar mixtures containing RFA, IFA, CFA, or RBA. Table 8.1 represents the embodied carbon factors of each constituent (kg CO₂ per kg constituent). Open literature values were used for evaluating embodied carbon in the mortar mixtures (Hammond et al. 2011), except the values for RFA, IFA, and RBA. Because these waste ashes are not typical and currently available, the embodied carbon values of RFA, IFA, and RBA were assumed based on the value for general ashes in the ICE database for this study.

Table 8.1. Embodied carbon factors for constituents of mortar

Constituent	Embodied carbon (kg CO ₂ /kg constituent)
Type I/II portland cement	0.930
Type IL portland cement	0.837
RFA	0.000*
IFA	0.008*
CFA	0.008
Fine aggregate	0.005
RBA	0.000*
Water	0.001

* Embodied carbon factors for RFA, IFA, and RBA were assumed.

Source: Hammond et al. 2011

The embodied carbon factor of Type IL portland cement was assumed to be 90% of Type I/II portland cement because the standard for blended cement allows for 5% to 15% limestone replacement in Type IL portland cement. The embodied carbon factors of RFA and RBA were conservatively assumed to be zero, as they are less than those of embodied carbon factors of general fly ashes from coal-fired plants, because natural gas and refuse-derived fuel are used during their production in the Ames Municipal Power Plant. The factor of IFA was assumed to be 0.008%, the same as that of CFA, because it was produced mainly from a coal-fired process at the ISU Power Plant.

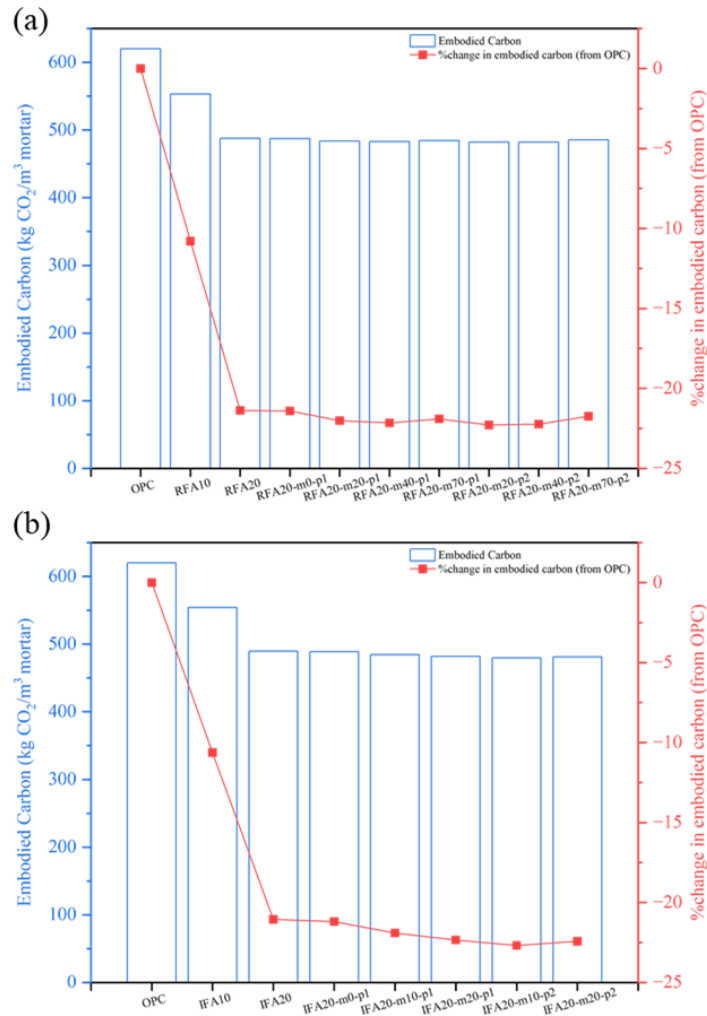
8.2 General Assessment

The embodied carbon of each mortar mixture tested in Chapters 6 and 7 was calculated according to the mixture proportion in a cubic meter of mortar. Table 8.2 presents the calculated embodied carbon for the mortar mixtures. As reported in many previous studies, embodied carbon in a mortar mixture is greatly dependent on the cement content in a unit volume of mortar (Gan et al. 2017, Purnell and Black 2012, Yang et al. 2015).

Table 8.2. Embodied carbon of the mortar mixes studied

Mixture ID	Embodied carbon in mortar (kg CO ₂ /m ³ mortar)	In-unit volume of mortar		
		Embodied carbon of cement (kg CO ₂ /m ³ mortar)	CO ₂ sequestered in ash (kg CO ₂ /m ³ mortar)	CO ₂ sequestration from carbon curing (kg CO ₂ /m ³ mortar)
OPC	620.1	613.2	–	–
RFA10	553.2	546.4	–	–
RFA20	487.6	480.8	–	–
RFA20-m0-p1	487.4	480.8	0.2	–
RFA20-m20-p1	483.6	480.8	4.0	–
RFA20-m40-p1	482.7	480.8	4.8	–
RFA20-m70-p1	484.3	480.8	3.3	–
RFA20-m20-p2	481.9	480.8	5.6	–
RFA20-m40-p2	482.3	480.8	5.3	–
RFA20-m70-p2	485.3	480.8	2.2	–
IFA10	554.3	546.9	–	–
IFA20	489.6	481.8	–	–
IFA20-m0-p1	488.7	481.8	0.8	–
IFA20-m10-p1	484.3	481.8	5.3	–
IFA20-m20-p1	481.6	481.8	7.9	–
IFA20-m10-p2	479.5	481.8	10.1	–
IFA20-m20-p2	481.1	481.8	8.5	–
CFA10	554.0	546.7	–	–
CFA20	489.2	481.4	–	–
CFA20-m0-p1	488.9	481.4	0.3	–
CFA20-m5-p1	486.6	481.4	2.5	–
CFA20-m5-p2	489.2	481.4	0.0	–
RBA10	613.5	607.3	–	–
RBA20	607.0	601.5	–	–
RBA20-m20-p1	602.0	601.5	5.0	–
RBA20-m70-p1	607.0	601.5	0.0	–
RBA20-m20-p2	604.4	601.5	2.6	–
RBA20-m70-p2	606.2	601.5	0.8	–
RBA20-wet	604.3	601.5	2.7	–
PLC	556.7	549.9	–	–
C-RFA20-m70-p1	315.4	431.5	3.3	120.6
C-IFA20	313.8	431.5	–	125.4
C-RBA20-m20-p1	384.3	539.4	5.0	155.5

Figure 8.1 shows the embodied carbon of each mortar mixture with standard curing and the percentage change in embodied carbon compared to the embodied carbon of OPC mortar. The reduction in the embodied carbon of mortar mixes containing waste fly ashes was almost similar to the replacement ratio of ashes for portland cement (20% in this study), indicating that maximizing replacement of cement with low embodied carbon materials is a controlling factor for reducing the embodied carbon of mortars. When 20% RBA was used to replace sand, it only reduced the embodied carbon of the OPC mortar by 2% to 3% because the embodied carbon of aggregates is much lower than that of cement.



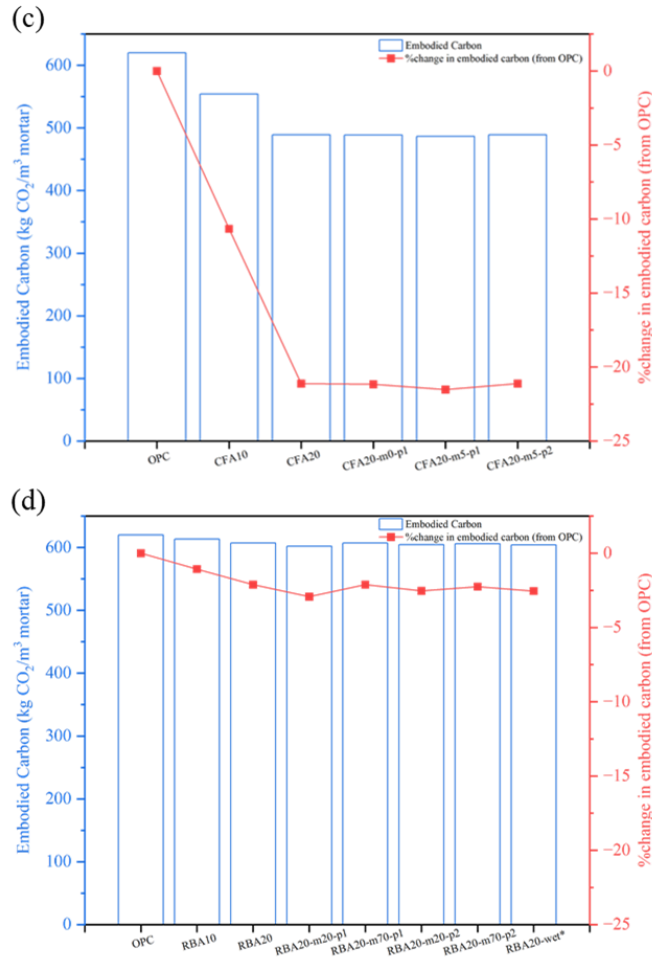


Figure 8.1. Embodied carbon of standard-cured mortar mixtures containing different waste ashes: (a) treated or non-treated RFA, (b) treated or non-treated IFA, (c) treated or non-treated CFA, and (d) treated or non-treated RBA

When carbon-treated fly ash was used as cement replacement, it had a limited effect on the embodied carbon of the mortar when compared to mortar containing untreated fly ash. This is because the amount of CO₂ sequestered in the carbon-treated ashes was relatively low (about 5% for RFA and 10% for IFA, see Tables 5.1 and 5.2). Thus, the carbon reduction resulting from the carbon treatment of the ashes was only 1% to 2% when 20% ashes were used for cement replacement in the mortar.

It should be noted that in terms of embodied carbon reduction, carbon treatment of waste ashes may not play a significant role when compared with the use of untreated waste ashes. However, the carbon treatment can effectively help oxidize the metallic aluminum and zinc in waste ashes, such as in the RFA studied, thus preventing gas generation, abnormal expansion, and strength reduction of the mortar containing waste ashes. The use of carbon-treated RBA as a sand replacement could also significantly improve the compressive strength of the mortar. However, carbon treatment of IFA and CFA did not improve the compressive strength of the resulting mortar.

Figure 8.2 shows the effect of carbon curing on the selected mortar mixtures in terms of embodied carbon. Compared with the embodied carbon of OPC, the IL cement cut approximately 10% of the embodied carbon due to the incorporation of limestone powder. In Figure 7.7, the amount of CO₂ sequestered during the carbon curing was greatly dependent on the cement content, resulting in an additional reduction in embodied carbon. The sequestered CO₂ of approximately 120 kg to 155 kg in a cubic meter of mortar, as shown in Table 8.2, was observed by carbon curing, leading to an additional reduction in embodied carbon aside from its reduction from cement or aggregate replacement. RFA20-m70-p1, C-RFA20-m70-p1, and C-RBA20-m20-p1 cut 49.1%, 49.4%, and 38.0% of the embodied carbon compared to the embodied carbon of OPC. Carbon curing was especially effective on mortar mixtures containing RBA (aggregate substitute) because cement is a major cause of embodied carbon.

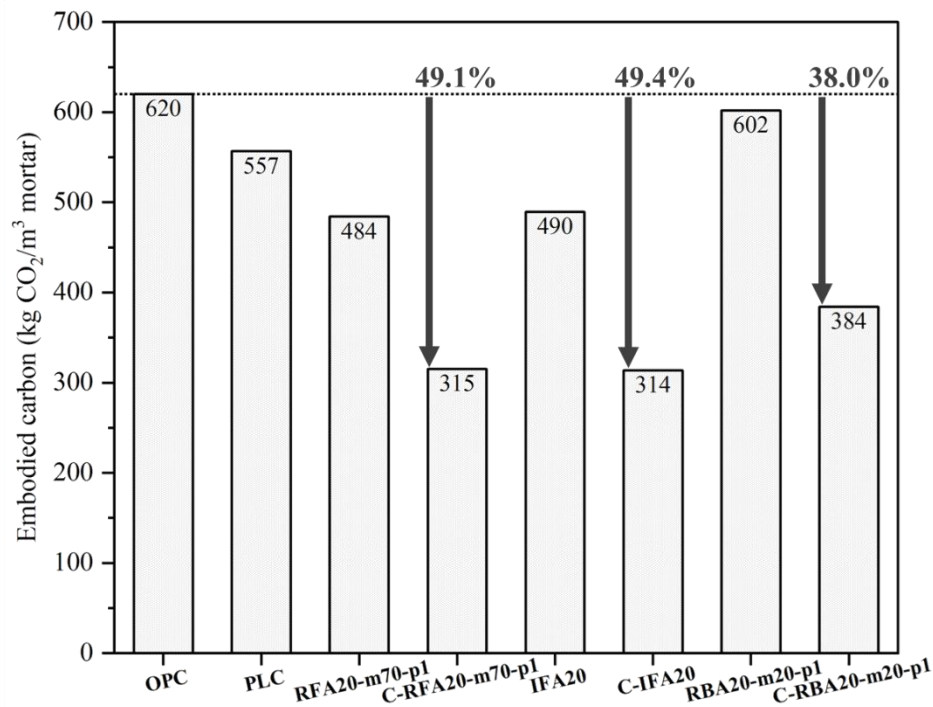


Figure 8.2. Embodied carbon of mixtures treated with carbon curing

8.3 Strength-Normalized Carbon Intensity

Importantly, the assessment of embodied carbon in concrete materials needs to be adjusted based on strength performance. This is because the higher strength of concrete materials requires less usage of them, reducing their embodied carbon during their life cycles. Table 8.3 presents the amount of embodied carbon (measured in kg CO₂e) in one cubic meter of mortar (m³) per unit of compressive strength (MPa), called the strength-normalized carbon intensity (SNCI), of the mortar mixes studied. That is,

$$\text{SNCI} = \text{Total embodied carbon in 1 m}^3 \text{ mortar} / \text{compressive strength} \quad (8.1)$$

The lower the SNCI value is, the closer the mortar is to carbon net-zero.

Table 8.3. Embodied carbon normalized by compressive strength

Mixture ID	Normalized embodied carbon in unit volume of mortar (kg CO ₂ /(MPa·m ³) mortar)	
	At 3 days	At 28 days
OPC	14.3	9.2
RFA10	16.9	11.0
RFA20	19.4	12.8
RFA20-m0-p1	17.5	11.3
RFA20-m20-p1	16.3	10.2
RFA20-m40-p1	13.9	10.1
RFA20-m70-p1	12.0	8.0
RFA20-m20-p2	18.6	10.7
RFA20-m40-p2	16.1	10.2
RFA20-m70-p2	15.2	8.5
IFA10	18.2	9.0
IFA20	20.9	11.5
IFA20-m0-p1	22.0	11.0
IFA20-m10-p1	20.9	11.6
IFA20-m20-p1	23.7	12.3
IFA20-m10-p2	19.6	10.6
IFA20-m20-p2	24.5	12.3
CFA10	15.8	7.9
CFA20	17.0	7.8
CFA20-m0-p1	16.8	7.8
CFA20-m5-p1	20.7	8.2
CFA20-m5-p2	22.7	8.8
RBA10	18.3	10.4
RBA20	19.2	11.9
RBA20-m20-p1	18.9	9.6
RBA20-m70-p1	19.2	9.7
RBA20-m20-p2	21.4	10.7
RBA20-m70-p2	20.8	10.2
RBA20-wet	18.4	10.4
PLC	14.1	9.2
C-RFA20-m70-p1	8.0	6.6
C-IFA20	8.6	6.3
C-RBA20-m20-p1	9.3	7.8

8.4 Simple Cost Savings Assessment

A simple cost savings analysis was conducted on the use of municipal solid waste incineration (MSWI) fly ash and bottom ash in concrete, and the results are shown in Table 8.4.

Table 8.4. Simple calculation of cost savings from use of MSWI fly/bottom ashes in concrete pavement

Concrete mix with different strength	3000 psi	4000 psi	5000 psi
Price of concrete (USD/yd³)	137	146	163
Approximate cement content (lb/yd ³)	500	600	700
Approximate sand content (lb/yd ³)	1500	1350	1200
Cement material cost in concrete (\$/yd ³)	30.0	36.0	42.0
Estimated cement transportation/shipment cost (\$0.196/ton/mile (500-miles rail shipping rates) for 200 miles in distance) (\$/yd ³ concrete)	8.9	10.7	12.4
Total cost for cement (\$/yd³ concrete)	38.9	46.7	54.4
Saving from 20% cement replacement by MSWI fly ash (\$/yd ³ concrete)	6.0	7.2	8.4
Cement shipping cost reduction, 200 miles in distance (\$/yd ³ concrete)	1.8	2.1	2.5
Total savings from cement replacement and shipping (\$/yd³ concrete)	7.8	9.3	10.9
Sand material cost in concrete (\$/yd ³ concrete)	8.3	7.4	6.6
Estimated sand shipment cost, 10 ton; 50 miles in distance (\$/yd ³ concrete)	30.6	27.6	24.5
Total cost for sand (\$/yd³ concrete)	38.9	35.0	31.1
\$ saved from 20% sand replaced by MSWI BA (\$/yd ³ concrete)	1.7	1.5	1.3
\$ saved from sand shipping (50 miles in distance) (\$/yd ³ concrete)	6.1	5.5	4.9
Total savings from sand replacement and shipping (\$/yd³ concrete)	7.8	7.0	6.2
\$ saved from 20% MSWI FA deposal (\$90/ton) (\$/yd ³ concrete)	4.1	4.9	5.7
\$ saved from 20% MSWI BA deposal (\$90/ton) (\$/yd ³ concrete)	12.2	11.0	9.8
Total savings from MSWI ash deposit (\$/yd³ concrete)	16.3	15.9	15.5
Total savings from cement replacement by MSWI fly ash (\$/yd ³ concrete)	11.9	14.2	16.6
Total savings from sand replacement by MSWI bottom ash (\$/yd ³ concrete)	20.0	18.0	16.0
Total savings from use of MSWI fly ash and bottom ash (\$/yd³ concrete)	31.9	32.3	32.6
(%)	23%	22%	20%

Based on the concrete cost per yard in Ames, Iowa (HomeBlue 2024), the average cost of concrete with a strength of 3000, 4000, and 5000 lb/in.² is approximately \$136.5, \$146.0, and

\$163.0, respectively. The average price of portland cement has been \$132.6 per metric ton (approximately \$6 per 100 pounds) over the last five years (IBISWorld 2024). The price of sand and gravel in 2024 (Jaganmohan 2024) is approximately \$12.2 (\$5.5 per 1000 lb). In the strength ranges of 3000 to 5000 lb/in.², the concrete mixture designs (per cubic yard of concrete) consist of approximately 550 to 650 lb of cement and 1400 to 1500 lb of sand.

As seen in Table 8.4, the savings from the use of MSWI fly ash and bottom ash in concrete come from the material and shipping costs of the amount of cement and sand replaced by MSWI fly ash and bottom ash as well as the cost of MSWI fly ash and bottom ash deposit. It should be noted that although the material cost, especially the sand cost, is minimal, the transportation costs of materials, especially the sand transportation cost, are prominent. In addition, the deposit costs for MSWI fly ash and bottom ash are significant. As a result, replacing cement and sand with 20% MSWI fly ash and 20% MSWI bottom ash could save over 20% of the total concrete cost in addition to providing a beneficial impact on the environment.

8.5 Summary of Carbon Intensity in the Mortar Containing Waste Ashes

Figure 8.3 summarizes the SNCI of the mortar mixes studied. The following observations can be made from the figure:

1. At early ages (3 days), the strength-normalized embodied carbon (SNCI) values of most mortar mixes containing waste ashes were higher than that of control mortar (made with 100% OPC) (14.3 kg CO₂/MPa·m³), except for the mortars containing 20% RFA that was carbon treated under a 40% or 70% moisture condition with 100 kPa pressure (RFA20-m40-p1 and RFA20-m70-p1). This is mainly because other mortars containing waste ashes had low compressive strength.
2. At the age of 28 days, the SNCI values of the control mortar decreased to 9.2 kg CO₂/MPa·m³ due to increased strength with age. Several other mortar mixes showed a lower value, including mortars made with RFA20-m70-p1/p2, IFA10 (untreated IFA and 10% replacement), CFA10/CFA20, CFA20-m0-p1, and CFA20-m5-p1/p2.
3. Carbon-cured mortar (C-RFA-m70-p1, C-IFA20, and C-RBA-m20-p1) showed lower SNCI values compared to the OPC and PLC at both 3 and 28 days. This was due to the sequestration of CO₂ into mortar during the carbon curing, cutting back on embodied carbon. In addition, the cement replacement with the ashes effectively reduced the embodied carbon.
4. In terms of embodied carbon, the embodied carbon of C-RBA-m20-p1 greatly decreased with the carbon-curing treatment, leading to a lower SNCI value than the standard-cured mixtures, even though the strength was not significantly improved.
5. Overall, from the SNCI viewpoint, use of up to 20% CFA with or without carbon treatment to replace cement in mortar is the most beneficial approach, followed by 20% RFA carbon treated under a 70% moisture condition with 100 kPa pressure (RFA20-m70-p1).
6. In terms of cement and transportation costs, the use of 20% carbon-treated waste fly ashes to replace cement in normal-strength concrete (3000 to 5000 psi) can result in concrete material cost savings of over 20%.

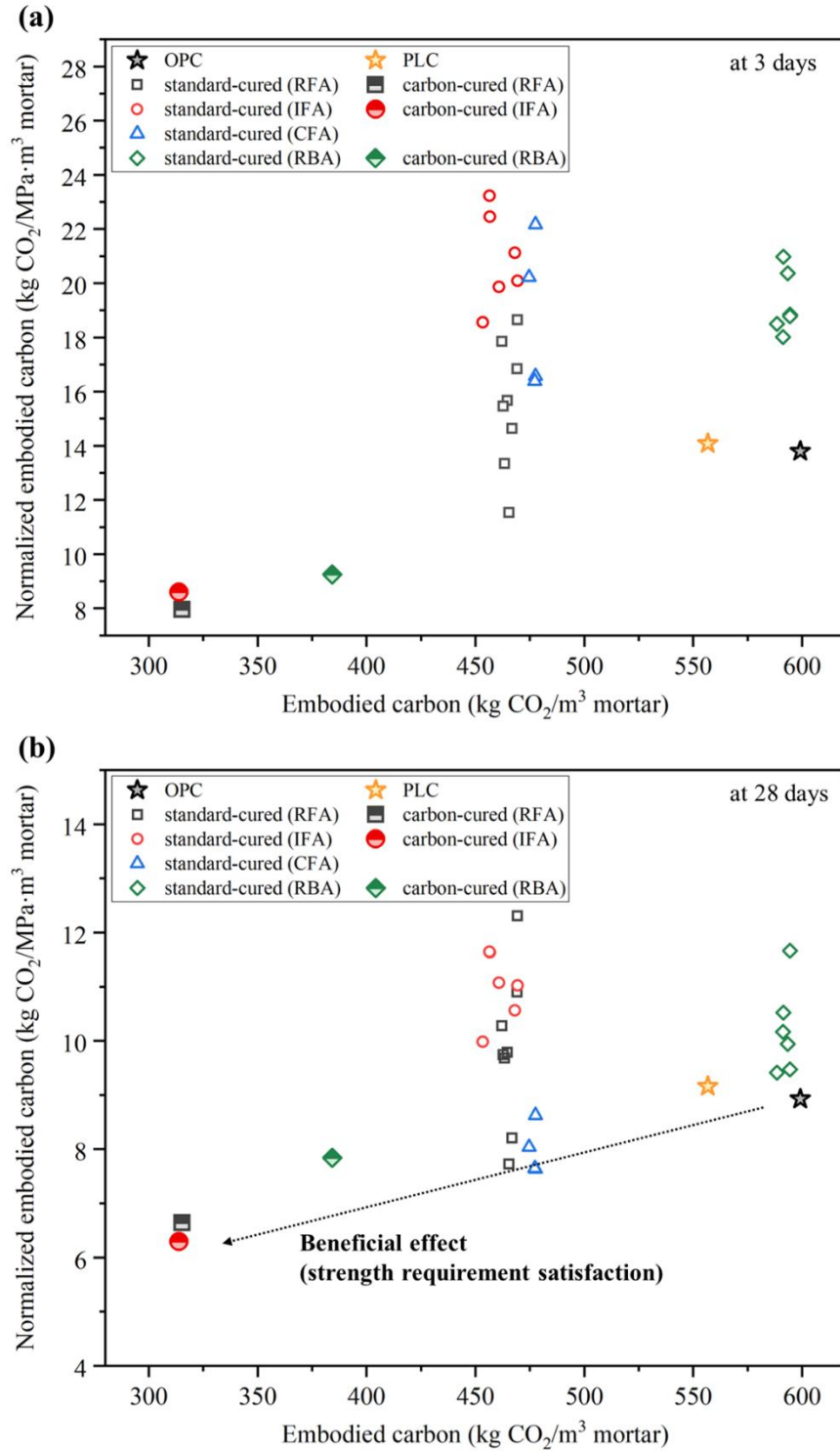


Figure 8.3. Embodied carbon normalized by compressive strength: (a) 3 days and (b) 28 days

9. CONCLUSIONS AND RECOMMENDATIONS

9.1 Summary of Observations

The following observations have been made in the present study:

1. Physical properties and morphology of raw ashes

- The specific gravity of RFA (2.09) and IFA (2.16) was similar to that of CFA (2.13), and the moisture content of RFA and IFA satisfied the ASTM C618 requirement (below 3%). RBA had a lower specific gravity of 2.23 and a higher absorption of 8.85%, while the river sand had a specific gravity of 2.67 and an absorption of 1.48%.
- The median particle sizes of RFA (70 μm) and IFA (60 μm) were much larger than that of CFA (16 μm). Their fineness values did not satisfy the ASTM C618 requirement.
- The morphology of RFA and IFA displayed mostly irregularly shaped particles, while CFA displayed mostly spherical particles. The particle shape of RBA was also similar to that of RFA, but there were rod-like crystals on the surface, which were ettringite.

2. Chemical properties and thermal stability of raw ashes

- The CaO content was 3.14% for RFA and 44.8 % for IFA, higher than that of CFA (24.3%), and all met the ASTM C618 requirement for CaO content in Class C fly ash. However, RFA and IFA did not meet the ASTM C618 requirements for $\text{SiO}_2 + \text{Al}_2\text{O}_3 + \text{Fe}_2\text{O}_3$ ($> 50\%$) and LOI ($< 6\%$). In addition, IFA had 22.5% SO_3 , significantly higher than the requirement ($< 5\%$), and RFA had 5.7% $\text{Na}_2\text{O}_{\text{eq}}$ ($\% \text{Na}_2\text{O} + 0.658 \times \% \text{K}_2\text{O}$), significantly higher than the requirement (0.6%). The commercial Class C fly ash, CFA, met all ASTM C618 requirements.
- Based on the XRD results, higher amounts of calcium carbonate and calcium sulfate in the ashes led to the above results. The crystalline phases of RFA were mostly composed of calcite, quartz, and anhydrite. On the other hand, IFA displayed the crystalline phases of anhydrite, quartz, and calcium oxide. The major crystalline phase of CFA was quartz. RBA showed major crystalline phases of ettringite, quartz, gehlenite, and calcite.
- The thermal stability of the ashes was related to the presence of calcite, anhydrite, and ettringite minerals, leading to higher LOI values in RFA, IFA, and RBA.

3. Optimal carbon treatment conditions for waste ashes

- The maximum temperature of an ash in the carbon treatment chamber was used as a carbonation index for determining an optimal condition. The maximum temperatures released from the waste ashes under different carbon treatment conditions were different among the ashes studied. While there is little difference in the maximum temperature resulting from different pressures applied (100 kPa and 200 kPa), the optimal moisture content for carbon treatment is 20% to 40% for RFA, 10% to 20% for IFA, around 10% for CFA, and 20% for RBA.

- At a high moisture content (>30%), some reactive fly ashes, like IFA and CFA, started to harden during carbon treatment due to hydration and carbonation reactions.
 - CFA, a conventional Class C fly ash, is highly reactive in water, requiring its carbon treatment under a low moisture condition. RFA is the least reactive among all of the fly ashes studied, allowing its carbon treatment under a moisture content of up to 70%. IFA contains a certain amount of lime, and its high reactivity with water leads to the ash hardening when above a moisture content of 20%. Therefore, the moisture content should be controlled in a range of 10% to 20% during the carbon treatment of IFA.
4. Carbon sequestration capacity and effect of carbon treatment on the properties of waste ashes
- Carbon sequestration was the highest in IFA, followed by RFA, RBA, and CFA. At a high CO₂ pressure (200 kPa), the optimal moisture content for carbon sequestration was lower and the carbon sequestration was improved.
 - The optimal moisture content at a CO₂ pressure of 100 kPa was 40% for RFA, 20% for IFA, and 20% for RBA. Under optimal conditions, the amount of CO₂ uptake in IFA, RFA, and RBA was approximately 10, 5, and 2 kg CO₂/kg anhydrous ash, respectively. However, the carbon treatment was not effective for the conventional fly ash, CFA.
 - Morphological changes to the carbon-treated RFA and IFA were observed. On the surface of the treated ash samples, calcium carbonate particles with a size of 1 to 5 μm were observed, and the particle surfaces became denser due to the production and aggregation of calcium carbonate. However, for CFA, no significant difference in the morphology before and after carbon treatment was found, although some agglomerations among small particles were noticed.
 - The ettringite on the RBA particle surfaces was clearly decomposed after carbon treatment under the treatment condition of 20% moisture content and 100 kPa pressure (sample C-RBA-m20-p1). The decomposition of ettringite due to carbonation was also identified in the TGA results. In addition, some irregularly shaped calcite particles were found on the surfaces of the carbon-treated RBA particles.
5. Effects of carbon-treated ashes on the properties of cement-based materials
- This research confirms that without any treatment, RFA contained a given amount of metallic aluminum and zinc, which could hydrate and generate air bubbles to cause severe cement expansion. During carbon treatment, the metallic aluminum is oxidized, and therefore the use of carbon-treated RFA in cement-based materials has no risk of expansion. Carbon treatment can be a promising technology for utilizing waste ashes that include metallic aluminum and zinc.
 - Carbon treatment effectively improved RFA and RBA to mitigate the strength reduction of mortar (20% replacement) without significant flowability loss. When carbon treated at the moisture condition of 70% under 100 kPa and 200 kPa pressure, 20% C-RFA replacement for cement led to a reduction in compressive strength of less than 10% and 15%, respectively, compared with the control mortar mix (100% portland cement) at the age of 28 days. When carbon treated at the moisture conditions of 20% and 70% under 100 kPa pressure, 20% SSD C-RBA replacement for river sand led to a reduction in compressive

strength of less than 7% compared with the mix made with 100% dry river sand at the age of 28 days. (Note: The mortar made with 100% dry river sand actually had a lower w/b ratio than the mortar made with 20% SSD C-RBA replacement for river sand.)

- In the test results of samples containing RFA, the strength activity index at 28 days was improved from 57% (RFA20) up to 90% (RFA20-m70-p1). The effect of carbon treatment on RFA was greatly dependent on moisture content. A moisture content of 70% was best for the treatment, leading to the effective removal of the metallic aluminum and the mitigation of strength reduction.
- In the test results of samples containing RBA, the carbon treatment for RBA improved the compressive strength, increasing the strength activity index at 28 days from 75% (RBA20) up to 93% (RBA20-m70-p1). This can be attributed to the surface refinement of the ash with calcium carbonate.
- Carbon treatment was not effective for IFA and CFA, which experienced no positive effect on mortar strength. Although the carbon treatment effectively transformed the CaO in IFA into calcium carbonate, the excessive sulfate content in the raw or carbon-treated IFA did not change, which hindered the strength development of the mortar.
- The carbon-treated CFA caused particle agglomeration and the prehydration of CFA, leading to negative effects on both flowability and strength development.

6. Strength-normalized carbon intensity of the mortar mixes studied

- The strength-normalized embodied carbon values decreased with the age of the mortar due to increased strength with age.
- At the ages of 28 and 56 days, the mortars with a lower value of strength-normalized embodied carbon than the control mortar are those containing RFA20-m70-p1/p2, IFA10,
- CFA10/CFA20, CFA20-m0-p1, and CFA20-m5-p1/p2, among which only the mortar with RFA20-m70-p1 also had a value of strength-normalized embodied carbon lower than the control mortar at 3 days.
- From the viewpoint of strength-normalized embodied carbon, the use of up to 20% CFA with or without carbon treatment or 20% RFA carbon treated under a 70% moisture condition with 100 kPa pressure (RFA20-m70-p1) to replace cement in mortar is the most beneficial approach.

9.2 Conclusions and Recommendations

The following are the conclusions and recommendations drawn from the present study:

1. The particle size and chemical composition of as-received RFA and IFA do not meet the requirement of ASTM C618, and therefore they cannot be used as supplementary cementitious materials directly.
2. Test results show that different CO₂ pressures (100 kPa or 200 kPa) have a limited impact on the effectiveness of carbon treatment, but the moisture content of waste ashes has a significant impact on the effectiveness of carbon treatment. Different ashes require different carbon treatment conditions to reach optimal carbon sequestration capacity. Generally,

reactive fly ash (like IFA and CFA) requires low moisture content to reach optimal carbon treatment, and high moisture content can lead to ash hardening during the treatment. Differently, less reactive ash (like RFA and RBA) allows for high moisture content during carbon treatment without hardening. This observation can be used to assist in the selection of carbon treatment conditions of waste ashes.

3. Under their optimal carbon treatment conditions, the CO₂ uptake of IFA, RFA, and RBA is approximately 10, 5, and 2 kg CO₂/kg of anhydrous ash, respectively. Such carbon sequestration capacity will offer additional benefits for embodied carbon reduction when the waste ashes are used in concrete.
4. After being carbon treated at a moisture condition of 70% under 100 kPa pressure, the strength activity index at 28 days of the RFA mortar was improved from 57% (RFA20, with no treatment) up to 90% (RFA20-m70-p1, with carbon treatment). After being carbon treated at a moisture condition of 70% under 100 kPa pressure, the strength activity index at 28 days of the RBA mortar was improved from 75% (RBA20, with no treatment) up to 93% (RBA20-m70-p1, with carbon treatment). These results suggest that from the strength viewpoint, carbon-treated RFA and RBA can be used as cement replacement and sand replacement in concrete, respectively.
5. Carbon treatment is not recommended for reactive ashes like IFA and CFA. Although the carbon treatment effectively transformed the CaO in IFA into calcium carbonate, it did not change the excessive sulfate content in IFA, which critically hindered the strength development of the mortar.
6. Embodied carbon in mortar mixtures is largely dependent on portland cement content. Therefore, maximizing the replacement of cement with low embodied carbon materials is very effective in reducing the embodied carbon of mortars. Although not playing a significant role in the embodied carbon reduction, carbon treatment of waste ashes can effectively help oxidize the metallic aluminum and zinc in waste ashes, such as in the RFA studied, thus preventing gas generation, abnormal expansion, and strength reduction of the mortar containing waste ashes.
7. Of all the waste ashes studied, only the mortar containing 20% RFA carbon treated under the 70% moisture condition with 100 kPa pressure (RFA20-m70-p1) showed a lower value of strength-normalized embodied carbon than the control mortar (made with 100% portland cement) at all ages up to 56 days. From the embodied carbon reduction viewpoint, 20% carbon-treated RFA is encouraged for use as cement replacement in mortar and concrete.
8. Mortars made with 20% carbon-treated RFA or 20% untreated IFA as a cement replacement and carbon cured for 13 hours can reduce embodied carbon by 49.1%. Additionally, mortars with 20% carbon-treated RBA as a sand replacement and carbon cured for 14 hours can reduce embodied carbon by 38.0%.
9. In terms of cement and transportation costs, the use of 20% carbon-treated waste fly ashes to replace cement in normal-strength concrete (3000 to 5000 psi) can result in concrete material cost savings of over 20%.
10. The durability of concrete containing carbonation-treated waste ashes, which was not covered in this study, must be investigated before the waste ashes can be practically used in field concrete.
11. Although the City of Ames produces 6 tons of waste ash daily, this amount is insufficient to meet the concrete industry's needs. A cost analysis is crucial to encourage the industry to

invest in production lines for waste ash treatment and to adopt these ashes as a viable material in concrete.

REFERENCES

- Adu-Amankwah, S., L. Black, J. Skocek, M. B. Haha, and M. Zajac. 2018. Effect of Sulfate Additions on Hydration and Performance of Ternary Slag-Limestone Composite Cements. *Construction and Building Materials*, Vol. 164, pp. 451–462.
- Anderson, J., and A. Moncaster. 2020. Embodied Carbon of Concrete in Buildings, Part 1: Analysis of Published EPD. *Buildings and Cities*, Vol. 1, No. 1, pp. 198–217.
- Ashraf, W., and J. Olek. 2016. Carbonation Behavior of Hydraulic and Non-Hydraulic Calcium Silicates: Potential of Utilizing Low-Lime Calcium Silicates in Cement-Based Materials. *Journal of Materials Science*, Vol. 51, pp. 6173–6191.
- Aubert, J. E., B. Husson, and A. Vaquier. 2004. Metallic Aluminum in MSWI Fly Ash: Quantification and Influence on the Properties of Cement-Based Products. *Waste Management*, Vol. 24, No. 6, pp. 589–596.
- Bertolini, L., M. Carsana, D. Cassago, A. Q. Curzio, and M. Collepardi. 2004. MSWI Ashes as Mineral Additions in Concrete. *Cement and Concrete Research*, Vol. 34, No. 10, pp. 1899–1906.
- Bui, P. T., Y. Ogawa, and K. Kawai. 2018. Long-Term Pozzolanic Reaction of Fly Ash in Hardened Cement-Based Paste Internally Activated by Natural Injection of Saturated Ca (OH) 2 Solution. *Materials and Structures*, Vol. 51, No. 6.
- Chen, B., and G. Ye. 2024. The Role of Water-Treated Municipal Solid Waste Incineration (MSWI) Bottom Ash in Microstructure Formation and Strength Development of Blended Cement Pastes. *Cement and Concrete Research*, Vol. 178.
- Chen, T., and X. Gao. 2019. Effect of Carbonation Curing Regime on Strength and Microstructure of Portland Cement Paste. *Journal of CO2 Utilization*, Vol. 34, pp. 74–86.
- Chen, T., X. Gao, and L. Qin. 2019. Mathematical Modeling of Accelerated Carbonation Curing of Portland Cement Paste at Early Age. *Cement and Concrete Research*, Vol. 120, pp. 187–197.
- Cosoli, G., A. Mobili, F. Tittarelli, G. M. Revel, and P. Chiariotti. 2020. Electrical Resistivity and Electrical Impedance Measurement in Mortar and Concrete Elements: A Systematic Review. *Applied Sciences*, Vol. 10, No. 24.
- Delbeke, J., A. Runge-Metzger, Y. Slingenberg, and J. Werksman. 2019. Chapter 2. The Paris Agreement. *Towards a Climate-Neutral Europe*. Routledge.
- Ebert, B. A., B. M. Steenari, M. R. Geiker, and G. M. Kirkelund. 2020. Screening of Untreated Municipal Solid Waste Incineration Fly Ash for Use in Cement-Based Materials: Chemical and Physical Properties. *SN Applied Sciences*, Vol. 2, No 5.
- Gan, V. J., J. C. Cheng, I. M. Lo, and C. M. Chan. 2017. Developing a CO2-e Accounting Method for Quantification and Analysis of Embodied Carbon in High-Rise Buildings. *Journal of Cleaner Production*, Vol. 141, pp. 825–836.
- Gao, Y., Y. Jiang, Y. Tao, P. Shen, C. S. Poon. 2024. Accelerated Carbonation of Recycled Concrete Aggregate in Semi-wet Environments: A Promising Technique for CO2 Utilization. *Cement and Concrete Research*, Vol. 180.
<https://doi.org/10.1016/j.cemconres.2024.107486>.
- Gartner, E., G. Walenta, V. Morin, P. Termkhajornkit, I. Baco, and J. M. Casabonne. 2011. Hydration of a Belite-Calciumsulfoaluminate-Ferrite Cement: AetherTM. *Proceedings of the 13th International Congress on the Chemistry of Cement*, Vol. 3, July, Madrid, Spain.

- Hammond, G., C. Jones, E. F. Lowrie, and P. Tse. 2011. Embodied Carbon. *The Inventory of Carbon and Energy (ICE) Version 2.0*.
- HomeBlue. 2024. Concrete Cost per Yard in Ames, Iowa. <https://www.homeblue.com/concrete/ames-ia-concrete-cost-per-yard.htm>.
- IBISWorld. 2024. Price of Cement. <https://www.ibisworld.com/us/bed/price-of-cement/190/>.
- Jaganmohan, M. 2024. Apparent Cement Consumption in the United States from 2010 to 2023. Statista. <https://www.statista.com/statistics/273367/consumption-of-cement-in-the-us/>.
- Jaganmohan, M. 2024. Average U.S. Price of Construction Sand and Gravel 2010-2023. Statista. <https://www.statista.com/statistics/219381/sand-and-gravel-prices-in-the-us/#:~:text=Average%20U.S.%20price%20of%20construction%20sand%20and%20gravel%202010%2D2023&text=In%20the%20United%20States%2C%20the,per%20metric%20ton%20in%202023>.
- Joseph, A. M., R. Snellings, P. Nielsen, S. Matthys, and N. De Belie. 2020. Pre-Treatment and Utilisation of Municipal Solid Waste Incineration Bottom Ashes towards a Circular Economy. *Construction and Building Materials*, Vol. 260.
- Li, P., M. Guo, M. Zhang, L. Teng, and S. Seetharaman. 2012. Leaching Process Investigation of Secondary Aluminum Dross: The Effect of CO₂ on Leaching Process of Salt Cake from Aluminum Remelting Process. *Metallurgical and Materials Transactions B*, Vol. 43, pp. 1220–1230.
- Liu, Y., Y. Zhuge, C. W. Chow, A. Keegan, D. Li, P. N. Pham, J. Huang, and R. Siddique. 2020. Properties and Microstructure of Concrete Blocks Incorporating Drinking Water Treatment Sludge Exposed to Early-Age Carbonation Curing. *Journal of Cleaner Production*, Vol. 261.
- Liu, Z., and W. Meng. 2021. Fundamental Understanding of Carbonation Curing and Durability of Carbonation-Cured Cement-Based Composites: A Review. *Journal of CO₂ Utilization*, Vol. 44.
- López-Arce, P., L. S. Gómez-Villalba, S. Martínez-Ramírez, M. Á. De Buergo, and R. Fort. 2011. Influence of Relative Humidity on the Carbonation of Calcium Hydroxide Nanoparticles and the Formation of Calcium Carbonate Polymorphs. *Powder Technology*, Vol. 205(1–3), pp. 263–269.
- Lu, B., S. Drissi, J. Liu, X. Hu, B. Song, and C. Shi. 2022. Effect of Temperature on CO₂ Curing, Compressive Strength and Microstructure of Cement Paste. *Cement and Concrete Research*, Vol. 157.
- Lu, J., S. Ruan, Y. Liu, T. Wang, Q. Zeng, and D. Yan. 2022. Morphological Characteristics of Calcium Carbonate Crystallization in CO₂ Pre-Cured Aerated Concrete. *RSC Advances*, Vol. 12, No. 23, pp. 14610–14620.
- Manz, O. E. 1999. Coal Fly Ash: A Retrospective and Future Look. *Fuel*, 78(2), 133-136.
- Monkman, S., and M. MacDonald. 2017. On Carbon Dioxide Utilization as a means to Improve the Sustainability of Ready-Mixed Concrete. *Journal of Cleaner Production*, Vol. 167, pp. 365–375.
- Mu, Y., Z. Liu, F. Wang, and X. Huang. 2018. Carbonation Characteristics of γ -Dicalcium Silicate for Low-Carbon Building Material. *Construction and Building Materials*, Vol. 177, pp. 322–331.
- Neto, J. D. S. A., G. Angeles, and A. P. Kirchheim. 2021. Effects of Sulfates on the Hydration of Portland Cement—A Review. *Construction and Building Materials*, Vol. 279.

- Ohenoja, K., J. Pesonen, J. Yliniemi, and M. Illikainen. 2020. Utilization of Fly Ashes from Fluidized Bed Combustion: A Review. *Sustainability*, Vol. 12, No. 7.
- Oral, Ç. M., and B. Ercan. 2018. Influence of pH on Morphology, Size and Polymorph of Room Temperature Synthesized Calcium Carbonate Particles. *Powder Technology*, Vol. 339, pp. 781–788.
- Peng, L., P. Shen, C. S. Poon, Y. Zhao, and F. Wang. 2023. Development of Carbon Capture Coating to Improve the Durability of Concrete Structures. *Cement and Concrete Research*, Vol. 168.
- Purnell, P., and L. Black. 2012. Embodied Carbon Dioxide in Concrete: Variation with Common Mix Design Parameters. *Cement and Concrete Research*, Vol. 42, No. 6, pp. 874–877.
- Qadir, W., K. Ghafor, and A. Mohammed. 2019. Evaluation the Effect of Lime on the Plastic and Hardened Properties of Cement Mortar and Quantified Using Vipulanandan Model. *Open Engineering*, Vol. 9, No 1, pp. 468–480.
- Smigelskyte, A., R. Siauciunas, H. Hilbig, M. Decker, L. Urbonas, and G. Skripkiunas. 2020. Carbonated Rankinite Binder: Effect of Curing Parameters on Microstructure, Strength Development and Durability Performance. *Scientific Reports*, Vol. 10, No. 1.
- Tsamatsoulis, D., and N. Nikolakakos. 2013. Optimizing the Sulphates Content of Cement Using Multivariable Modelling and Uncertainty Analysis. *Chemical and Biochemical Engineering Quarterly*, Vol. 27, No. 2, pp. 133–144.
- Visser, J. H. M. 2014. Influence of the Carbon Dioxide Concentration on the Resistance to Carbonation of Concrete. *Construction and Building Materials*, Vol. 67, pp. 8–13.
- Wieczorek-Ciurowa, K., J. Paulik, and F. Paulik. 1980. Influence of Foreign Materials upon the Thermal Decomposition of Dolomite, Calcite and Magnesite Part I: Influence of Sodium Chloride. *Thermochimica Acta*, Vol. 38, No. 2, pp. 157–164.
- Yang, K. H., Y. B. Jung, M. S. Cho, and S. H. Tae. 2015. Effect of Supplementary Cementitious Materials on Reduction of CO₂ Emissions from Concrete. *Journal of Cleaner Production*, Vol. 103, pp. 774–783.
- Yu, M. Y., J. Y. Lee, and C. W. Chung. 2010. The Application of Various Indicators for the Estimation of Carbonation and pH of Cement Based Materials. *Journal of Testing and Evaluation*, Vol. 38, No. 5, pp. 534–540.
- Zajac, M., I. Maruyama, A. Iizuka, and J. Skibsted. 2023. Enforced Carbonation of Cementitious Materials. *Cement and Concrete Research*, Vol. 174.
- Zhang, D., B. R. Ellis, B. Jaworska, W. H. Hu, and V. C. Li. 2021. Carbonation Curing for Precast Engineered Cementitious Composites. *Construction and Building Materials*, Vol. 313.
- Zhang, D., V. C. Li, and B. R. Ellis. 2018. Optimal Pre-Hydration Age for CO₂ Sequestration through Portland Cement Carbonation. *ACS Sustainable Chemistry & Engineering*, Vol. 6, No. 12, pp. 15976–15981.
- Zhang, D., and Y. Shao. 2016. Early Age Carbonation Curing for Precast Reinforced Concretes. *Construction and Building Materials*, Vol 113, pp. 134–143.
- Zheng, S., P. Ning, L. Ma, X. Niu, W. Zhang, and Y. Chen. 2011. Reductive Decomposition of Phosphogypsum with High-Sulfur-Concentration Coal to SO₂ in an Inert Atmosphere. *Chemical Engineering Research and Design*, Vol. 89, No 12, pp. 2736–2741.

APPENDIX A. ADDITIONAL XRD TEST RESULTS

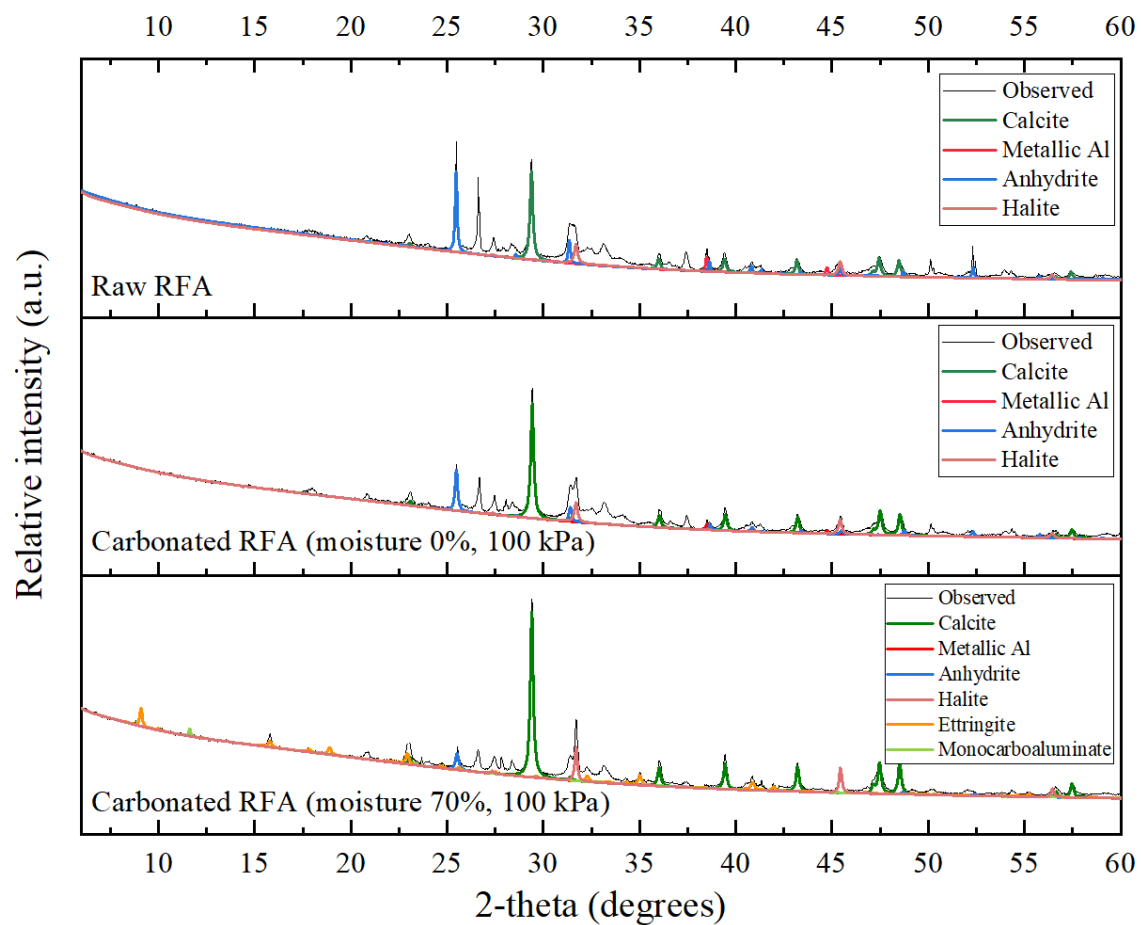
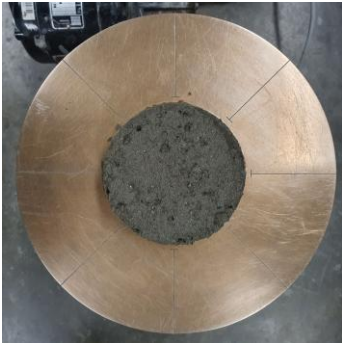

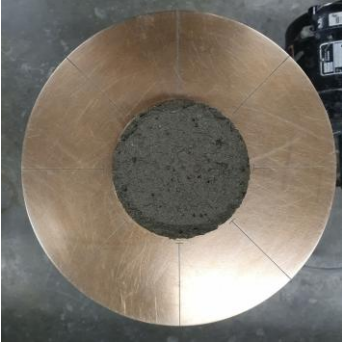

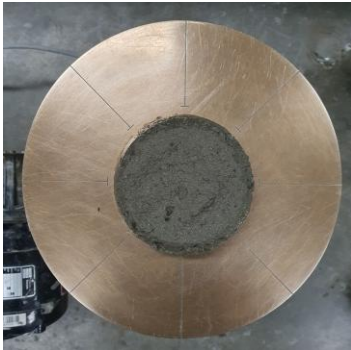




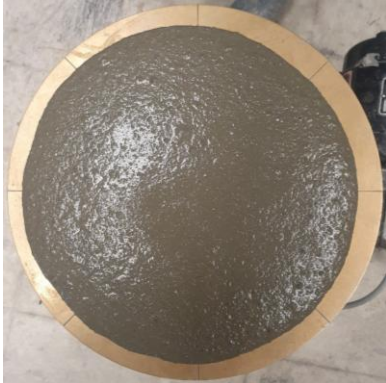
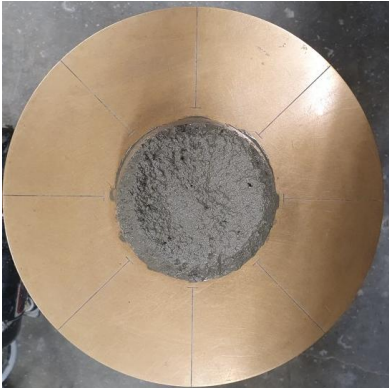

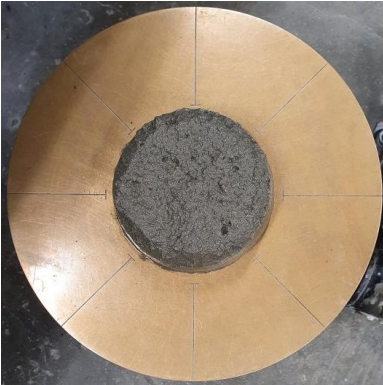


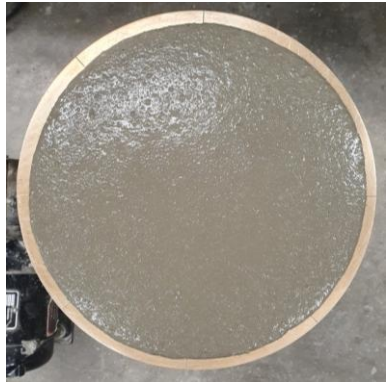
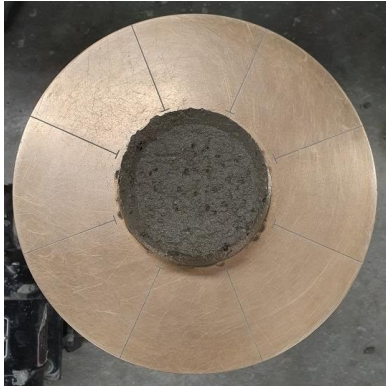
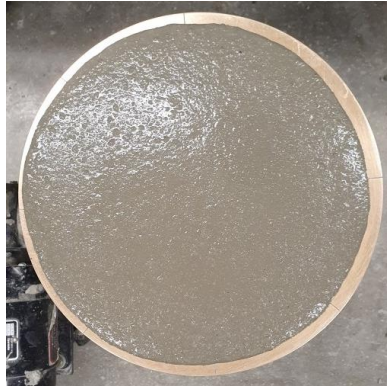
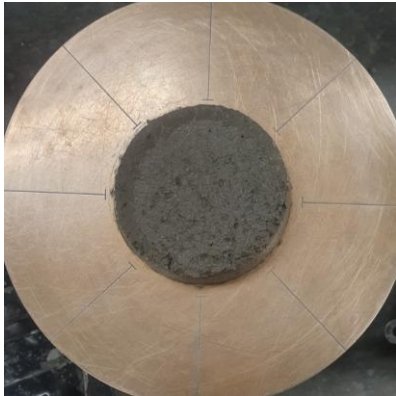



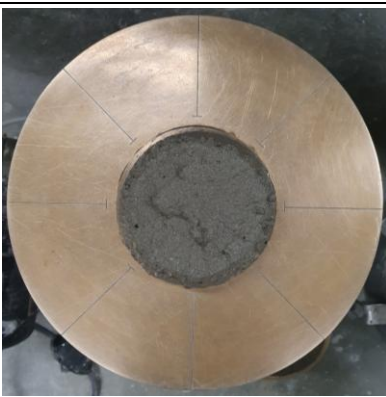





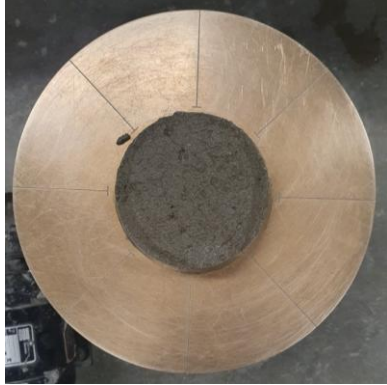

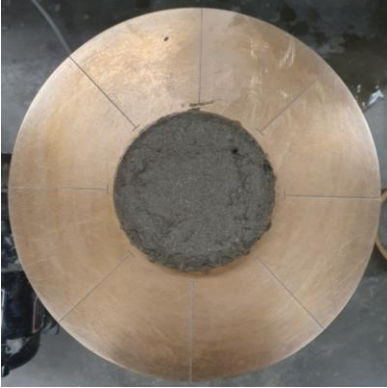



Figure A1. XRD patterns of the carbon-treated RFA at a CO₂ pressure of 100 kPa



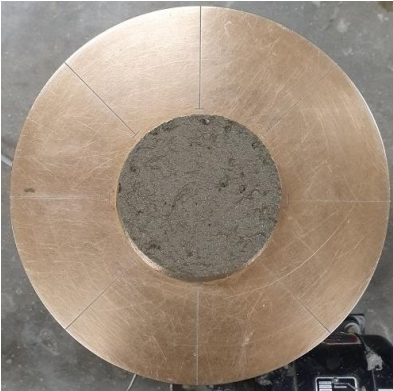



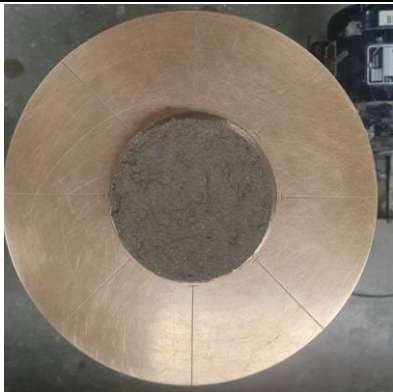

APPENDIX B. PHOTOS FROM FLOW TABLE TESTS

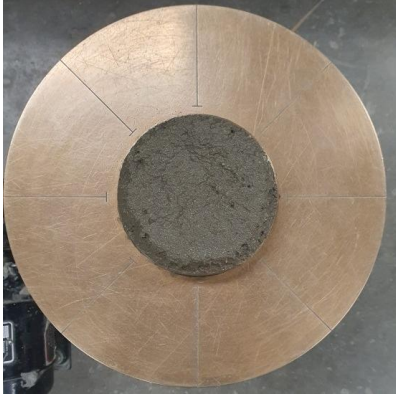

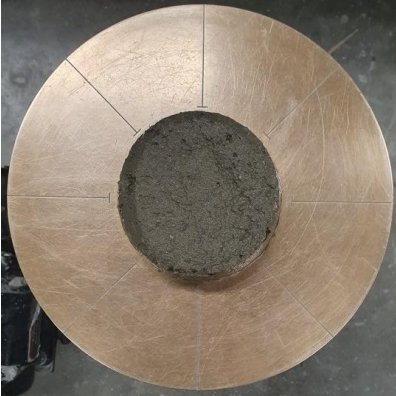
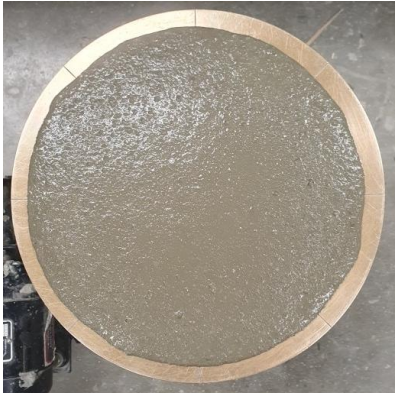
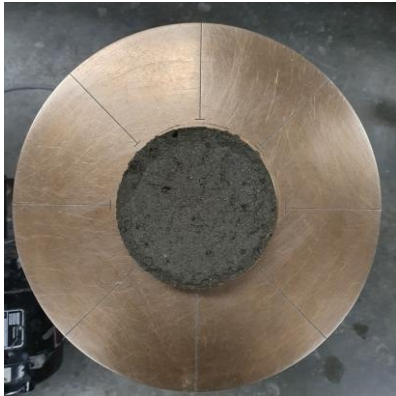



Mixture name	Initial flow	Final flow after 25 drops
OPC		
RFA10		
RFA20		
RFA20-m0-p1		





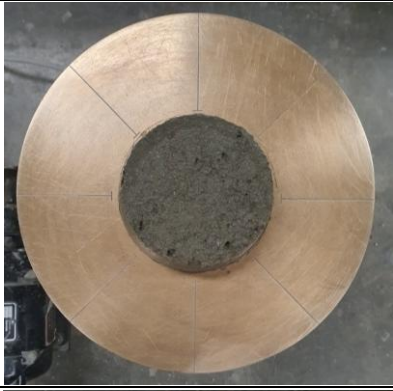
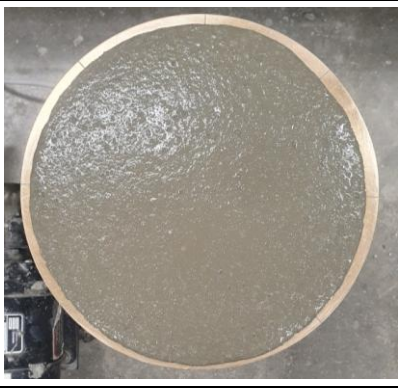


Mixture name	Initial flow	Final flow after 25 drops
RFA20-m20-p1		
RFA20-m40-p1		
RFA20-m70-p1		
RFA20-m20-p2		

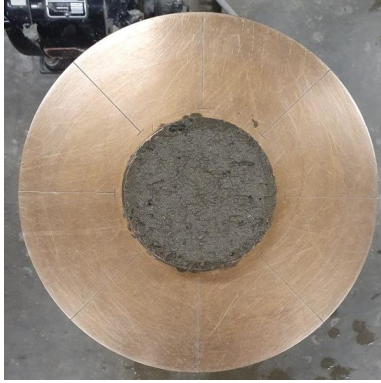

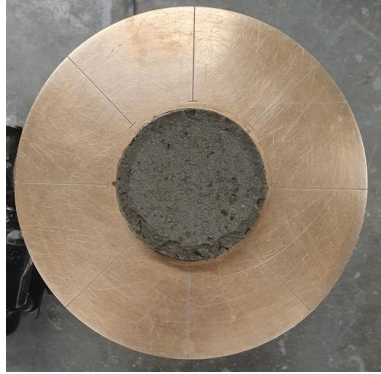


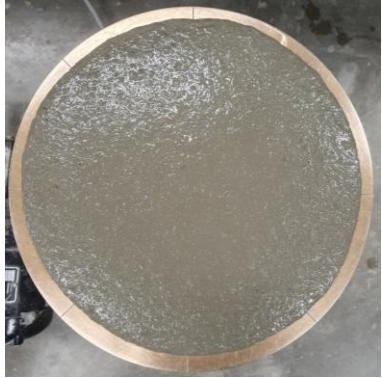
Mixture name	Initial flow	Final flow after 25 drops
RFA20-m40-p2		
RFA20-m70-p2		
IFA10		
IFA20		

Mixture name	Initial flow	Final flow after 25 drops
IFA20-m0-p1		
IFA20-m10-p1		
IFA20-m20-p1		
IFA20-m10-p2		

Mixture name	Initial flow	Final flow after 25 drops
IFA20-m20-p2		
CFA10		
CFA20		
CFA20-m0-p1		

Mixture name	Initial flow	Final flow after 25 drops
CFA20-m5-p1		
CFA20-m5-p2		
RBA10		
RBA20		

Mixture name	Initial flow	Final flow after 25 drops
RBA20-m20-p1		
RBA20-m70-p1		
RBA20-m20-p2		
RBA20-m70-p2		

Mixture name	Initial flow	Final flow after 25 drops
RBA20-m20-p5		
RBA20-m70-p5		
RBA20-wet-p5		

**THE INSTITUTE FOR TRANSPORTATION IS THE FOCAL POINT FOR TRANSPORTATION
AT IOWA STATE UNIVERSITY.**

InTrans centers and programs perform transportation research and provide technology transfer services for government agencies and private companies;

InTrans contributes to Iowa State University and the College of Engineering's educational programs for transportation students and provides K–12 outreach; and

InTrans conducts local, regional, and national transportation services and continuing education programs.



**IOWA STATE
UNIVERSITY**

Visit InTrans.iastate.edu for color pdfs of this and other research reports.